Chemical genetics of Vertebrate development

By

Charles H Williams III

Dissertation

Submitted to the Faculty of the
Graduate School of Vanderbilt University
in partial fulfillment of the requirements
for the degree of

DOCTOR OF PHILOSOPHY
in
Cell and Developmental Biology
May, 2017
Nashville, Tennessee

Approved:

Charles C Hong, M.D., Ph.D. (Mentor)
Ken Lau, Ph.D.
David Bader, Ph.D.
Craig Lindsley, Ph.D.
Guoqiang Gu, Ph.D. (Chair)

ACKNOWLEDGEMENTS

I thank my committee members for their support during this thesis. Stephen Dalton for hiPSC-NCC work. Isabel Dominguez for dn-CK2α construct. Current and former Labmates Audrey frist, Johnathan Hempel, Adrian Cadar, Young Chun, Jamie Rickmyre and Erin Booton; Programs of Developmental biology, VICC, VICB, Department of Cardiology, and Cell and Developmental Biology. NIH for funding.

ABSTRACT

Small molecules have value in their ability to modulate protein activity in ways that are not accessible using conventional genetic methods, and their potential to be developed into therapeutics. As genetic causes of human disease are identified, many are found to play an integral role in embryonic development as well. The purpose of this dissertation is to utilize vertebrate embryonic development as a platform for discovery and characterization of chemical probes using phenotype guided development. I discovered three molecules, Eggmanone, Incaskin, and Ogremorphin based on ability to perturb development of a composite of 29 anatomical features. Using these anatomical features as a query against the wealth of reference genotype-phenotype data in ZFIN, I identified the targets of the small molecules as PDE4, CK2α, and GPR68. Using eggmanone, I characterize a novel role for PDE4 in regulation of HH signaling, and show that it could be a useful therapeutic target for smo inhibitor resistant cancers. Using incaskin, I show an unbiased phenotypic clustering methodology for target deconvolution; furthermore, I show that incaskin is a highly selective, potent CK2α inhibitor which provides a therapeutic approach for targeting cancers down stream of APC in Wnt signaling. Using ogremorphin, a first in class inhibitor of GPR68, I show that proton sensing GPR68 is critical neural crest migration. Furthermore, I show that proton-sensing GPR68 represents a novel chemically tractably therapeutic avenue for development of an anti-metastatic agent. This body of work contributes to novel discovery of small molecules, signaling, and developmental biology

TABLE OF CONTENTS

Page

LIST OF FIGURES

LIST OF TABLES

CHAPTER 1

INTRODUCTION

Phenotypic Screening

For much of human history, therapies for various ailments came about from astute phenotypic observations and serendipity (Mueller and Scheidt, 1994). For instance, the origins of digoxin, a cardiac glycoside currently in use for heart failure, can be traced directly to a traditional herbal remedy for dropsy made from the foxglove plant (Mueller and Scheidt, 1994; Norman, 1985). With the advent of modern biochemistry and molecular biology, drug discovery became dependent on the target-based approach to systematically screen for thousands and even millions of agents that modulate a particular biological target chosen based on a rational therapeutic hypothesis. In the decades that followed, an unprecedented number of new therapeutics have transformed modern medicine and pharmaceutical industry (Kinch et al., 2014). However, despite the disproportionate focus and funding on target based approaches for the past two decades, the pharmaceutical industry as a whole delivered fewer “first-in-class” drugs using this approach than using a phenotypic approach ((Swinney and Anthony, 2011). In fact, the cost, and the risks, of developing a new pharmaceutical entity have skyrocketed in the recent decades, with the costs of developing a new drug seeming to grow exponentially, a trend termed “Eroom’s Law,” to contrast with the Moore’s Law describing exponential growth in computing power (Scannell et al., 2012). There are a number of reasons for this alarming decline in efficiency of pharmaceutical development. Obvious reasons

include unforeseen off-target effects and toxic metabolites that result in deleterious effects in humans. While late stage failure in clinical trials captures headlines, a key reason for the sustained decline in productivity may lie in the earliest stages of drug discovery: specifically, poor target selection. For an industry grown around target-based discovery, picking a wrong target based on an invalid therapeutic hypothesis can be a death knell, a situation made worse by the fact that consequences might not be apparent until significant expenditure of time and effort. There are numerous causes of poor target selection, but chief among them appears to inadequate insight into human pathophysiology provided by *in vitro* and preclinical models (Bracken, 2009; Worp et al., 2010).

Given the pitfalls of target-based screening, phenotypic screening has reemerged as an attractive alternative and complementary approach to drug discovery. As the name implies, this approach focuses on phenotypic perturbations – observable changes in complex biological function caused by small molecules - to identify chemical modulators of physiological or disease processes in a target agnostic manner. The observed phenotype results from integration of all cellular pathway perturbations in the context of an active biological system, be it an individual cell or an entire organism. A phenotypic screen identifies chemotypes that affect a biologically meaningful target or targets, including key nodes responsible for integrating cell pathways and behaviors. Importantly, since a phenotypic screen is conducted without regard to *a priori* knowledge of targets, it has the potential to discover new therapeutic targets, which may have greater impact at the systems level than established targets. Moreover, in contrast to target-based screens, a phenotypic screen permits discovery of compounds that effect a desired

outcome via engaging multiple targets in a synergistic manner that may not have been otherwise anticipated. Indeed, recent studies have shown that polypharmacology is not necessarily deleterious, and that engagement of multiple targets can sometime be more effective for treatment of certain disease (Roth et al., 2004). While a knowledge of the precise pharmacological target is traditionally considered essential, although not required by the FDA, to push a drug development forward; there is increasing willingness to be target agnostic provided there is a compelling biological rationale and an unmet medical need (Mullard, 2015).

In contrast to traditional observational approaches, which were low-throughput and therefore depended on serendipity, the modern phenotypic screen combines the advantages of phenotype-based approaches with the latest high-throughput chemical screening capabilities. In this review, we will provide a brief overview of various models used in phenotypic screens, with a focus on zebrafish based screens, which has emerged as a powerful *in vivo* model amenable to high-throughput and high-content analyses, and a look to the future of phenotypic screening.

Phenotypic screening modalities

Modalities of phenotypic screens can be broken into two components: the biological model and the assay outputs. These two factors must be considered prior to any screen. A number of model systems have been used in phenotypic screening, ranging from single cells, to organoids and whole organisms.

Cell based screens vary in scope of potential readouts from a simple cell viability assay to complex cell behavior analyses. At the simple end of the spectrum, most

screens for potential anti-cancer agents are cell viability assays using established cancer cell lines (Shoemaker, 2006). At the complex end, Lum and colleagues have screened small molecules in HCT116 human colorectal cancer cells using multiplexed luciferase assays and dot blotting to monitor multiple pathways simultaneously (Kulak et al., 2015). By assessing multiple pathways in a quantitative manner, they were able to collapse the cellular phenotypes elicited by individual compounds into a "fingerprint." Traditionally, determining mechanism of action (MOA) can be laborious, however; such an approach provides mechanistic insights by clustering compound induced "fingerprints" to those obtained from an siRNA library (Kulak and Lum, 2013). Cell based screens have also been conducted in an image based analytics paradigm. Peppard and colleagues identified novel autophagy regulators in HeLa cells expressing LC3 (microtubule-associated protein light chain3)-GFP (green fluorescent protein) fusion protein as an autophagy readout. LC3 is normally cytosolic, however during autophagy is recruited to autophagosomal membranes, which manifest as GFP granules in this read out. When nutrient starved cells are treated with lysomotropic agent hydroxychloroquine (HC), which inhibits the lysosome, LC3-GFP degradation by autophagy is blocked. Using HCS imager *Incell 3000,* a 250,000 compound screen was conducted to identify inhibitors of the formation of autophagosomes, which was thresholded as *<4 GFP granules* (Peppard et al., 2014) Notably, the authors validated this assay with wortmannin, a known inhibitor of autophagosome formation and used this as a positive control to set the threshold.

While most cell based screens have been conducted in established cell lines grown in simple monolayers or suspension, investigators have developed 3-D organoid models of tumor cells, with the aim of developing an *in vitro* model that is more relevant

to human tumor biology, including the role of metabolically quiescent tumor stem cells and the effect of hypoxia gradient within solid tumors. For instance, Walsh and colleagues have developed a model of spheroids derived from primary human tumors, utilizing intrinsic fluorescence properties of FAD and NADH called optical metabolic imaging (OMI). OMI has previously been shown to serve as an early endpoint biomarker for drug response (Walsh et al., 2013). Using this technique the authors carried out a screen for small molecules that altered metabolic activity of tumor spheroids (Walsh et al., 2014).

In the past few years, human induced pluripotent stem cells (hiPSCs) have emerged as a promising human biological platform for phenotypic screening. Since their initial description less than a decade ago, researchers have created iPSC models of a myriad of human diseases using patient-derived iPSCs (Tang et al., 2016). For example, Burkhardt and colleagues have generated hiPSC from ALS patients and demonstrated that neurons differentiated from these hiPSCs exhibit TDP-43 aggregation, a pathological hallmark of ALS. Using an image-based screen based on TDP-43 aggregation in neurons generated from ALS hiPSCs, they discovered that known small molecule inhibitors of the Na+/K+ ATPase, GSK3 and CDK could ameliorate this phenotype, providing supporting not only for prior studies that have implicated these proteins as potential ALS therapeutic targets but also the use of patient-derived iPSCs for drug discovery (Burkhardt et al., 2013).

Cell based screens, while providing an inexpensive, quantitative and high throughput platform for phenotypic screening, suffer from several disadvantages. Despite advances in engineered tissue constructs, cultured cells do not exist in a native biological

context and lack critical tissue interactions and paracrine factors which clearly play an important role *in vivo*. Compound liabilities such as poor metabolic stability, suboptimal bioavailability and undesirable off-target as well as on-target effects are not recognized early on during the primary screen. Such issues can be addressed from the start with *in vivo* chemical screening of living organisms and whole animals. Thus far, large-scale *in vivo* phenotypic screens have been conducted in various model multicellular organisms ranging from nematode such as *c. elegans* to vertebrates such as zebrafish. For instance, Petraschek and colleagues have performed a small molecule screen for compounds that affect aging in the nematode. From this screen, they identified 60 compounds that increase *c. elegans* lifespan without obvious deleterious effects. Concordant with existing genetic models of aging, over half of the hit compounds increased the animal's resistance to oxidative stress (Ye et al., 2014). Importantly, this screen revealed a large number of candidate targets that are conserved in humans and hence represent potential therapeutic targets to slow aging. Of course, *c. elegans* is still a very simple animal organism, with a rudimentary physiology, lacking for instance discrete circulatory system. Moreover, *c. elegans* has a very short life cycle (approximately 3.5 days) and each adult hermaphrodite has precisely 959 cells, making them less suitable for modeling certain diseases like cancer. Finally, due to their substantial evolutionary divergence from man (Figure 1), the targets of small molecules identified in invertebrates like c*. elegans* and *Drosophila* may not be conserved in man and even then the human orthologs may have divergent functions, making phenotypic screens using invertebrates less than ideal for drug discovery.

	C. elegans	D. melanogaster	D. rerio	M. musculus	HiPSC
Generation Time	3–5 days	10–14 days	3–4 months	6–8 weeks	NA
Brood size	250-300	80-300	100-300	5-8	NA
Media	Solid or liquid	Solid	Liquid	N/A	Liquid
Number of Genes	~19,000	~14,000	~26,000	~20,000	~20,000
Genome size (million bases)	100	140	1,400	2,000	3,200
Evolutionary Divergence from Man (million years)	990	990	450	90	0
AA identity hALK2	35	57	70	98	100
Cost per plate ($)	<1	<1	~1	5790*	20-1000**
Relative throughput/ easy of scalability	++++	+++	+++	+	++++

Figure 1 Comparison of model organisms used in phenotypic screens.
*Commonly accepted numbers for generation time and brood size are listed, along with media for animal maintenance, evolutionary divergence, gene number and genome size. Also listed, the evolutionary divergence from man and the amino acid sequence identity to the human BMP receptor ALK2 (hALK2). Unit cost: approximate cost of animals needed to screen a 96-well plate of compound libraries, in triplicate. *For mice, this is the approximate cost to purchase 288 mice from Jackson Labs. **Cost of iPSC varies significantly depending on differentiated cell type, culture methods and screening conditions. Relative throughput/ease of scalability: ++++, very high (close to* in vitro *HTS); +++, high (up to tens of thousands compounds/week); +, low (up to hundreds of compounds/week)*

Zebrafish screens

We believe that zebrafish represent a “sweet spot” for large-scale phenotypic screens in terms of biological complexity, physiologic similarities to humans, small size and fecundity. Zebrafish are also far less costly to maintain in large numbers necessary to conduct a large-scale screen than mammals like mice. Although zebrafish have many important physiological differences from humans, they have numerous similarities such homologous organ systems and complex tissue architectures. Moreover, the majority of the functional domains of human proteins and zebrafish orthologs are highly conserved; many, if not a majority, of the small molecules discovered in zebrafish screens should have similar effects, or at least identical targets, in man. The first proof of principle that zebrafish could be useful for a large-scale *in vivo* phenotype screen came from a study

that was conducted by Peterson and colleagues in 2000. In this study, the authors demonstrated that zebrafish embryos can be arrayed and screened in a 96-well format, and that small molecules which affected embryonic development and body patterning could be identified based on discrete perturbations to various anatomic structures (Peterson et al., 2000). Moreover, given the rapid development of zebrafish, which have a functional circulatory system by 24-hours post fertilization (hpf) and free swimming larvae by 72-hpf, the timeframe required for a phenotypic readout is similar to many cell based assays. Sixteen years since this landmark study, dozens, if not hundreds, of chemical screens have been carried out in zebrafish (Rennekamp and Peterson, 2015). The phenotypic screens can be broadly be categorized into four major types by assay output: morphological, therapeutic, pathway and behavioral (Williams and Hong, 2011). These four categories cover the majority of assays that have been performed in zebrafish and are meant to serve as a general framework for discussion of different assay types, rather than be comprehensive or mutually exclusive. Screens for compounds that modulate a diverse range of form and function, such as regeneration, lipid absorption and angiogenesis (Rennekamp and Peterson, 2015), while not specifically discussed here can be considered within the frame of the four categories.

Morphological

As the name indicates, the morphological screen involves identification of hit compounds based on their ability to cause specific and reproducible morphologic deviations from normal. The main feature of the morphology-based approach is the variable data depth of the screen, since they are by definition multi-dimensional (Williams and Hong, 2011). The screener has the choice between obtaining “shallower data” by focusing exclusively on a single anatomical feature to “deeper data” to detect any

discernable morphologic changes throughout the embryo. In a screen for compounds that result in altered dorsoventral (DV) patterning, we used tail length as a primary endpoint (Yu et al., 2008), since embryos with dorsalized pattern have grossly shortened, twisted tail (Mullins et al., 1996). This single point screen has resulted in the discovery of dorsomorphin, the first small molecule inhibitor of the bone morphogenetic protein (BMP) pathway (Hao et al., 2013; Yu et al., 2008) as well as a Wnt pathway modulator (Hao et al., 2013). Even when focused on a single feature, the phenotypic screen can obtain additional information, increasing data depth. For example, Colanesi and colleagues performed a chemical screen looking specifically at the pigmentation of zebrafish embryo. From this simple phenotypic screen, they could subdivide the hit compound into 10 categories based on specific pigmentation alterations; these included reduced numbers of iridiophores and/or melanophores, changes in color depth in either cell type, ectopic numbers of chromatophores, abnormal shape of melanophores and so on (Colanesi et al., 2012).

Since the zebrafish embryo is transparent, the screener can simultaneously score for specific changes to a predefined morphologic feature and any morphologic changes in the rest of the body. We adopted this “all comer” approach to identify a novel hedgehog pathway inhibitor and a lysophosphatidic acid (LPA) receptor inhibitor (Hao et al., 2010a; Shelton et al., 2013; Williams and Hong, 2015; Williams et al., 2015). Importantly, because this screening approach is unbiased with respect to pathways and targets, it has the potential to allow discovery of novel mechanistic insights to regulation of pathways involved in embryonic development. Moreover, since it is open to all possible morphologic perturbations, the depth of phenomic data acquired is limited only by

technology related to high-content image analysis. In addition, morphological screens are not limited to anatomical features visible by standard microscopy. For example, multiple groups have utilized transgenic fish expressing fluorescent markers in the endothelium to identify compounds that perturb the vasculature (Reynolds et al., 2016; Tran et al., 2007). Similarly, others have utilized transgenic fish expressing a fluorescent marker in cardiomyocytes to screen for compounds that effect both heart structure and function (Burns et al., 2005; Ni et al., 2011). It is also possible to conduct a fairly large-scale screen involving *in situ* hybridizations to screen for compounds that perturb expression patterns of a cell or tissue marker. For example, Zon and colleagues carried out an *in situ* hybridization-based screen to identify small molecules, such as leflunomide, which affect *crestin*-expressing neural crest cell development (White et al., 2011).

By definition, the morphology based screens are flexible, compatible with many derivations to discover small molecules that perturb many cell types and anatomical structures. Morphologic screens also serve as starting points for finding molecules that affect cell behaviors as well; for example, looking at the quantity and location of leukocytes or neutrophils at a singular time point after tail resection provides information about where those cells are located, as seen in Liu et al, and Robertson et al. From here the authors used secondary assays to identify compounds that modulate the migration of these cells (Liu et al., 2013b; Robertson et al., 2014). An obvious shortcoming of the morphology-based screen is the lack of direct therapeutic relevance; nevertheless, the discovery of dorsomorphin by this approach has directly contributed to new therapeutic strategies for numerous human diseases such as heterotopic ossification, anemia, IBD,

and cancers (Hong and Yu, 2009; Hover et al., 2015, 2016, Owens et al., 2013, 2015; Wang et al., 2012) and has spawned several ongoing drug development programs.

Therapeutic

The therapeutic screen uses zebrafish with a disease phenotype to identify small molecules that specifically ameliorate this phenotype. In contrast to the morphological screen in which deviations from norm are the "hit" criteria, in this category, a return towards the normal phenotype would be a "hit". In the first of such therapeutic screens in zebrafish, Peterson and colleagues used the *gridlock* mutant, a zebrafish model of aortic coarctation lacking normal tail circulation at 24 to 48-hpf, to identify small molecules which restored tail circulation (Peterson et al., 2004). Similarly, Peal and colleagues used the *breakdance* mutant, a zebrafish model of Long QT proarrhythmic syndrome due to a mutation in the KCNH2 potassium channel, to screen for compounds that ameliorate the proarrhythmic phenotype. In a relatively small screen of 1200 compounds, they identified two compounds that restored normal heart beating and therefore have potential as anti-arrhythmic agents (Peal et al., 2011). In addition, other human disease models, such as Duchenne muscular dystrophy (DMD), have been successfully screened for compounds that suppressed the disease phenotypes (Kawahara and Kunkel, 2013).

Therapeutic screens have been successfully carried out in non-genetic disease models as well. Cardiomyopathy is a relatively common serious sequela of cancer treatment with the chemotherapeutic doxorubicin. Peterson and colleagues developed a zebrafish model of doxorubin-induced cardiomyopathy, and conducted a counter-screen for cardioprotective compounds (Liu et al., 2014). Of the 3000 screened compounds, they discovered two, visnagin and diphenylurea, which protected cardiac function without mitigating the chemotherapeutic effects. In a similar manner, the Peterson group also

screened for chemoprotectors against cyanide poisoning, and identified four potential antidotes (Nath et al., 2013). In a search for candidate compounds that can accelerate recovery after acute kidney injury (AK), Cosentino et al screened for small molecules that increase proliferation of renal progenitor cells in zebrafish embryos (Cianciolo Cosentino et al., 2013). This screen identified histone deacetylase inhibitor methyl-4-(phenylthio)butanoate (PTBA), which enhanced recovery after acute kidney injury (Cosentino et al., 2013) and reduced postinjury renal fibrosis in mice (Skrypnyk et al., 2015). Finally, investigators have developed *Mycobacterium marinum* infection and human carcinoma xenograft models in zebrafish (Jung et al., 2012; Takaki et al., 2012). These two models allow for identification of compound that selectively kill pathogen or tumor cells without affecting the health and viability of zebrafish. The paradigm of therapeutic screening in zebrafish is attractive because of its immediate therapeutic relevance. While such screens show promise, using the correct model for screening is critically important to ensure the validity of the therapeutic target. With the ease of genetic editing through CRISPR/Cas9, this platform would be particularly well suited for monogenic diseases with well understood pathophysiology, as zebrafish based models could be rapidly developed and screened.

Pathway

The pathway screen involves identification of hit compounds based on their ability to perturb the function of a specific pathway of interest. As with other phenotypic screens, the assay is unbiased with respect to a particular molecular target; however, it limits the scope of potential targets as the hit must interact with a specific pathway in a measurable manner. This modality relies on pathway-specific read outs in the zebrafish. One of the first pathway screens in zebrafish was conducted by Molina and colleagues. In this study,

the authors took advantage of the fact that gene expression of *dual specific phosphatase-6 (dusp6),* a feedback regulator of FGF (fibroblast growth factor) signaling, is itself a robust reporter of FGF pathway activations. They used a transgenic zebrafish expressing a destabilized GFP expressed under the control of a dusp6 promoter. In this platform, the GFP fluorescence intensity provides quantitative read out of the signaling activity (Molina et al., 2009). From this screen, Molina and colleagues identified a compound (E)-2-benzylidene-3-(cyclohexylamino)-2,3-dihydro-1H-inden-1-one (BCI), and used chemical genetic epistasis and computational approaches to show that the compound targeted dusp6 itself. One drawback of GFP reporters in zebrafish is that quantification of fluorescence can be difficult given the dynamic nature of the transgene expression pattern and that the orientation of the zebrafish in a well can dramatically affect the apparent signal intensive. To address some of these issues, *in vivo* luciferase reporter fish lines have been developed (Becker et al., 2012; Weger et al., 2013).

Finally, a single assay could have a combination of morphological, therapeutic and pathway outputs For example, in the *axin* mutant embryos, ectopic activation of the canonical Wnt/β-catenin signaling results in an eyeless phenotype (van de Water et al., 2001), and the *axin* mutant phenotype can be recapitulated with BIO, an inhibitor of GSK3β, a key component of the β-catenin destruction complex inhibitor. Moreover, windorphen, a canonical Wnt pathway inhibitor, can rescue the eyeless phenotype in *axin* mutants (Hao et al., 2013). Using this Wnt pathway-specific morphologic phenotype as a read out, Nishiya and colleagues conducted a chemical suppression screen and discovered that GGTI-286, a geranylgeranyltransferase 1 (GGTase I) inhibitor, could block canonical Wnt signaling downstream of the β-catenin destruction complex (Nishiya

et al., 2014). In the developing zebrafish embryo, individual pathways do not exist in isolation; therefore, a phenotypic screen designed to interrogate one signaling pathway may lead to serendipitous and sometimes context specific interaction with other pathways.

Behavioral

One of the major unmet therapeutic areas is in neuropsychiatric diseases, for which many target based drug discovery efforts have failed. Such difficulties and the fact that many current neuropsychiatric medicines trace their roots to clinical observations on neurobehavioral effects of drugs originally intended for other indications have motivated investigators to consider behavioral screens to discover novel, and hopefully physiologically relevant, neuropsychiatric drug targets. For this, zebrafish larvae seem ideal since they are amenable to high-throughput chemical screens and they exhibit numerous complex behaviors reminiscent of some human behaviors. In one of the first behavior-based chemical screen in zebrafish, Rihel and colleagues screened over 5,000 compounds for modulators of restfulness or wakefulness. This screen resulted in the identification of 463 unique structures that altered zebrafish behavior (Rihel et al., 2010). Of these compounds, known modulators of major neurotransmitters were found to recapitulate many of the behavioral effects observed in mammals. For example, clonidine, a α2-adrenergic receptor agonists used as a treatment for ADHD (attention deficit hyperactivity disorder) and gaining use as a sedative, was found to also have sedating effects in zebrafish. Subsequent behavioral screens for compounds that modulate responses to photic and acoustic stimuli yielded compounds that not only modulate immediate responses to these stimuli, but also more complex behaviors such as habituation (Kokel and Peterson, 2011; Wolman et al., 2011). This technology has

been expanded to a battery of tests to identify novel neuroactive compounds with a distinct behavioral profile, a “fingerprint,” which can then be used to inform mechanism of action studies (Bruni et al., 2016; Rennekamp et al., 2016). With ongoing advances in behavioral analysis algorithms, it may one day be possible to screen for compounds that modulate increasingly complex behaviors. Given difficulties in developing drugs for neuropsychiatric diseases by targeted approaches, zebrafish-based behavioral screens represent a bold new path for this important unmet medical need as well as opportunities to improve our understanding of animal behavior.

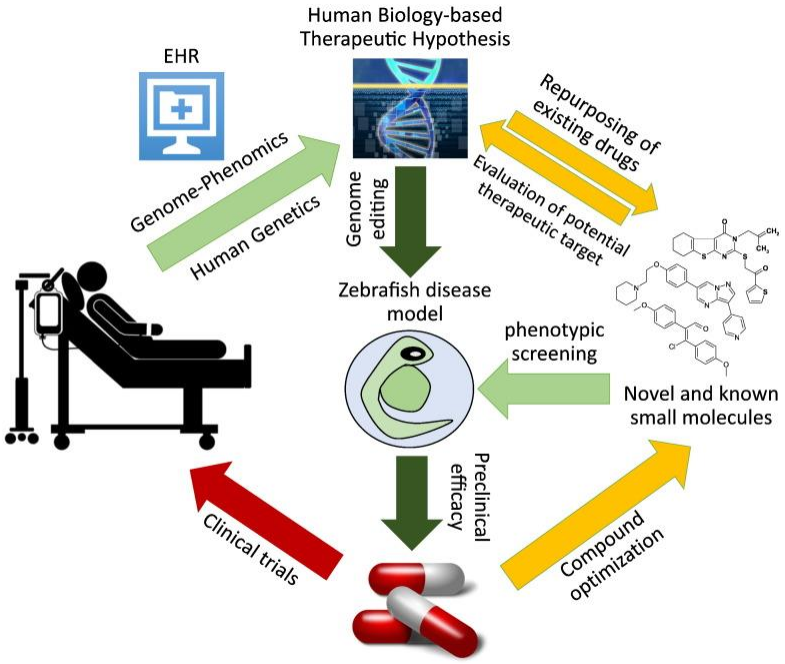

Figure 2 Proposed zebrafish phenotypic screens incorporating human genome–phenome information to accelerate therapeutic discovery.
Human genome–phenome information provided by electronic health record (EHR)-coupled DNA database and by human genetic diseases studies drive formulation of therapeutic hypotheses ("human biology-based therapeutic hypotheses"). To test these hypotheses, zebrafish models of human genetic diseases are generated by genomic editing and employed in phenotypic screen for novel or known compounds which ameliorate the disease phenotypes. These compounds are then advanced for further development, including compound optimization and testing in appropriate preclinical disease models. Alternatively, a target-agnostic morphology-based screen is carried out. Subsequently, targets of hit compounds identified, and each target evaluated in silico against human genome–phenome database to determine whether a viable therapeutic hypothesis can be formulated. If so, these hits are advanced for further development, including compound optimization and testing in appropriate preclinical disease models.

Beyond discovery

While still relatively new, the impact of zebrafish-based chemical screens has been notable. In the past decade, the rate of published zebrafish screens has risen steadily, with an average impact factor of 9.5, as of 2013 (Rennekamp and Peterson, 2015). While dissemination of knowledge through the publication of a chemical screen is the primary goal for academics, a secondary, implicit goal is therapeutic discovery, ultimately to impact human health. Among a number of compounds originally identified in zebrafish

chemical screens with therapeutic potential, several have resulted in industry partnerships for preclinical and clinical development. For instance, Oricula Therapeutics is developing Proto-1 for prevention of hearing loss, Novo Biosciences is developing a metalloproteinase-13 (MMP13) inhibitor for peripheral neuropathy, and La Jolla Pharmaceuticals is developing BMP receptor inhibitors for fibrodysplasia ossificans progressiva (FOP) and other rare diseases. The most advanced therapeutic lead resulting from a zebrafish screen is the PGE2 inhibitor Prohema(North et al., 2007), which has shown promising results in a randomized, controlled Phase II study of patients undergoing hematopoietic stem cell (HSC) transplantation for the treatment of hematologic malignancies (Fate Therapeutics, 2016). Given these early successes, it seems reasonable to anticipate that there will be many more therapeutic leads resulting from zebrafish chemical screens in the coming decades.

Next Steps: Genomics and drug discovery

There are currently about 7,000 known rare diseases in man, and roughly 4,000 of these have been linked to a single genetic cause (Lander, 2015; Stelzer et al., 2016). Some, like familial hypercholesterolemia, are fairly common, found in 1 in 500 individuals, while other are extremely rare like Fibrodysplasia Ossificans Progressiva (FOP), found in 1 in 2 million individuals. Taken together, about 10% of the US population is estimated to be afflicted with a rare disease, representing a significant healthcare burden (Heemstra et al., 2009). Of the disease associated genes in the Online Mendelian Inheritance in Man (OMIM) database, 82% have at least one zebrafish ortholog (Howe et al., 2013). With the advances in genome editing technology, such as the clustered regularly

interspaced short palindromic repeats CRISPR/Cas9 nuclease technique, it is now feasible to generate zebrafish models of virtually all human Mendelian diseases (Figure 2). Once a disease phenotype or a surrogate phenotype is established in zebrafish mutants, a therapeutic screen for compounds that ameliorate these phenotypes should be straightforward. With the advances in genomic sequencing technologies, the number of ultra-rare genetic diseases is expected to increase significantly in the coming decade. In such a scenario, one can easily envision harnessing the power of zebrafish phenotypic screens, perhaps using a panel of known bioactive small molecules or FDA approved drugs, to help accelerate drug discovery and repurposing efforts for rare genetic diseases (Figure 2).

A unique advantage of phenotypic screens is the discovery of novel, previously unrecognized components involved in a biological process or a disease pathophysiology, and chemical tools to modulate them. However, the discovery of new pharmacological targets and new pharmacological classes by themselves do not ameliorate the most important reason for the high rate of failure in drug development: uncertainties associated with target selection. Based on the first principles, the risks associated with target selection are inherently lower for human Mendelian conditions. For instance, the knowledge that rare individuals lacking proprotein convertase subtilisin/kexin type 9 (PCSK9) have better lipid profiles and are protected from atherosclerosis and myocardial infarctions was an important factor in rapid development and approval of PCSK9 inhibitor for treatment of hypercholesterolemia (Cohen et al., 2005, 2006; Kotowski et al., 2006; Zhao et al., 2006). But the power of human genetics need not stop with rare Mendelian conditions. At Vanderbilt University Medical Center (VUMC), a large human DNA

repository, named BioVU, has been linked to de-identified electronic health records (EHR) within the Synthetic Derivative (SD) database. Using BioVU as a human genome-phenome analysis platform, a phenome-wide association study (PheWAS) can be carried out to determine what clinical phenotypes are associated with single nucleotide polymorphisms (SNPs) in a given gene (Figure 2;Denny et al., 2016). Using this approach, we not only identified potential new indications of our small molecule BMP inhibitors but also potential on-target side effects, which will be valuable for eventual clinical trials and post-marketing surveillance (CCH, personal communication).

How might zebrafish-based phenotypic screens leverage the power of human genetics to accelerate drug discovery? As discussed above, zebrafish models of human Mendelian genetics can be used to carry out therapeutic screens for compounds that ameliorate the disease phenotype (Figure 2). Alternatively, a novel pharmacological target identified in unbiased morphologic screens can be interrogated by phenome-genome databases such as BioVU to determine whether alterations in that gene are associated with a disease phenotype and/or therapeutic effects, dramatically lowering the risks of a drug development program (Figure 2). If carried out on a large scale, such efforts might dramatically accelerate drug discovery and repurposing efforts to meet the anticipated need for targeted therapies for rare and common diseases (Figure 2). In summary, zebrafish is a versatile platform that has a bright future as a drug discovery tool in the Era of Personalized Medicines.

Phenoclustering for target identification

Chemical genetic screening for small molecules that affect in vitro and in vivo phenotypes is drug development paradigm that is increasing recognized as a viable alternative to the classical target-based drug discovery paradigm. As a model organism for such screening, the zebrafish is becoming a favorite because of its rapid development, high fecundity, low cost, vertebrate orthologies and liquid aquaculture allowing for precise and scalable screening. However, because of the organism's complexity, screening can yield numerous and often complex phenotypes. The traditional method of target identification is affinity chromatography, which is both time and labor intensive with predilection for identifying the most abundant proteins that may or may not be biologically relevant. Although newer approaches such as drug affinity responsive target stability (DARTS) and yeast three hybrid systems are promising, target identification requires a separate platform distinct from the original in vivo screening models(Williams and Hong, 2011). By contrast, a key advantage of an ***in vivo*** phenotype-based chemical screen using zebrafish and other animal models is that the developing animal itself can provide crucial clues as to the pathway being disrupted. As such, biological responses to small molecules with known activity can be quantified and used as a reference for clustering responses of unknown compounds, with a supposition that tightly clustered compounds will have similar mechanisms of action (Figure 3).

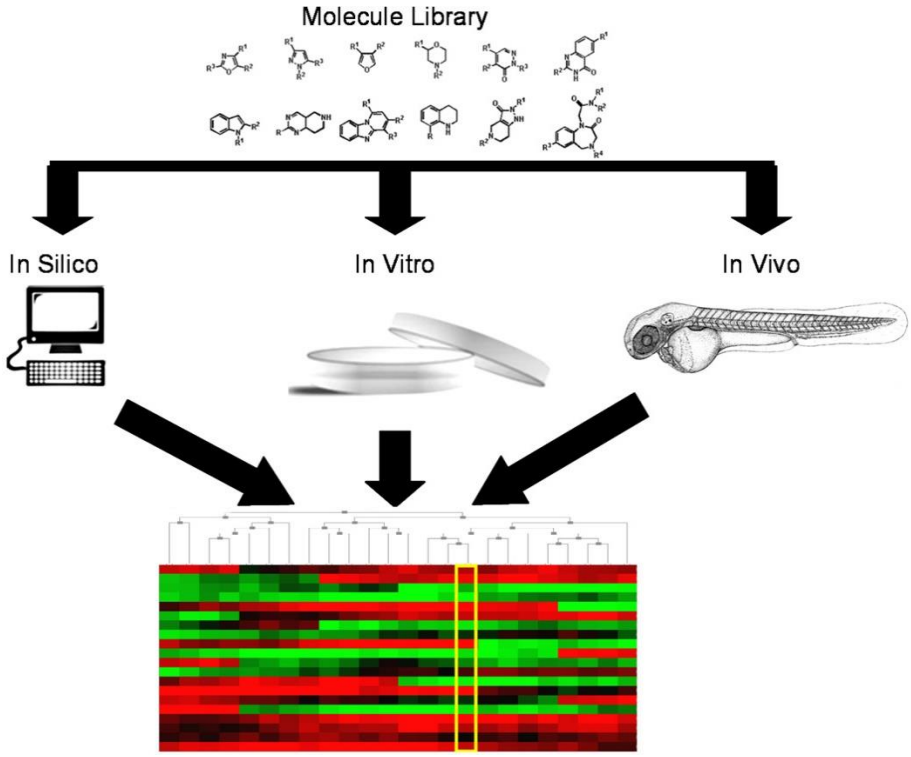

Figure 3 Annotation of small molecule libraries through hierarchical clustering can be done in a number of models; in silico, in vitro and in vivo
The data generated for the query compound in these models is then compared to a reference data set through clustering. The nearest neighbor should have a similar or the same target as the query compound (yellow).

In silico Clustering

High-throughput screening has become a staple of drug development; and has resulted in the formation of a large repertoire of information on PubChem. As of August, 2011, over 30 million chemically unique compounds have been deposited in the PubChem database. Furthermore, over 500 thousand bioassay records have been uploaded, representing over 130 million experimental bioactivity results. With this wealth of data Han and colleagues were able to mine the PubMed bioactivity spectra by hierarchical clustering and were able to understand the biological mechanisms of target-small molecule interactions(Han et al., 2009). One such example was the compound myricetin (PubChem CID:5281672), a flavonoid that is commonly found in natural food

source. By examining the bioactivity spectra, they found that the molecule is an inhibitor of several proteins such as aldehyde dehydrogenase, Leishmania Mexicana pyruvate kinase, and stress-activated protein kinase. This finding was confirmed in a literature search where the mechanism of action of this molecule had been described(Han et al., 2009). This was a principle proof that structurally similar compounds have similar bioactivity spectra. Therefore, the same group later used a similar method and investigated 37 small molecules in the context of their PubChem bioactivity spectra and chemical similarity. They found that compounds that were then examined in the context of the NCI-60 clustered into groups with similar mode of actions, which strongly correlated with chemical structures(Cheng et al., 2011). The NCI-60 is a project run by DTP (Developmental Therapeutic Program) and NCI (National Cancer Institute), designed to screen up to 3,000 compounds per year for potential anticancer activity against 60 different human tumor cell lines, representing leukemia, melanoma and cancers of the lung, colon, brain, ovary, breast, prostate, and kidney. The service is provided at no cost to the individual who submits their compound. Given the results of this study, the authors suggest that the NCI-60 activity spectra could be used as a standardized resource for identifying compounds that have similar mechanisms of action through a clustering approach.

In vitro Clustering

Phenoclustering is being applied in vitro with high-throughput annotation of cell morphology after exposure to known and previously undescribed bioactive molecules. For example, Tanaka and colleagues screened 107 compounds that were structurally similar in 5 separate cell lines. By looking at features such as area form factor and staining with Hoechst and alpha-tubulin they were able to identify a more potent a structural analog of PP, hydroxy-PP, which binds not only the src-family kinase Fyn but rather a completely different biomolecule, the oxidoreductase CBR1(Tanaka et al., 2005). This method could be expanded and utilized with a more diverse chemical library, and possibly more read outs to allow for in vitro phenotypic target identification.

Another in vitro clustering approach utilizes the gene responses (transcriptomic fingerprint) elicited by exposure to small molecule. Connectivity Map and Mantra are two platforms developed for mouse and human genomes(Iorio et al., 2010; Lamb et al., 2006). In short, the gene response for an unknown compound is ranked and then clustered against a database of compounds with known mechanisms of actions and the mechanism is inferred. With this new technique, it was possible to infer a new mechanism of action for the FDA approved drug Fausudil, suggesting that it could be used as a therapeutic agent to induce autophagy(Iorio et al., 2010).

In vivo clustering

Conceptually, phenoclustering has been widely used by developmental biologists for many years. Arguably, the pioneers of the "***in vivo*** phenomics" are Eric Wieschaus and Christiane Nusslein-Volhard, whose seminal contribution was, not just in identification of mutations that cause patterning defects in Drosophila embryo, but in classification the mutant loci into groups based on distinct patterning defects(Nüsslein-Volhard and Wieschaus, 1980). From drosophila to other model organisms, clustering of mutant loci resulting from large-scale mutagenesis screens based on morphologic phenotypes has become a central theme in developmental genetics. One such example of a large-scale forward genetic screen in vertebrates was the Tubingen Screen carried out at the Max-Planck Institute. Mutants were first clustered according to defects in areas such as jaw/ craniofacial development, retinal development, early arrest, pigmentation, and neural development(Haffter et al., 1996). They were then further clustered according to similarity of the defects - for example, the early arrest mutants were clustered by the timing of developmental arrest. The core logic behind such clustering is that mutations that have similar phenotypes are related by developmental pathway or mechanism. In other words, mutants that exhibited similar phenotypes were found to be caused by mutations in the same gene or in the genes in the same developmental pathway. By analogy, compounds found to cause specific phenotypes in a high content chemical genetic screen can be clustered based on distinct phenotypes, and compounds that elicit similar phenotypes presumed to target a common gene or distinct genes in a common developmental pathway.

To facilitate target identification of bioactive compounds discovered in phenotype based chemical screens, phenomic clustering will involve comparison of the small molecule-induced phenotypes to an annotation of phenotypes generated when each gene in the organism's genome is disrupted. In recent years, RNAi-based phenoclustering has been successfully used in to elucidate individual gene functions in C. elegans and Drosophila(Boulton et al., 2002; Fuchs and Boutros, 2006; Piano et al., 2002). Moreover, Sugimoto and colleagues have developed a database of RNAi knockdown phenotypes in c. elegans which can be mined for genes that exhibit the phenotype a small molecule elicits(Sugimoto, 2004). The wealth of phenome-genome data makes c. elegans a choice model for phenotypic chemical screens.

Few studies have undertaken the use of phenoclustering in vertebrate models. Kokel and colleagues recently used the zebrafish model in a high-throughput screen to identify neuroactive small molecules(Kokel and Peterson, 2011). The major hurdles to using a hierarchical clustering analysis in the context of a chemical screening are deciding the appropriate measurements that need to be made; and generating enough data points to be able to harness the full power of clustering analysis. By utilizing photomotor response (PMR), a startle response to high-intensity light, Kokel, et al. screened 14,000 small molecules(Kokel and Peterson, 2011). Simply put, this assay measured whether the zebrafish embryos moved more or less in response to light stimuli. Since a single qualitative reading, such as increased or decreased movement, is insufficient, they developed multiple quantifiable read outs. Moreover, rather than simply quantifying motion in four broad phases of PMT (Background, Latency, Excitation, and Refractory), Kokel further divided the Excitation period into three segments and the Refractory period

into two, obtaining a 14 data-point barcode for each small molecule(Kokel and Peterson, 2011).

A pilot study with several known small molecules with known neuroactivity across different mechanisms (adrenergic, dopaminergic, and serotonergic) demonstrated that, not only were the PMR profiles reproducible across days, embryos, and replicates, but the pharmacological effects mirrored that of what happens in mammalian systems. For example, isoproterenol, a psycho-stimulant, increased activity throughout PMR while apomorphine, a dopamine agonist, lengthened PMR latency. With these profiles and others in place, a large-scale screen of 14,000 compounds yielded 1,627 hit compounds that were then clustered(Kokel and Peterson, 2011). Interesting, many of the clustered hits that shared a similar activity profile also showed similar chemical scaffolding, demonstrating the strength of this approach to identify chemical motifs having similar bioactivities. The true strength of clustering utilized by this method is the potential for target identification. Of 15 compounds that exhibited a "slow-to-relax" phenotype, two, STR-1 and STR-2, were novel compounds that clustered closely with eserine, a known inhibitor acetylcholinesterase (AChE). Indeed, Kokel et al. demonstrated that STR-1 and STR-2 are novel AChE inhibitors(Kokel and Peterson, 2011). In a similar behavioral study using zebrafish, Rihel et al. used rest/wake behavior as a platform for small molecule screening. Implementing a similar behavioral fingerprint and then utilizing hierarchical clustering, they uncovered novel mechanisms involved in the regulation of rest-wake behaviors, including the role of ERG potassium channels and immunomodulators like NSAIDs(Rihel et al., 2010). Importantly, this method could facilitate target identification. For example, MRS-1220, an adenosine A3 receptor antagonist, which clustered with

monoamine oxidase (MAO) inhibiting antidepressants, was found to inhibit ***in vitro*** MAO activity with an IC_{50} of ~1 μM(Rihel et al., 2010).

Advances for in vivo phenoclustering

As an ***in vivo*** model for phenoclustering, the zebrafish has incredible potential. Among small animal models amenable to large scale chemical screens, zebrafish is the lone vertebrate, sharing the highest genetic homology to humans. Moreover, the structural, physiological and behavioral similarities permit elegant behavioral studies as described above as well as other studies that examine specific organ systems(Williams and Hong, 2011).

As for morphology-based phenoclustering, analyzing the shape of an organ in the zebrafish via standard microscopy might not yield enough quantitative data points for hierarchical clustering. Nonetheless, there are exciting emerging technologies that could overcome the limitation of morphology-based chemical screens(Sabaliauskas et al., 2006). For example, Canada and colleagues developed a system for high-throughput histology and image capture for whole mount zebrafish, as well as a program SHIRAZ, an automated histology image annotation system for zebrafish phenomics(Canada et al., 2011). The authors focused on the retina, which consists of seven easily discernable layers, and quantified for each layer various phenotypic attributes, such as absence, necrosis, disorganization, and hypotrophy(Canada et al., 2011). By utilizing this technology, it may be possible to conduct large-scale morphology-driven phenotypic small molecule screens that generate more than enough data to allow for hierarchical

clustering, and, with a trained set using known bioactive compounds, target identification as well.

Signaling pathways

In the course of the study of chemical genetics of vertebrate development the unbiased nature of screening methodology causes diversification of knowledge with projects operating on separate distinct parts of development and distinct signaling pathway. The three molecules identified and studied operate on three different pathways, *hedgehog wnt, and proton sensing.*

Hedgehog Pathway and inhibitors

The hedgehog (HH) signaling pathway was first discovered in 1980 by Nusslein-Volhard and Wieschaus and their analysis of mutations found in the fruit fly drosophila melanogaster(Nüsslein-Volhard and Wieschaus, 1980). This progressed to the identification of three orthologs of the HH ligand in vertebrates; sonic hedgehog (SHH), indian hedgehog (IHH), and desert hedgehog (DHH) in the 1990s (Echelard et al., 1993; Krauss et al., 1993; Roelink et al., 1994). These early discoveries identified the importance of this pathway as one of the major signaling pathways active during embryonic development. It was soon after this discovery that ectopic HH activity was implicated in cancer(Fan et al., 1997; Oro et al., 1997). Since these early findings, hedgehog signaling has been implicated in numerous mechanisms of cancer proliferation, propagation, and survival(Hanna and Shevde, 2016). Given the importance of this pathway in both development and disease, studies have dissected many of the components of hedgehog signaling and a concerted effort has been made in both

academia and industry to develop therapeutics targeting this pathway. In this review, we will examine the canonical components of HH signaling, the non-canonical effectors of HH signaling, and small molecule modulators that have been developed for the pathway.

Hedgehog ligand biogenesis and release

The starting point of canonical HH signaling begins with the formation of the ligand. Although there are three ligands in vertebrates SHH is the most widely expressed and well-studied. SHH exhibits a dose dependent response in the developing neural tube and understanding the morphogenic gradient is still a very active field of study. SHH is first produced as a propeptide that undergoes proteolytic cleavage to produce an N-terminal signaling fragment that concomitantly attaches a cholesterol moiety (Porter et al., 1995, 1996). Palmitoylation also occurs as a further lipid modification with the aid of the acyltransferase Skinny hedgehog/HHAT(Chamoun et al., 2001). This lipid modified SHH leaves the producing cell with the aid of both the transmembrane protein Dispatched and the secreted protein SCUBE2(Caspary et al., 2002; Hollway et al., 2006). While these critical molecules are known, the exact mode by which SHH gets to the receiving cell is still not well understood. Several models have been proposed ranging from freely diffusing soluble SHH, exosome particles and actin based cytonemes(Vyas et al., 2014; Zeng et al., 2001). How and where these mechanisms are employed will be of great interest as they may provide novel druggable targets for HH related disorders.

Hedgehog signal transduction

When HH ligand is encountered by the receiving cell it binds the receptor Patched1, with the aid of one or more accessory molecules including Boc, Cdon, and Gas1(Izzi et al., 2011). While it is not fully understood how these co receptors work, Patched, when bound, relieves the repression of Smooothened (Smo) to trigger

downstream signal transduction events. HH signaling is ultimately regulated through three transcription factors Gli1-3. This transcription factor is bound and sequestered by Suppressor of Fused (Sufu)(Kogerman et al., 1999). Furthermore, SuFu also regulates Gli protein level, and proteolytic processing into a repressor form (Chen et al., 2009b). However, SuFu is also thought to play a positive role, as loss of SuFu can also reduce Hh induction of high-threshold neural tube fates, such as floor plate(Oh et al., 2015). In vertebrates, the primary cilium is utilized for transducing HH signaling (Corbit et al., 2005). The current model places Smo becoming enriched at the cilium tip through targeting by Pitchfork and Gprasp2(Jung et al., 2016). At this time, the kinesin Kif7 and the SuFu-Gli complex translocate to the ciliary tip as well(Pedersen and Akhmanova, 2014; Tukachinsky et al., 2010). While the components of the pathway are enriched at the tip of the primary cilium it is thought that SuFu, through an as yet unidentified mechanism, dissociates from the Gli transcription factor, allowing it to become transcriptionally active. Gli2 and Gli3, when they are not active, undergo proteolytic cleavage in the cytoplasm to form a transcriptional repressor Gli2-R and Gli3-R. However, Gli1does not contain a repressor domain and can only function as an activator(Li et al., 2011; Schrader et al., 2011). Phosphorylation of Gli is a critical regulator of HH activity; the kinase CK1 promotes HH by sustaining Gli activity, GSK3B promotes Gli3 processing when sequestered by SuFu, AMPK phosphorylation of Gli1 suppresses activity, and PKA phosphorylation of Gli promotes and represses HH activity in a residue dependent manner (Kise et al., 2009; Li et al., 2015; Niewiadomski et al., 2014; Shi et al., 2014). The combinatorial activity of these three transcription factors ultimately define and control transcriptional response of target genes.

Non-canonical Hh signaling

In addition to the signaling cascade described above other signaling pathways are thought to interact with HH signaling, in one or more contexts. One such pathway is the Ras-raf-mek pathway; in pancreatic cancer ectopic Kras activity results in increased Gli activity(Ji et al., 2007; Nolan-Stevaux et al., 2009). Similarly in gastric cancer, the Ras-mek-erk pathway positively affects Gli transcriptional activity(Seto et al., 2009). Other extracellular ligands such as TGFB are also thought to control hedgehog signaling. In fibroblasts it was found that TGFB signaling through smad3 potently induced Gli-1 and Gli-2 expression(Dennler et al., 2007). In breast cancer MDA-231 cells, this HH activity functioned independently of Smo(Johnson et al., 2011). More directly it was shown that Gli2 has a SMAD3 transcriptional binding site(Dennler et al., 2007). Furthermore, studies with JQ1, an inhibitor of BRD4, a bromodomain and extraterminal (BET) family of member inhibited Gli1 expression in HH driven tumors, and revealed that BRD4 directly occupies Gli1 and Gli2 promotors(Long et al., 2014; Tang et al., 2014). Finally, PDE4D has been established as a critical regulator of Gli activity independent of SuFu (Williams et al., 2015).

Small molecules targeting the hedgehog pathway

The discovery and development of small molecule tool compounds represent an invaluable resource for researchers. Furthermore, these small molecules can potentially be developed into therapeutic agents for HH driven pathologies such as BCC, Gorlin syndrome and medulloblastoma. As described above, the HH pathway is has numerous components but can be categorized into three general categories; molecules that act on or before Smo, those that act on targets downstream of Smo, and noncanonical approaches (Figure 4).

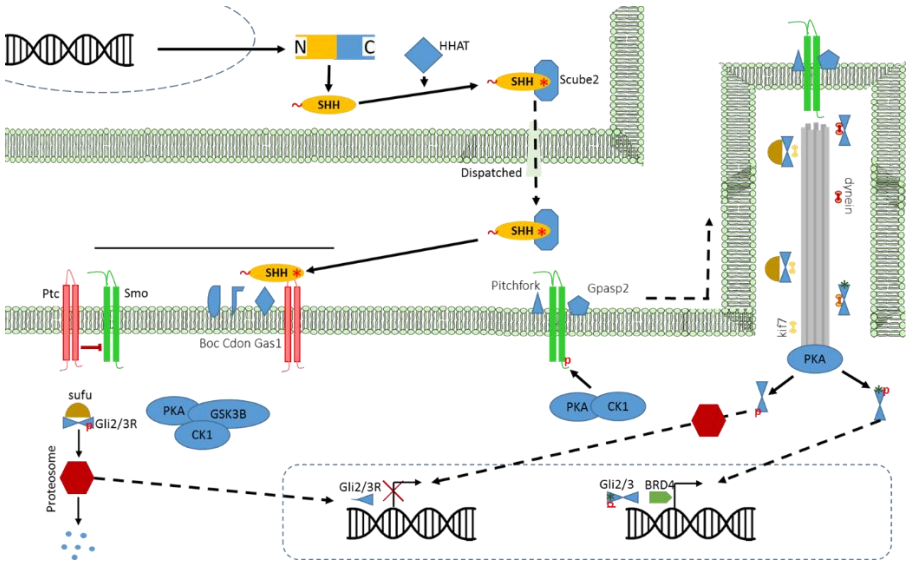

Figure 4 Schematic of Hedgehog signaling

There is currently a single inhibitor that functions upstream of Smo, Robotnikinin. This Macrocyclic molecule binds directly to the N-terminal SHH fragment and prevents the ligand from binding the receptor Patched(Stanton et al., 2009). Smo antagonists represent a large and successful body of molecules. The first HH inhibitor, still considered the status quo in research is Smo inhibitor Cyclopamine (Chen, 2016). This compound was initially discovered from its teratogenic effects on sheep grazing on *Veratrum californicum*. The use of this small molecule tool and SAG (Smo agonist) have been invaluable for determining the role of HH in numerous cancers(Chen, 2016). Subsequently, Smo antagonists have been advanced into clinical trials by several companies including Genentech (GDC-0449), Novartis (LDE225), Bristol-Meyers Squibb (BMS-833923), and Pfizer (PF-04449913). Notably GDC-0449 and LDE225 have both been FDA approved for Basal Cell Carcinoma.

While these advances with Smo inhibitors have been spectacularly successful, a number of researchers have uncovered that BCC can become refractory to Smo inhibition

at a rate of ~21% of patients (Brinkhuizen et al., 2014; Chang and Oro, 2012; Sharpe et al., 2015). Possible solutions to this and other resistances lie in targeting downstream of Smo. The number of compounds that antagonize HH down stream of Smo is limited by the number of known targets. The majority of development has centered on Gli antagonists such as GANT58 and GANT61(Lauth et al., 2007). One such Gli antagonist Arsenic Trioxide has made it into Phase IV studies for leukemia. There has also been a discovery of a series of molecular scaffolds HPI1-4 that antagonize hedgehog signaling through various mechanisms, primarily downstream of Smo(Hyman et al.). One molecule, Ciliobrevin (HPI-4), was later identified as a dynein ATPase inhibitor that targets the primary cilium which is critical for HH signaling(Firestone et al., 2012). These other inhibitors and targets of the canonical HH pathway represent possible avenues of future therapeutic development

Another option for targeting Smo inhibitor resistant cancers is to target the non-canonical pathways, for which many have inhibitors that have made it into man. It has been shown that pathways such as RAS/MAPK activate and contribute to the Smo inhibitor resistance in BCC (Zhao et al., 2015). Therefore, inhibitors like Sorafenib an FDA approved RAF inhibitor or PD0325901 (a MEK inhibitor in Phase III trials) could serve as adjuvant or therapy for resistant BCC. Further the use of LY2157299 (in Phase II), a TGF-B inhibitor could also serve to target HH driven cancers that are refractory to Smo inhibition(Perrot et al., 2013). Targeting activity of Gli indirectly with BRD4 or PDE4 inhibitors, JQ1 and Eggmanone also represent a therapeutic strategy(Stecca and Pandolfi, 2015; Williams et al., 2015).

Wnt Pathway and inhibitors

The wnt ligand was initially discovered as *wingless* in a screen of drosophila mutants in 1980 by Nusslein Volhard and Weischaus. Around the same time Int-1 was discovered as a factor that was upregulated during the oncogenic transformation caused by MMTV (Nusse and Varmus 1982). The two genes were reconciled after half a decade of research as the same gene, merging the names into Wnt-1(Rijsewijk et al 1987). Using the drosophila model, a cascade of components were determined using epistasis, resulting in the identification of porcupine, dishevelled, armadillo and zeste-white3 (Cadigan and Nusse, 1996; van den Heuvel et al., 1993; Manoukian et al., 1995; Riggleman et al., 1990; Siegfried et al., 1994). Further discoveries were made possible when mouse wnt-1 was injected into a xenopus embryo, resulting in a duplication of the primary axis (McMahon and Moon, 1989a, 1989b). This elegant and robust assay allowed researchers to identify and interrogate other components such as TCF/LEF, frizzled and LRP(Behrens et al., 1996; Bhanot et al., 1996; Merriam et al., 1997; Wehrli et al., 2000).

Although wnt was identified as having an oncogenic role in 1982 an renewed fervor for its clinical roles occurred in the early 1990s when APC (adematous polyposis coli), was identified as an oncogene driving a hereditary form of colon cancer (Nakamura et al., 1991). This protein was later found to interact with the human ortholog of armadillo, b-catenin (Rubinfeld et al., 1993). Since the time of these discoveries careful genetic, molecular and biochemical studies have elucidated where and how these and other components are orchestrated during signaling in development and disease.

Wnt ligand biogenesis and release

The starting point of canonical wnt signaling begins with the formation of the ligand. There are 19 vertebrate wnt ligands that can activate the pathway. The wnt ligand is

synthesized in the ER (endoplasmic reticulum) of the producing cell. This protein is lipid modified in a process dependent in on the ER embedded acetyltransferase Porcupine(Galli et al., 2007). In the absence of Porcupine Wnt proteins accumulate in the ER (van den Heuvel et al., 1993). This palmitolated wnt is transferred to the Golgi complex which houses the protein Wntless (Hausmann et al., 2007). Wntless complexes with the wnt ligand to facilitate its subsequent extracellular release(Herr and Basler, 2012). The Wnt ligand is associated with the protein Dlp, which facilitates binding to the Frizzled receptor(Yan et al., 2009). While these critical molecules are known, the exact mode by which Wnt gets to the receiving cell is still not well understood. Several models have been proposed ranging from freely diffusing soluble Wnt, exosome particles, actin based cytonemes and even filopodia(Gross et al., 2012; Stanganello and Scholpp, 2016; Stanganello et al., 2015). How and where these mechanisms are employed will be of great interest as they may provide novel druggable targets for wnt related disorders.

Wnt signal transduction

When wnt ligand binds to the receiving cell through the receptor Frizzled, with the aid of co receptors LRP5 and LRP6(Baig-Lewis et al., 2007; Bhanot et al., 1996). Frizzled is a 7-transmembrane receptor that share structural similarities to G-protein coupled receptors (GPCRs). Although it is not fully understood, how or whether, G proteins are essential mediators for wnt signaling it has been shown that G□q depletion can mitigate wnt signaling(Liu et al., 2005). The key event upon wnt binding of Frizzled (Fz) and LRP is the phosphorylation of LRP(Zeng et al., 2005). These phosphorylation sites, mediated through CK1 and GSK3B, recruit Dvl and Axin to LRP6 upon activation (Davidson et al., 2005; Mao et al., 2001; Wong et al., 2003; Zeng et al., 2005). While not fully understood, when DVL and axin are recruited, it relieves the repression of □-catenin (caused by the

APC destruction complex) to trigger downstream signal transduction events(Stamos and Weis, 2013).

In the absence of a Wnt stimulus, β-catenin, a structural protein and transcriptional activator for wnt signaling is degraded (Ozawa et al., 1989; Rubinfeld et al., 1993). This degradation is regulated by a multiprotein “destruction complex” consisting of Axin, APC and the kinases Casein kinase 1 (CK1) and GSK3□. These kinases sequentially phosphorylate a “degron” recognized by β-TrCP (Aberle et al., 1997; Lagna et al., 1999). β-TrCP as a consequence causes B-catenin to become proteosomally degraded, and unable to activate transcription(Aberle et al., 1997). Ultimately, the outcome of Wnt signaling results in the transactivation of genes □-catenin (Figure 5). Wnt pathway activation causes β-catenin accumulation in the nucleus, in a manner that is not well understood. Nuclear □-catenin primarily interacts with TCF/LEF family of DNA-bound transcription factors (Arce et al., 2006; Behrens et al., 1996). TCF represses transcription through the repressor Groucho. However upon β-catenin binding to TCF, transcriptional activators take the place of Groucho (Daniels and Weis, 2005) (Daniels and Weis, 2005). These transcriptional co-activators are chromatin/histone modifying proteins such as CBP/300 Histone acetyl transferases, PAF1, and BRG1(Mosimann et al., 2009; Willert and Jones, 2006).

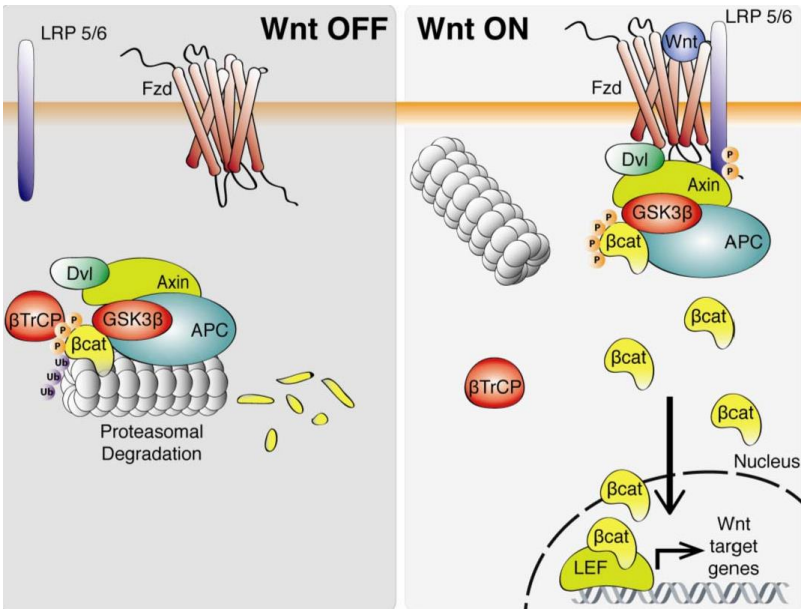

Figure 5Schematic of WNT signalling
Figure taken from "Trends in Cell Signaling Pathways in Neuronal Fate Decision", book edited by Sabine Wislet-Gendebien, ISBN 978-953-51-1059-0

Small molecules targeting the Wnt pathway

The discovery and development of small molecule tool compounds represent an invaluable resource for researchers. Furthermore, these small molecules can potentially be developed into therapeutic agents for wnt/□-catenin driven pathologies including but not limited to familial adenomatous polyposis, colon cancer, melanoma and adenocarcinoma(Bodmer, 2006; Mohammed et al., 2016; Rimm et al., 1999). Although there is excitement about potentially developing therapeutics for wnt driven pathologies, there are currently no FDA approved molecules that target Wnt signaling. As described above, the wnt pathway is has numerous components but can be categorized into three parts; Extracellular/receptor level molecules, cytoplasmic/ destruction complex level molecules, and nuclear/ CBP level molecules.

There are currently two biologics developed that target the reception of wnt ligand. The first, OMP-54F28 is a soluble form of frizzled cysteine rich domain(Le et al., 2015).

OMP-54F28 therefore binds free WNT ligand that is in the extracellular space. This biologic is in Phase I dose escalation studies for both late stage pancreatic cancer and recurrent ovarian cancer. The second is OMP-18R5 a frizzled antibody. This particular antibody although developed against Frizzled 7, interacts with Frizzled 1,2,5,and 8 as well through a shared epitope in the extracellular domain(Gurney et al., 2012). This biologic was placed on partial clinical hold during its phase 1a trial(Le et al., 2015). Additionally, the small molecule LGK974 targets WNT secretion through the inhibition of the acetyl-transferase porcupine(Liu et al., 2013a). Singaporean A*STAR (agency for science technology and research) lead Experimental Therapeutics Center used this paradigm to develop ETC-159 which is in Phase1 clinical trials.(Duraiswamy et al., 2015). While these agents have been efficacious in preclinical models of various cancers, cancers that are driven by APC, or other ligand independent mechanisms of activated wnt signaling would be refractory to the treatment.

There are 4 major mechanisms for wnt inhibition downstream of the receptor, in the cytosol. First are the DVL inhibitors, 3289-8625 and FJ9(Fujii et al., 2007; Grandy et al., 2009). Second are the Tankyrase inhibitors IWR-1 and XAV939(Chen et al., 2009a; Huang et al., 2009b). These molecules increase b-catenin degradation through stabilization of axin. This target is being developed and has a promising lead compound G007-LK for in vivo usage(Voronkov et al., 2013). The third and fourth mechanisms are CK1a agonism and CK2α antagonism. These casein kinases both regulate B-catenin activity. CK1a is allosterically activated by Pyrvinium (a previously FDA approved anti-helminthic), and CK2α is targeted by the inhibitors TBB, apigenin and CX-4945(Barua et

al., 1979; Cozza et al., 2011; Thorne et al., 2010). Notably, CX-4945 is currently in phase 1 for advanced solid tumors or multiple myeloma.

Finally, there are two mechanisms in the nucleus to block the transcriptional response to wnt signaling. The first are molecules that block b-catenin interactions, PFK115-584, CCGP049090 (Minke et al., 2009). Second are molecules that inhibit activation of translational co-activators CBP and P300 histone acetyl transferases, which are blocked by ICG-001 and windorphin respectively(Emami et al., 2004; Hao et al., 2013). Notably, ICG-001 is in clinical trials for colon cancer and leukemias.

H+ extrusion and sensing

pH sensing is an oft overlooked aspect of physiology outside the function of the stomach, kidneys, and buffering of blood. At a cellular level a large focus is placed on cytosolic pH regulation and the acidification of lysosomes. However it is becoming apparent that H+ ions are more than a byproduct mitochondrial metabolism but also serve a critical role in diseases ranging from inflammatory diseases like asthma and arthritis, to cancer and heart disease(Odunewu-Aderibigbe and Fliegel, 2014; Okajima, 2013; Webb et al., 2011). The following section will review proton extrusion mechanisms, and mechanisms that sense these protons, ASICs, TRPs and GPCRs (Figure 6).

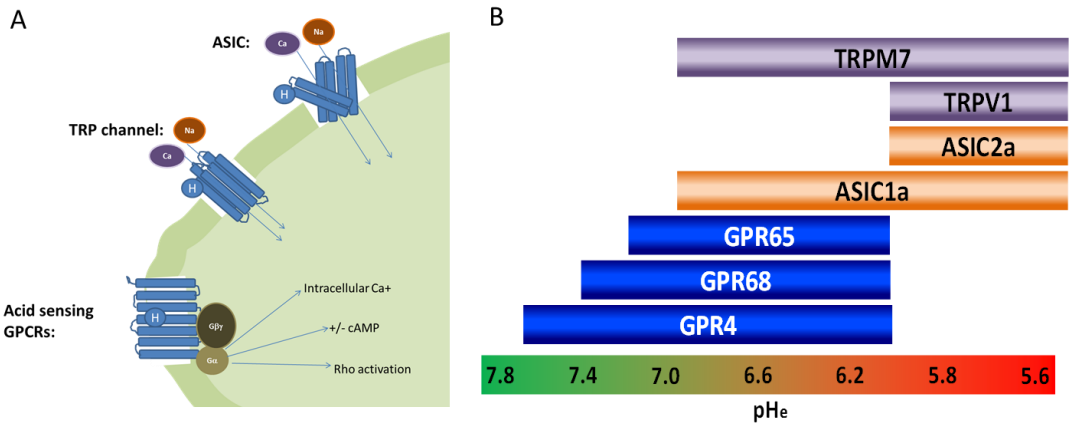

Figure 6 Proton sensing mechanisms
(A) Diagrammatic representation of GPCR TRP and ASIC activity (B) Activity ranges of TRP ASIC and GPCRs

H+ extrusion

There are 4 major ways that protons are extruded from the cell, Na^+-H^+ exchanger (NHE), H^+-K^+ ATPase, vacuolar-type H^+ ATPase (v-ATPase) and H+ channels. NHE release protons from cells across the plasma membrane through the exchange of a Na+ ions. NHE1 is a major form of this family of proteins which is ubiquitously expressed (Mattei et al., 1988). Homozygous missense mutations in NHE1 have been linked to Lichtenstein-Knorr syndrome, which is characterized by progressive ataxia and hearing loss(Guissart et al., 2015) H^+-K^+ ATPase is a hetero dimer, assembled from an alpha and Beta subunit. The pump can extrude protons against the concentration gradient by utilizing the hydrolyzation of ATP. H+-K+ ATPase is often targeted for treatment of gastroesophageal reflux and peptidic ulcers with proton pump inhibitors (PPI) such as omeprazole. However usage of PPI have been linked to dementia(Gomm et al., 2016; Trifirò et al., 2006). Vacuolar ATPase (v-ATPase) is similar to H+-K+ ATPase in utilizing ATPase to drive protons across the plasma membrane against the concentration

gradient. V-ATPase is a large 300kD+ molecular assembly that is found in the membranes of many organelles, including lysosomes and secretory vesicles.(Mazhab-Jafari and Rubinstein, 2016). Mutations in multiple components of v-ATPase have been linked to distal renal tubular acidosis (dRTA)(Karet et al., 1999; Stover et al., 2002). H+ channels are unique among the proton extrusion mechanisms as they allow the transport of protons along the concentration gradient. These voltage sensitive channels open during membrane depolarization(Cherny et al., 1995). These four mechanisms account for the majority of all proton efflux in vertebrates.

H+ sensing

There are 3 major ways that protons are sensed by the cell, acid sensing ion channels (ASICs), transient receptor potential channels (TRP channels) and acid sensing G- protein coupled receptors (GPCRs). ASICs are trimeric proteins that respond to pH ranges 4.5-6.8 and import Cations such as Ca+ and Na+(Wemmie et al., 2013). ASICs are widely expressed in both the peripheral and central nervous system(Zeng et al., 2014). The function of multiple ASIC family members have been linked to neuronal function, and health (Wemmie et al., 2013).

ASICs and TRP channels were once thought to be the only way cells sensed extracellular pH until Ludwig established the proton sensing ability of the orphan receptors GPR68 and GPR4. They belong to a family of GPCRs (G Protein Coupled Receptors) that are activated by decreasing pH_e (extracellular pH), being inactive at pH 7.4 and fully active at pH 6.8(Ludwig et al., 2003). The members of this class of receptors are GPR68 (OGR1), GPR4, GPR65 (TDAG8), and GPR132 (G2α), which share an amino acid homology (Ishii et al., 2005; Liu et al., 2010; Ludwig et al., 2003; Murakami et al., 2004; Radu et al., 2005; Saxena et al., 2012; Seuwen et al., 2006; Sun et al., 2010; Wang et

al., 2004; Yang et al., 2007). These receptors activate a wide array of different G-proteins: GPR68 stimulates G_q leading to phospholipase C activity resulting in Ca+ flux, and G_s to stimulate cAMP synthesis(Ludwig et al., 2003; Saxena et al., 2012). GPR4 activates G_s which in turn activates adenylyl cyclase causing cAMP (cyclic adenosine monophosphate) accumulation(Chen et al., 2011). It has been demonstrated that GPR65 in macrophages also activates G_s which causes cAMP accumulation and subsequent PKA (cyclic AMP activated protein kinase A) activation (Mogi et al., 2009). Finally GPR132, although it is a member of this family, has less defined pH sensing capabilities and activates RhoA through G_{a13} in response to LPA (lysophosphatidic acid).(Kabarowski et al., 2000; Murakami et al., 2004) These three mechanisms account for the majority of all proton efflux in vertebrates.

H+ sensing in development

Few studies have investigated the role of pH regulation in development. In Xenopus, intracellular acidification was found to be important for development of the posterior part of the embryo(Gutknecht et al., 1995). Conversely, intracellular alkalization was found to be necessary for the specification of anterior neural cell fates (Uzman et al., 1998). Furthermore, disruption of the H^+-V-ATPase, a proton pump, disturbed pH regionalization and craniofacial morphogenesis in Xenopus (Vandenberg et al., 2011). Finally, in both Xenopus and zebrafish, the H^+-V-ATPase plays a conserved role in establishing left-right asymmetry(Adams et al., 2006). Together these studies highlight the importance of transient proton efflux in the developing vertebrate embryo.

However, how these effluxes are translated into a cellular response is not understood. The effects of the extracellular pH are thought to be mediated through one of three mechanisms: ASICs (acid sensing ion channels), TRP (transient receptor

potential) channels, and acid sensing GPCRs (Glitsch, 2011). ASICs and TRPs share a number of similarities; both are ion channels responsive to a wide pH range are expressed mainly in nervous tissue, and are found in distant evolutionary phyla such a c. elegans(Brand et al., 2012; Xiao and Xu, 2011). Notably, proton mediated signaling has been characterized in excitatory cells. In the retina, protons have been shown to mediate lateral inhibition(Wang et al., 2014). In isolated neurons localized proton transients have been shown to activate ASICs(Zeng et al., 2015). By contrast, acid sensing GPCRs sense a narrow pH range, are widely expressed, and found only in the vertebrate lineage(Seuwen et al., 2006). Acid sensing GPCRs have been shown to function in numerous cells outside the neuronal lineage; loss of GPR4 causes wide spread vascular abnormalities, GPR68 regulates contraction in airway smooth muscle cells, a multiple family members have been shown to regulate inflammation (Okajima, 2013; Saxena et al., 2012; Yang et al., 2007). Taken together, the ability to modulate proton sensing GPCRs might represent new avenues for treatment of multiple diseases and pathologies.

CHAPTER 2

MATERIALS AND METHODS

Chemical Screen

All zebrafish experiments were approved by Vanderbilt University Institutional Animal Care and Use Committee. Chemical screen for small molecules that perturb dorsoventral axis was performed as previously described (Hao et al., 2010b, 2013; Williams et al., 2015; Yu et al., 2008). Briefly, pairs of WT zebrafish were mated, and fertilized eggs were arrayed in 96-well microtiter plates (5 embryos/well) containing 100 □l E3 water. At 4-hpf, small molecule library from Vanderbilt High Throughput Screening Facility was added to each well to the final concentration of 10□M. Embryos were incubated at 28.5C until 24 and 48-hpf, when they were examined for gross morphologic changes indicative of dorsalization of the embryonic axis. A total of 30,000 compounds were screened.

Whole-Mount Zebrafish In Situ Hybridization

In situ hybridization was performed as previously described (Westerfield, 2000). Zebrafish krox20, pax2.1, ptc1, foxd3 probes were synthesized as previously described (Concordet et al., 1996; Krauss et al., 1991; Oxtoby and Jowett, 1993; Stewart et al., 2006).

Whole Mount Immunofluorescence

Unless otherwise stated, manipulations were performed at RT. Embryos were fixed in 4% paraformaldehyde (PFA) at 4 °C overnight. Embryos were blocked with blocking solution (1x PBS, 1% BSA, 1% Triton-X100, 0.1% DMSO) for 2 hours. Embryos were incubated with primary antibodies diluted in block solution overnight at 4 °C. Embryos were washed in 1x PBS with 1% Triton-X100 for 60 min. Embryos were incubated with secondary antibodies diluted in blocking solution for 2 hours. Primary antibodies specific against Myh1/2/4/6 (F-59) were obtained from Santa Cruz (1:50 dilution). Fluorescence immunocytochemistry was performed using anti-mouse secondary antibody Alexa 488 (1:500 dilution, Invitrogen).

Alcian Blue staining

Staged embryos and larvae were anesthetized with Tricaine and killed by immersion in 4% formaldehyde (prepared from paraformaldehyde, and buffered to pH 7 in phosphate-buffered saline (PBS)). The fixed animals were rinsed in acid–alcohol (0.37% HCl, 70% EtOH), and stained overnight in Alcian blue (Schilling et al.,1996a) After differentiation in several changes of acid–alcohol the preparations were rehydrated. Following rinsing and clearing in a solution of 50% glycerol and 0.25% KOH, the cartilages were visualized under a stereo microscope.

Zebrafish Injections

Plasmid encoding dnCK2α was a kind gift from Isabel Dominguez(Dominguez et al., 2004). RNA was synthesized as previously described(Dominguez et al., 2004). OGR1 morpholino 5'-TTTTTCCAACCACATGTTCAGAGTC-3' was synthesized by Genetools. Morpholino and mRNA was injected as previously described(Westerfield, 2000)

Cell Culture and Transfection

STF293, HEK293, Hela, DU145, and RKO cells were cultured in DMEM supplemented with 10% FBS (GIBCO) and 1% penicillin-streptomycin (Cellgro). SW480 cells were cultured in RPMI supplemented with 10% FBS (GIBCO) and 1% penicillin-streptomycin (Cellgro). HCT116 cells were cultured in DMEM/F12 supplemented with 10% FBS (GIBCO) and 1% penicillin-streptomycin (Cellgro).

Luciferase Reporter Assays

For WNT/b-catenin signaling assay, STF293 cells (HEK293 cells stably transfected with TOPFLASH (TCF/LEF1-optimized promoter)-firefly luciferase reporter) (Thorne et al., 2010) were seeded in 96-well plates, and incubated overnight with the various concentrations of compound and WNT3a-conditioned media (made according to directions in the American Type Culture Collection website). The cells were then lysed, and cell extracts were subjected to Steady-Glo luciferase assay (Promega) according to manufacturer's instructions. The results were normalized to cell titer, as determined using Cell Titer-Glo luminescence assay (Promega)

Western Blotting

Cells were lysed in CelLytic cell lysis buffer (Sigma) or M-PER lysis buffer (Thermo Scientific) supplemented with protease inhibitor cocktail (Sigma) and phosphatase inhibitor cocktail 2 (Sigma). Cell lysate was resolved in SDS-PAGE and transferred onto PVDF membrane. The b-catenin, and alpha-tubulin were detected by Odyssey system (Li-Cor bioscience) after incubation with the appropriate primary and secondary antibodies. Primary antibodies used include mouse anti-active b-catenin (Millipore), rabbit anti-pan b-catenin (Santa Cruz), rabbit anti-phospho-S370 PTEN (Abcam), rabbit anti-

cleaved caspase 3(Cell Signaling technology), mouse anti-□ tubulin (Santa Cruz) goat anti-Gli2 and goat anti-Gli3 (R & D Systems); rabbit antip-T197-PKA-C, (Cell Signaling technology), rabbit anti-Lamin-A/C (Cell Signaling technology). The secondary antibodies used include IRDye 680-conjugated goat anti-rabbit IgG (Li-Cor Bioscience, 1:5000 dilution).

Immunostaining of β-catenin translocation

Human colon carcinoma RKO cells were treated with 20μM windorphen in the presence or absence of Wnt3a for 24 hours. The cells were fixed in 4% paraformaldehyde and blocked in PBS-Tween-BSA (0.2% Tween 20 and 1mg/ml BSA in PBS) overnight at 4°C. The cells were then incubated with mouse anti-active-beta catenin antibody (Millipore Clone 8E7) for 4 hours at room temperature. After three times of wash with PBS, the cells were then incubated with the secondary anti-mouse Alexa-594 antibody (Cell Signaling) for two hours, and DAPI was used to nucleus counterstaining.

Immunostaining of PKA phosphorylation and Gli2 ciliary translocation

NIH3T3 cells were plated on poly-D-lysine-coated glass coverslips and were cultured at 37 °C, 5% CO2 in DMEM medium containing 10% fetal bovine serum until reaching 75% confluency, at which time the culture medium was switch to 0.5% serum for cilia formation. Cells were treated with 20 nM SAG in the presence or absence of 5 μM eggmanone. Untreated cells were used as a control. After overnight incubation, cells were washed with PBS, fixed for 10 min. in 4% PFA, permeabilized 20 min. at –20 °C with cold methanol, blocked with PBS/1% BSA, and incubated with primary antibodies: anti-phosphoThr197PKA catalytic domain (Cell Signaling, Danvers, MA), Arl13b (Tamara Caspary), anti-γ tubulin (Sigma Aldrich, St. Louis, MO), anti-IFT88 (Proteintech, Chicago,

IL) and/ or anti-Gli2 (Jonathan Eggenschwiler, Univ. of Georgia). Cells stained for IFT88 required acetone permeabilization in lieu of methanol. For co-IF of p-PKA and Arl13b, an additional overnight blocking step using unconjugated rabbit IgG was required between primary antibody incubations since both antibodies were produced in rabbit. Fluorescent conjugated secondary antibodies were used for visualization.

Cancer Cell Viability Assay

The following cancer cell lines were seeded into 96-well plates and incubated overnight: Hela, SW480, RKO, DU145 and HCT116. The following day, media was replaced with media containing incaskin/ eggmanone at varying concentrations. Cells were incubated for an additional 72 hr., at which time CellTiter Blue (Promega) was added to each well as per manufacturer's recommendations. After 3 hr. of incubation, plates were read in a Modulus microplate reader (Promega) at 590nm and cell titer results were normalized to wells containing cells without incaskin compound.

RT-PCR

NIH3T3 cells were stimulated with 3 μM purmorphamine in the presence of eggmanone or DMSO for 24 hours. Sufu-/- cells were treated for 24 hours. Cells were collected and RNA isolated with the RNeasy kit (Qiagen, Valencia, CA). After subsequent cDNA amplification using Superscript III (Invitrogen, Carlsbad, CA), samples were quantified by comparing Q-PCR cycle thresholds (Ct) for gene expression normalized to GAPDH. The following TaqMan probe and primer sets (Applied Biosystems) were used: GAPDH (Mm99999915_g1), Gli1 (Mm00494646_g1) and Ptc1 (Mm01306905_m1). Melanoma and hiPSC-NCC cells we collected and RNA isolated with the RNeasy kit (Qiagen, Valencia, CA). After subsequent cDNA amplification using Superscript III

(Invitrogen, Carlsbad, CA), samples were quantified by comparing Q-PCR cycle thresholds (Ct) for gene expression normalized to GAPDH. Zebrafish embryos were raised, staged and collected according to standard conditions, and trizol-chloroform extraction was performed to isolate RNA(Westerfield, 2000). After subsequent cDNA amplification using Superscript III (Invitrogen, Carlsbad, CA), samples were quantified by comparing Q-PCR cycle thresholds (Ct) for gene expression normalized to actb1. Primer sequences found below:

GPR4	qDreCED0009735	15:28172077-2817222
GPR65	qDreCID0014173	17:2589919-2594987
GPR68	qDreCED0006683	17:38892083-38892229
GPR132-1	qDreCED0007674	17:39927946-39928094
GPR132-2	qDreCED0021794	20:18408237-18408372
GPR132-3	qDreCID0022336	15:12244897-12268724
actb	qDreCED0020462	1:7727158-7728668

GPR4	CCCTCCTGTCATAATTCCATCC	TGGTCTACAGGGAAGAGATGAG
GPR65	TGGCTGTTGTCTACCCTTTG	CCACAACATGACAGCATTGAAG
GPR68	GTTTGAAGGCGGCAGAAATG	GTGGAATGAGGAGGCATGAA
GPR132	TTCAGGAGCATCAAGCAGAG	CGAAGCAGACTAGGAAGATGAC
GAPDH	GTTTGAAGGCGGCAGAAATG	GTGGAATGAGGAGGCATGAA
ITGB3	GGACACAGCCAACAACCCAC	AGGAGGCATTCTGGGACAAAG

CCND1	CCGTCCATGCGGAAGATC	GAAGACCTCCTCCTCGCACT
CD44	CACGTGGAATACACCTGCAA	GACAAGTTTTGGTGGCACG
ZEB2	GAAAGTGGCATGTATGCATGTGA	CGATAAGGTGGTGTTTGTGTTTG
SNAIL2	ATTGCCTTGTGTCTGCAAGATCT	TCTGTCTGCAAAAGCCCTATTG
MMP2	GGCCCTGTCACTCCTGAGAT	GGCATCCAGGTTATGGGGGA
MMP9	TTGACAGCGACAAGAAGTGG	GCCATTCACGTCGTCCTTAT
N-cadherin	CACTGCTCAGGACCCAGAT	TAAGCCGAGTGATGGTCC

PDE Assays

Assays were performed by Caliper Life Science (Hopkinton, MA). Reactions were carried out in 100 mM HEPES, pH 7.5, 5 mM MgCl2, 1 mM DTT, 0.0015% Brij-35, with 20 pM PDE enzyme and 1.0 µM cAMP substrate. Twelve compound concentrations were screened for each assay in duplicate. To 1 µL of 100X compound in 100% DMSO was added a 2X solution of enzyme in 49.5 µL and the mixture was incubated for 10 minutes (final DMSO concentration was 1%). To the mixture was added 49.5 µL of 2X cAMP substrate, and the reaction was incubated at R.T. for one hour. The reaction was stopped by addition of a solution consisting of 100 mM HEPES pH 7.5, 24 mM EDTA, 0.015% Brij-35, and 5% DMSO and read on LabChip® EZ Reader. Cyclic AMP substrate and 5'-AMP product are separated by charge using electrophoretic mobility shift and product formed is compared to control wells to determine inhibition. Results were analyzed with GraphPad and fit to non-linear regression with variable slope.

Target Profiling Assays for Kinases, GPCRs and Phosphatases

Kinase profiling assays were performed by DiscoverRx (San Diego, CA) using a phage display model. GPCR profiling assays were performed by Millipore (St. Louis, MO) using in cells expressing Gα15, a promiscuous G protein that enhances GPCR coupling to downstream Ca2+ signaling pathways. Phosphatase profiling assay was performed by Millipore (Dundee, UK)

Generation of Zepac clustering method

Data on Phenotype of zebrafish genes was downloaded from ZFIN.org. Phenotypes seen within the first 48 hours were then curated. And multiple descriptors for each anatomical feature per gene were concatenated. Genes with no noted phenotype for anatomical features were imputed as normal. This database was then converted into nominal values of 0 = normal or 1 = abnormal or into levenshtein distances in Excel. The database was then imported into Orange and open source data mining software. For nominal clustering Jaccard similarity index was used, for levenshtein values phenotypic changes were viewed as vectors with distance and therefore Euclidean distance was used.

VBA script for levenshtein calculation in excel

```
Public Function WeightedDL(source As String, target As String) As Double

    Dim deleteCost As Double
    Dim insertCost As Double
    Dim replaceCost As Double
    Dim swapCost As Double

    deleteCost = 1
```

```
insertCost = 1.1
replaceCost = 1.1
swapCost = 1.2

Dim i As Integer
Dim j As Integer
Dim k As Integer

If Len(source) = 0 Then
   WeightedDL = Len(target) * insertCost
   Exit Function
End If

If Len(target) = 0 Then
   WeightedDL = Len(source) * deleteCost
   Exit Function
End If

Dim table() As Double
ReDim table(Len(source), Len(target))

Dim sourceIndexByCharacter() As Variant
ReDim sourceIndexByCharacter(0 To 1, 0 To Len(source) - 1) As Variant

If Left(source, 1) <> Left(target, 1) Then
   table(0, 0) = Application.Min(replaceCost, (deleteCost + insertCost))
End If

sourceIndexByCharacter(0, 0) = Left(source, 1)
sourceIndexByCharacter(1, 0) = 0

Dim deleteDistance As Double
Dim insertDistance As Double
Dim matchDistance As Double
```

```
For i = 1 To Len(source) - 1

   deleteDistance = table(i - 1, 0) + deleteCost
   insertDistance = ((i + 1) * deleteCost) + insertCost

   If Mid(source, i + 1, 1) = Left(target, 1) Then
      matchDistance = (i * deleteCost) + 0
   Else
      matchDistance = (i * deleteCost) + replaceCost
   End If

   table(i, 0) = Application.Min(Application.Min(deleteDistance, insertDistance), matchDistance)
Next

For j = 1 To Len(target) - 1

   deleteDistance = table(0, j - 1) + insertCost
   insertDistance = ((j + 1) * insertCost) + deleteCost

   If Left(source, 1) = Mid(target, j + 1, 1) Then
      matchDistance = (j * insertCost) + 0
   Else
      matchDistance = (j * insertCost) + replaceCost
   End If

   table(0, j) = Application.Min(Application.Min(deleteDistance, insertDistance), matchDistance)
Next

For i = 1 To Len(source) - 1

   Dim maxSourceLetterMatchIndex As Integer

   If Mid(source, i + 1, 1) = Left(target, 1) Then
      maxSourceLetterMatchIndex = 0
   Else
```

```
    maxSourceLetterMatchIndex = -1
End If

For j = 1 To Len(target) - 1

    Dim candidateSwapIndex As Integer
    candidateSwapIndex = -1

    For k = 0 To UBound(sourceIndexByCharacter, 2)
        If sourceIndexByCharacter(0, k) = Mid(target, j + 1, 1) Then candidateSwapIndex = sourceIndexByCharacter(1, k)
    Next

    Dim jSwap As Integer
    jSwap = maxSourceLetterMatchIndex

    deleteDistance = table(i - 1, j) + deleteCost
    insertDistance = table(i, j - 1) + insertCost
    matchDistance = table(i - 1, j - 1)

    If Mid(source, i + 1, 1) <> Mid(target, j + 1, 1) Then
        matchDistance = matchDistance + replaceCost
    Else
        maxSourceLetterMatchIndex = j
    End If

    Dim swapDistance As Double

    If candidateSwapIndex <> -1 And jSwap <> -1 Then

        Dim iSwap As Integer
        iSwap = candidateSwapIndex

        Dim preSwapCost
        If iSwap = 0 And jSwap = 0 Then
            preSwapCost = 0
```

```
            Else
                preSwapCost = table(Application.Max(0, iSwap - 1), Application.Max(0, jSwap - 1))
            End If

            swapDistance = preSwapCost + ((i - iSwap - 1) * deleteCost) + ((j - jSwap - 1) * insertCost) + swapCost

        Else
            swapDistance = 500
        End If

        table(i, j) = Application.Min(Application.Min(Application.Min(deleteDistance, insertDistance), matchDistance), swapDistance)

    Next

    sourceIndexByCharacter(0, i) = Mid(source, i + 1, 1)
    sourceIndexByCharacter(1, i) = i

Next

WeightedDL = table(Len(source) - 1, Len(target) - 1)
End Function
```

Jaccard similarity calculation

$$J(A,B) = \frac{|A \cap B|}{|A \cup B|}.$$

Euclidean distance calculation

$$\begin{aligned} \mathrm{d}(\mathbf{p}, \mathbf{q}) = \mathrm{d}(\mathbf{q}, \mathbf{p}) &= \sqrt{(q_1 - p_1)^2 + (q_2 - p_2)^2 + \cdots + (q_n - p_n)^2} \\ &= \sqrt{\sum_{i=1}^{n} (q_i - p_i)^2}. \end{aligned}$$

Library preparation and RNA-sequencing

RNA samples were submitted to the Vanderbilt VANTAGE core for RNA-seq. RNA quality was determined using the 2100 Bioanalyzer (Agilent Technologies; Santa Clara, CA). The RNA integrity number (RIN) of each sample was 10. Libraries were prepared using the TruSeq RNA Sample Prep Kit (Illumina; San Diego, CA) to enrich for poly(A)-containing mRNA and generate cDNA. Library quality was also confirmed using the 2100 Bioanalyzer. The libraries were sequenced using a 150 bp paired read protocol on the Illumina HiSeq 2500 (Illumina).

Sequence alignment, differential expression and pathway analysis

Sequence alignment and differential expression were performed using GALAXY server. TopHat was used to align paired sequence reads to the UCSC human reference genome hg19 using default parameters, and differential expression was calculated using cuffdiff. Comparisons were made between vehicle- and OGM treated WM115 cells. Pathway analysis was done using Database for Annotation, Visualization and Integrated Discovery (DAVID) v6.8(Huang et al., 2009a).

Chemical synthesis

The following syntheses were carried out by Vanderbilt Synthesis Core:

Synthesis of GPR68 antagonist.

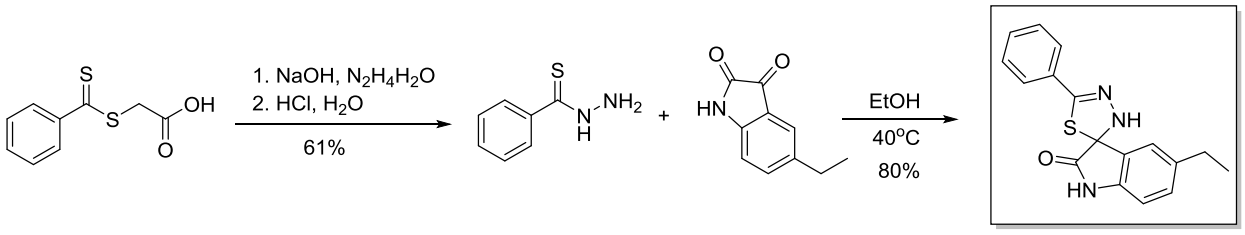

Benzothiohydrazide. To a solution of 2-((phenylcarbonothioyl)thio)acetic acid (3.0 g, 14.13 mmol) in NaOH solution (10 M, 30 mL) was added hydrazine (1.11 mL, 35.33 mmol)

at 0 ºC. The reaction mixture was stirred for 5 hr. at room temperature, acidified to pH 5 using 2*N* HCl then chilled on ice. A white solid was filtered and recrystallized from tepid water to afford the title compound as white crystals (1.30 g, 61 %).

5-ethyl-5'-phenyl-3'H-spiro[indoline-3,2'-[1,3,4]thiadiazol]-2-one.

Benzothiohydrazide (0.7 g, 4.6 mmol) and 5-ethylindoline-2, 3-dione (0.89 g, 5.05 mmol) were dissolved in ethanol (9 mL). The reaction mixture was heated at 40 ºC for 2 hr. and cooled to room temperature. The precipitate was filtered, washed with ethanol, and recrystallized from methanol to afford the spiro compound as yellow solid (1.36 g, 95 %).

Eggmanone Synthesis

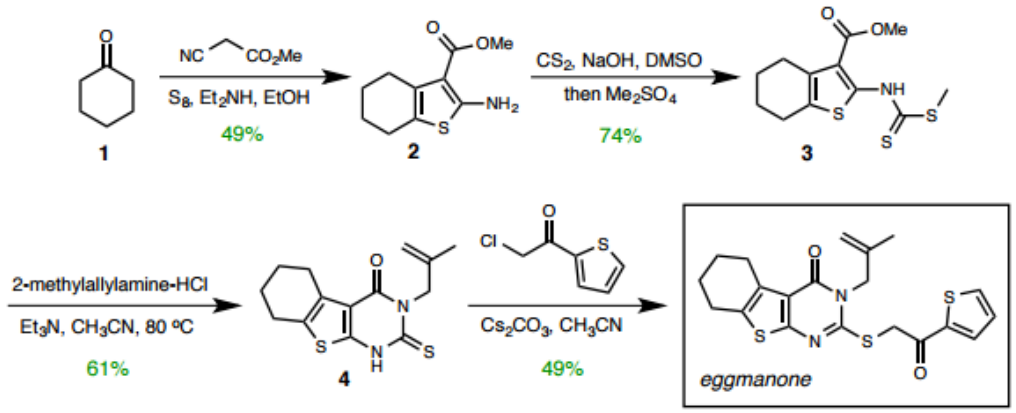

Eggmanone was synthesized starting from commercially available cyclohexanone. Elaboration of cyclohexanone utilizing the Gewald protocol provided the 2-aminothiophene after stirring at RT overnight, which was reacted with CS2 followed by dimethylsulfate to give the dithiocarbamate (Fondjo, et al., 2006; Alagarsamy, et al.,

2006). Cyclization to the 2-thioxo-2,3- dihydrothienopyrimidinone was realized with 2-methylallylamine•HCl and triethylamine in acetonitrile at 80 °C overnight (Ivachtchenko, et al., 2004). Finally, S-alkylation with 2- (chloroacetyl)thiophene provided eggmanone after stirring at RT for 4 hours.

CHAPTER 3

EGGMANONE

Introduction

Hedgehog (Hh) signaling represents an important therapeutic target for the treatment of cancer. While its signal transduction and resulting downstream gene transcription are essential to vertebrate embryonic patterning and development, aberrant Hh signaling is responsible for a variety of malignancies including basal cell carcinoma (BCC), medulloblastoma, small cell lung cancer, and pancreatic cancer(Kar et al., 2012; Ng and Curran, 2011). Classical Hh signaling requires the presence of the extracellular ligand Sonic hedgehog (Shh), which upon binding to the transmembrane receptor Patched (Ptc) causes Ptc to remove its inhibitory influence on the G protein-coupled receptor Smoothened (Smo) (Ryan and Chiang, 2012). Activation of Smo then leads to nuclear translocation of the Gli family of transcription factors and induction of Hh target gene transcription. In the absence of the hedgehog family of ligands, Gli2 and Gli3 are processed to their repressor forms leading to transcriptional inhibition. Many details regarding signal transduction between Smo activation and Gli-mediated gene transcription remain unclear.

A wide array of small molecules that target Smo, including the canonical Hh inhibitor cyclopamine, have been shown to mediate tumor progression (Carney and Ingham, 2013; Taipale et al., 2000). Additionally, the Smo antagonist vismodegib is approved by the United States Food and Drug Administration for the treatment for

advanced BCC (Robarge et al., 2009; Von Hoff et al., 2009). However, downstream-of-Smo oncogenic mutations and acquired resistance due to Smo binding pocket mutations have limited the efficacy of this and other clinically promising therapeutics (Yauch et al., 2009). Therefore, the identification of novel downstream Hh signaling mediators could represent a new therapeutic opportunity for Hh-dependent malignancies.

Results

Discovery of eggmanone, a novel small molecule hedgehog inhibitor, from an in vivo chemical genetic screen

A screen of approximately 30,000 small molecules for their ability to effect alterations in embryonic zebrafish dorsoventral patterning identified a series of structurally related compounds represented by the prototype termed eggmanone (Figures 7A). Eggmanone reliably and selectively reproduced the zebrafish Hh-null phenotype with features ranging from ventral tail curvature, small eyes, loss of pectoral fins and enlarged, rounded somites to loss of neurocranial chondrogenesis and impaired slow muscle formation (Figures 7B-7D) (Barresi et al., 2000; van Eeden et al., 1996a, 1996b; Hirsinger et al., 2004; Wada et al., 2005). Consistent with loss of Hh signaling, we confirmed abrogation of the Hh-target gene *Patched* (*Ptc*)*-1* expression in bud-stage adaxial cells, pectoral fin fields, and the somites resulting from eggmanone treatment (Figures 7E and 7F).

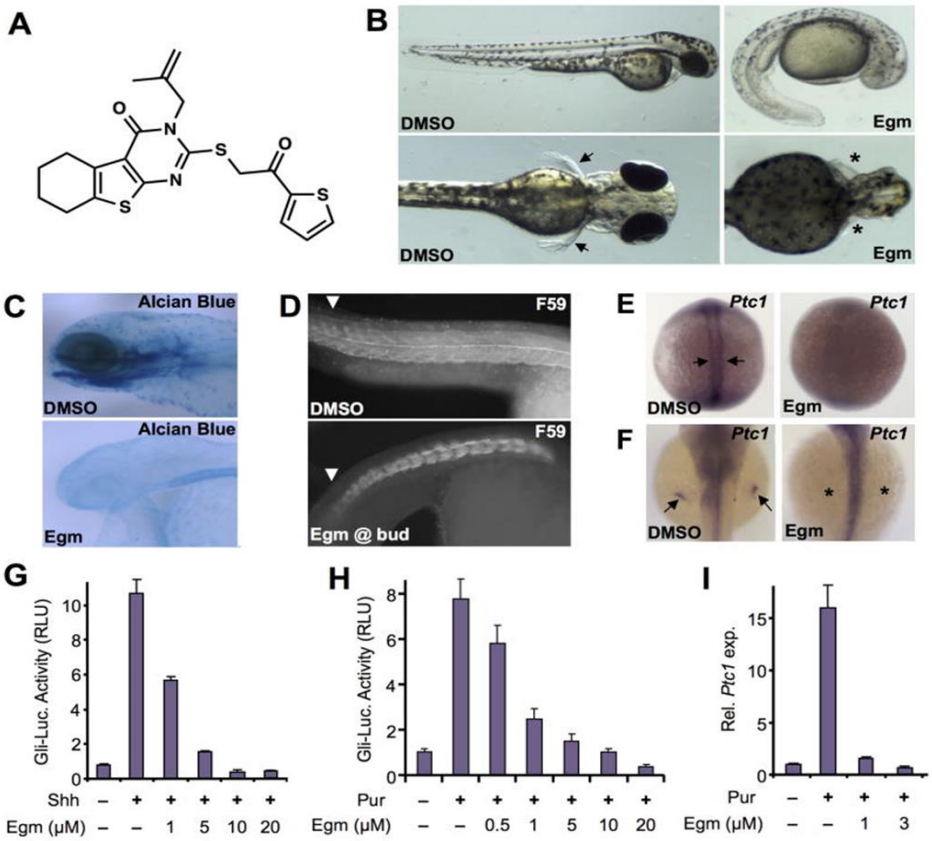

Figure 7 Eggmanone affects embryonic zebrafish patterning through inhibition of Hedgehog signaling

(A) Chemical structure of eggmanone (Egm), (3-(2-methylallyl)-2-((2-oxo-2-(thiophen-2-yl)ethyl)thio)-5,6,7,8-tetrahydrobenzo[4,5]thieno[2,3-d]pyrimidine-4(3H)-one). (B) Zebrafish embryos treated with 2 μM Egm starting at 4-hours post fertilization (hpf) exhibited a range of phenotypes found in Hh pathway mutants, including ventral tail curvature, loss of pectoral fins, and smaller eyes. (C) Alcian blue staining following 2 μM Egm treatment at 4-hpf revealed altered craniofacial development including the jaw. (D) Trunk slow muscles immunostained with anti-MyHC antibody (F59) showed altered slow muscle formation upon Egm treatment (2 μM). (E) Egm treatment (1 μM) abolished Hh-responsive Ptc1 expression in adaxial cells at 12 hpf (arrows). (F) Egm treatment (1 μM) ablated Hh-responsive Ptc1 expression in the pectoral fin bud at 48-hpf (arrows and asterisks). (G) Egm inhibited Sonic hedgehog (Shh)-responsive Gli-luciferase (Gli-Luc) reporter activity in a dose-dependent manner when stimulated with Shh conditioned medium (n = 4 for each condition, results represented as mean relative luciferase units (RLU) ± standard error of the mean (SEM); p-value <0.0184, starting at 1 μM). (H) Egm inhibited purmorphamine-induced (3 μM) Gli-Luc reporter activity in a dose-dependent manner (mean ± SEM, n = 4 for each condition; p-value <0.0054, starting at 0.5 μM). (I) Egm inhibited purmorphamine-induced (3 μM) Ptc1 expression in NIH3T3 fibroblasts (mean ± SEM, n = 3, expression normalized to GAPDH, p-value <0.003, starting at 1 μM).

Given that eggmanone elicited a loss-of-Hh phenotype in zebrafish, we tested its ability to directly affect Hh signaling in the mouse Hh reporter cell line Shh-Light2 (Taipale et al., 2000). Eggmanone inhibited Hh-inducible Gli-responsive luciferase (Gli-Luc) activity in a

dose-dependent manner when stimulated with the exogenous ligand Shh (Figure 7G). In contrast, cells transiently overexpressing Gli2 retained their Gli-Luc activity following eggmanone treatment (Figure 8D). Moreover, luciferase reporter assays for other key signaling pathways, such as BMP, were negative (Figure 8E). Taken together, our results indicate that eggmanone's pharmacological target lay specifically in the Hh pathway upstream of Gli.

Eggmanone exerts its Hh-inhibitory effects downstream of Smo

Since most Hh inhibitors act through Smo, we examined eggmanone's effects at the level of Smo signaling. Specifically, eggmanone retained its Hh-inhibitory activity when Shh-Light2 cells were stimulated with the Smo-agonist purmorphamine, blocking both Gli-Luc activity and *Ptc1* expression (Figures 7H and 7I) (Sinha and Chen, 2006). Importantly, eggmanone failed to compete for Smo binding with BODIPY-cyclopamine when HEK293 cells overexpressing Smo were pre-treated with 5 nM of the fluorescent ligand followed by treatment with concentrations of eggmanone up to 10 μM (Figure 8F) (Chen et al., 2002). Therefore, these results confirmed that eggmanone targeted the Hh pathway downstream of Smo, and taken in concert with our previous findings, we demonstrated that eggmanone acts between Smo and Gli-mediated transcription to block Hh signaling.

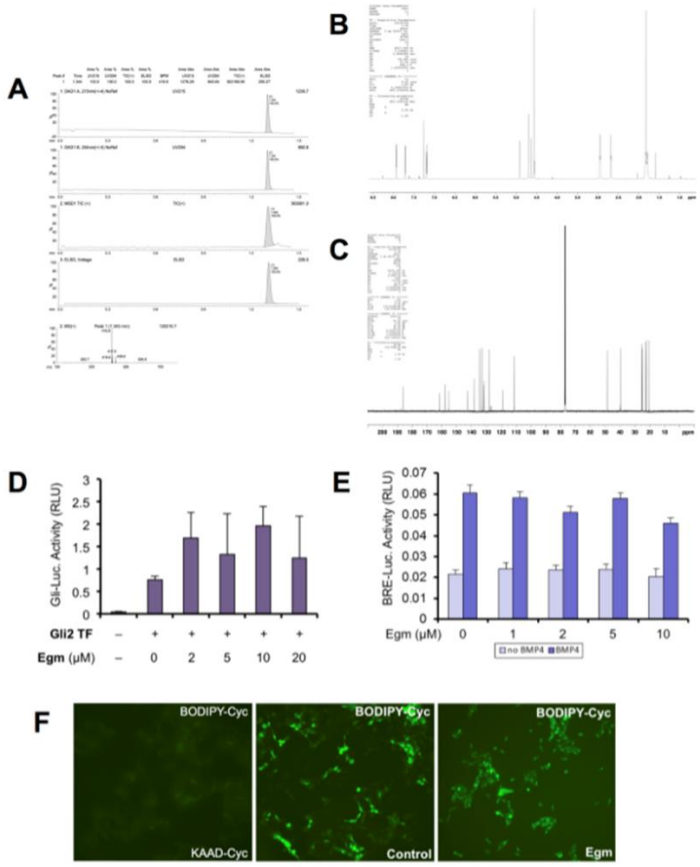

Figure 8 Eggmanone acts within the Hedgehog pathway, downstream of Smoothened and upstream of Gli transcription.

(A) Liquid chromatography/mass spectrometry analysis confirmed the purity of synthesized eggmanone. LCMS, single peak, UV=215 nm, RT=1.344 min, 100.0%, m/z = 416.6 [M+1]. (B)1H NMR (600 MHz, CDCl3): δ 7.93 (dd, J = 3.7, 0.8 Hz, 1H), 7.72 (dd, J = 4.9, 0.9 Hz, 1H), 7.19(dd, J = 4.8, 3.9 Hz, 1H), 4.92 (s, 1H), 4.70 (s, 2H), 4.63 (s, 1H), 4.56 (s, 2H), 2.95 (dd, J = 6.2, 5.9 Hz, 2H), 2.69 (dddd, J = 6.1, 6.0, 1.9, 1.5 Hz, 2H), 1.87-1.76 (m, 4H), 1.82 (s, 3H). (C) 13CNMR (150 MHz, CDCl3): δ 186.2, 161.4, 158.0, 155.2, 142.8, 138.2, 134.5, 133.0, 131.8, 131.5, 128.2, 118.7, 111.1, 48.5, 39.4, 25.4, 25.1, 22.9, 22.2, 20.3. (D) Egm showed no significant effect on Gli-luciferase reporter activity under Gli2 overexpression conditions. Values reported as mean relative luminescence units (RLU) ± standard error of the mean (SEM). (E) Egm had no significant effects on BMP4-responsive reporter (BRE-Luc) activity in C2C12BRA reporter cells. BRE-Luc (BMP responsive element-driven luciferase) cells were stimulated with 50 ng/mL BMP4 ligand. Values reported as mean RLU ± SEM. (F) Egm (10 μM) did not compete with BODIPY-cyclopamine (5 nM) for Smo binding, in contrast to KAAD-cyclopamine (200 nM), which effectively competed with BODIPY-cyclopamine (5 nM) for Smo binding in cells transiently overexpressing Smo. Scale bar 10 μm.

To rule out its action at alternative Smo binding sites, we investigated eggmanone's ability to inhibit Hh signaling in Sufu−/− mouse embryonic fibroblasts (MEFs), which display constitutively active signaling downstream of Ptc and Smo (Chen et al., 2009; Lin et al., 2014). Specifically, eggmanone significantly reduced transcription levels of Gli1 and Ptc1, whereas, as expected, the Smo antagonist cyclopamine showed no inhibition (Figure 9A). Thus, taken in concert with our previous findings, eggmanone acts between Smo and Gli-mediated transcription to block Hh signaling.

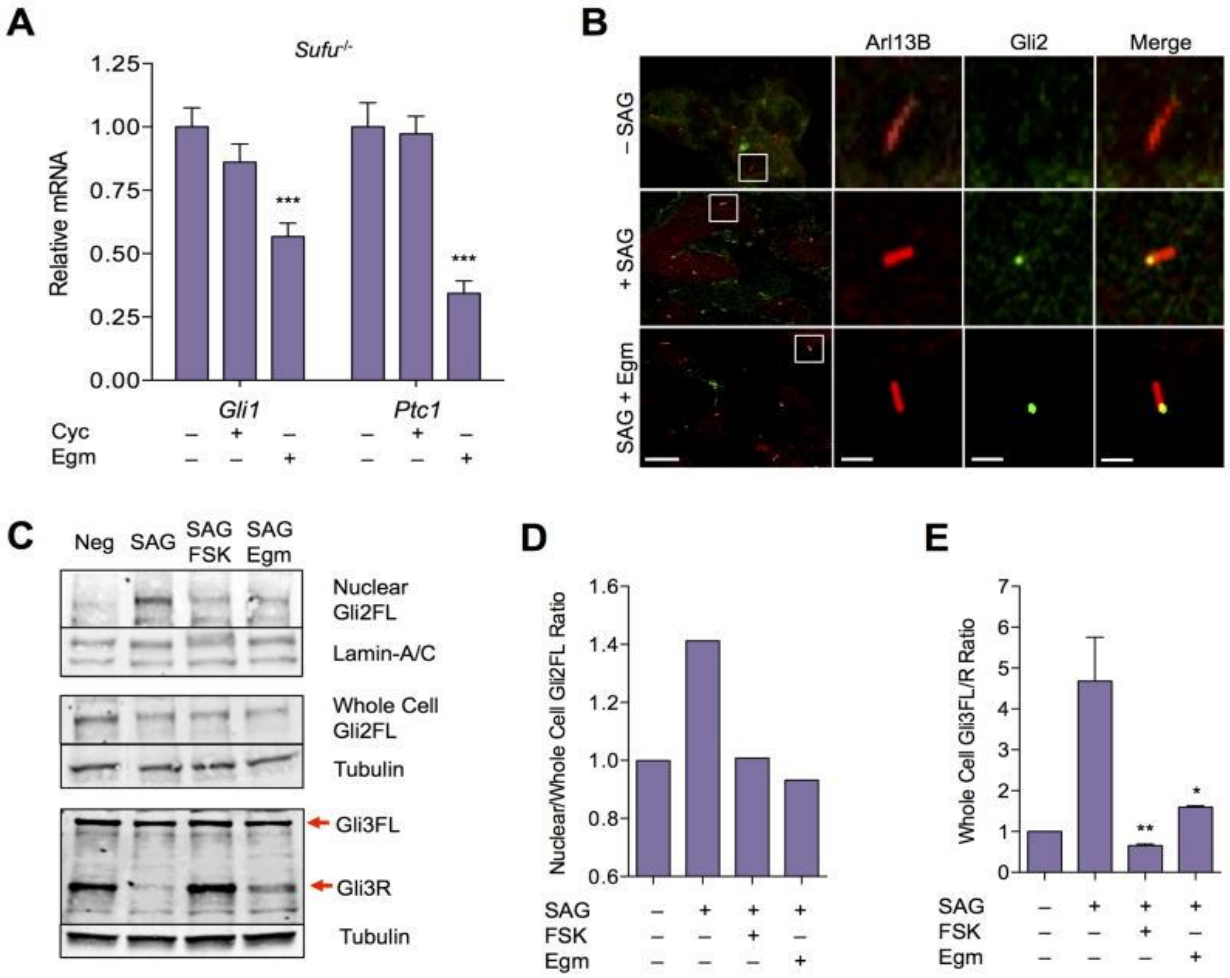

Figure 9 Eggmanone alters the activity of Gli transcription factors

*(A) Quantitation of mRNA transcripts of Gli1 and Ptc1 in Sufu−/− cells when treated with 10 μM Cyc (mean ± SEM, n = 7, not significant) or 10 μM Egm (mean ± SEM, n = 10, *** = <0.0001), expression normalized to GAPDH. (B) Immunostaining for the cilium marker Arl13b (red) and Gli2 (green) of unstimulated MEFs (top), MEFs stimulated with SAG (20 nM) in the presence of DMSO control (middle) or 5 μM Egm (bottom). Co-localization of Gli2 (yellow) in the primary cilium remained unchanged in Egm treated MEFs. Representative cilium (white box) magnified to the right, scale bar of left column 10 μm; columns 2–4 scale bar 0.2 μm. (C) Representative western blot for full length Gli2 in nuclear (top, n = 4) and whole cell (middle, n = 2) fractions of NIH3T3 cells. Western blot of Gli3 (bottom, n = 3) from whole cell lysate of C3H10T1/2 cells. Neg, unstimulated. SAG, stimulated with SAG (100 nM) for 1.5 hours (Gli2) or 24 hours (Gli3). SAG+FSK, co-treated with SAG and FSK (30 μM). SAG+Egm, co-treated with SAG and Egm (10 μM). Corresponding western blots for nuclear Lamin-A/C and whole cell α-tubulin as loading controls. FL, full-length, active forms of Gli2 and Gli3. R, repressor form of Gli3. (D) Quantitative analysis of the mean ratio of normalized nuclear full length Gli2 to normalized whole cell Gli2 from (C). (E) Quantitative analysis of the ratio of full length to repressor form of Gli3 from (C) (mean ± SEM, n = 3 for each condition; ** = 0.0095; * = 0.028, vs. SAG).*

Eggmanone differentially affects Gli transcription factors

The primary cilium plays a critical role in Hh signal transduction (Corbit et al., 2005; Rohatgi et al., 2007). Smo translocation to the cilium propagates Hh pathway activation through the ciliary trafficking of Gli (Wong et al., 2009). Therefore, we examined whether eggmanone affected Gli trafficking to the primary cilium, where Gli transcription factors undergo activation prior to proteolytic processing and subsequent translocation to the nucleus to either promote or inhibit transcription (Haycraft et al., 2005; Liu et al., 2005). Thus, under pathway stimulation with SAG (Frank-Kamenetsky et al., 2002; Chen et al., 2002b), a Smo agonist, MEFs stained for Gli2 confirmed trafficking of Gli2 to the primary cilium (Figure 9B). Importantly, with co-treatment of SAG and eggmanone, Gli2 properly localized to the proximal tip of the cilium as marked by the ciliary maintenance protein Arl13b. Additionally, with the recent report of ciliobrevin D, a small molecule that antagonizes the cytoplasmic motor dynein resulting in defective retrograde transport and causes gross ciliary malformation, we sought to examine whether eggmanone affected cilium structure and trafficking (Hyman et al., 2009; Firestone et al., 2012). In NIH3T3 cells stained for the ciliary maintenance protein Arl13b, cilium structure was unaffected by eggmanone, and in contrast to ciliobrevin D, the ciliary transport protein IFT88 remained intact following eggmanone treatment (Figure 10). Thus, in light of unaltered structure and ciliary trafficking of Gli, we focused on elucidating eggmanone's effects on Gli processing and nuclear translocation.

Under regulation by Hh signaling, each Gli transcription factor is differentially processed to form either Gli full length (FL) activators or Gli repressors (R) which then translocate to the nucleus to either activate or inhibit downstream gene transcription.

However, the relative importance of Gli processing and nuclear translocation varies between individual factors. For instance, the differential processing of Gli3 is more sensitive to the Hh pathway status than Gli2, which remains predominantly in its GliFL form regardless of Hh activity (Hui and Angers, 2011). Thus, we separately investigated Gli2FL nuclear accumulation and proteolytic processing of Gli3FL to Gli3R. Hh pathway stimulation with SAG led to an increase in the fraction of Gli2FL in the nucleus, and this nuclear accumulation was inhibited by eggmanone and the adenylyl cyclase (AC) activator forskolin (FSK) (Figures 2C, 2D). SAG treatment also inhibited processing of Gli3FL to Gli3R, and both eggmanone and FSK restored Gli3R formation (Figures 9C, 9E) (Humke et al., 2010). Taken together, these data suggest that eggmanone functions upstream of Gli processing and nuclear translocation to exert its Hh-inhibitory effects.

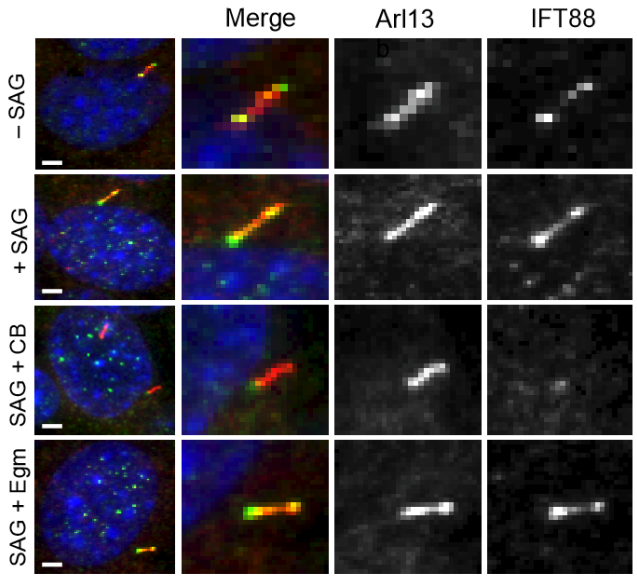

Figure 10 Eggmanone does not affect ciliary structure or IFT
Immunostaining for the cilium marker Arl13b (red) and IFT88 (green) of NIH3T3 cells without stimulation (top), stimulated with SAG (20 nM) in the presence of DMSO control (second), 100 µM ciliobrevin D (CB, third), or 5 µM Egm (bottom). Scale bar 2 µm.

Eggmanone causes selective activation of protein kinase A at the basal body

An emerging understanding of Gli transcription factor activity involves direct phosphorylation by PKA at two separable steps: repressor formation, and activation for nuclear translocation (Pan et al., 2009; Wolff et al., 2013; Tuson et al., 2011; Wang et al., 1999; Zeng et al., 2010; Niewiadomski et al., 2014). As our Gli2 and Gli3 western data (Figure 9) correlated well with this picture, we next investigated eggmanone's effects on PKA autophosphorylation. Immunostaining and quantification of phospho-threonine 197-PKA (p-T197-PKA) following eggmanone treatment strikingly indicated a significant increase in PKA activity at the base of the primary cilium, corresponding to the basal body, when co-stained with the ciliary maintenance protein Arl13b (Figures 11A, 11B). However, western blotting of whole cell lysates indicated no significant increase in p-PKA levels upon eggmanone treatment (Figure 11C), hinting at the possibility of localized PKA activation by eggmanone. PKA's localization to the basal body has been previously reported as a mechanism for control of Gli processing prior to its trafficking to the nucleus to inhibit Hh signaling (Tuson et al, 2011). To confirm this localization, co-staining of p-T197-PKA and γ-tubulin, which associates with the basal body, further revealed robust PKA activation at the basal body due to eggmanone treatment (Figure 11D, 11E). Taken together with the Gli processing and translocation data, localized PKA activation may be responsible for mediating eggmanone's effects on Hh signaling.

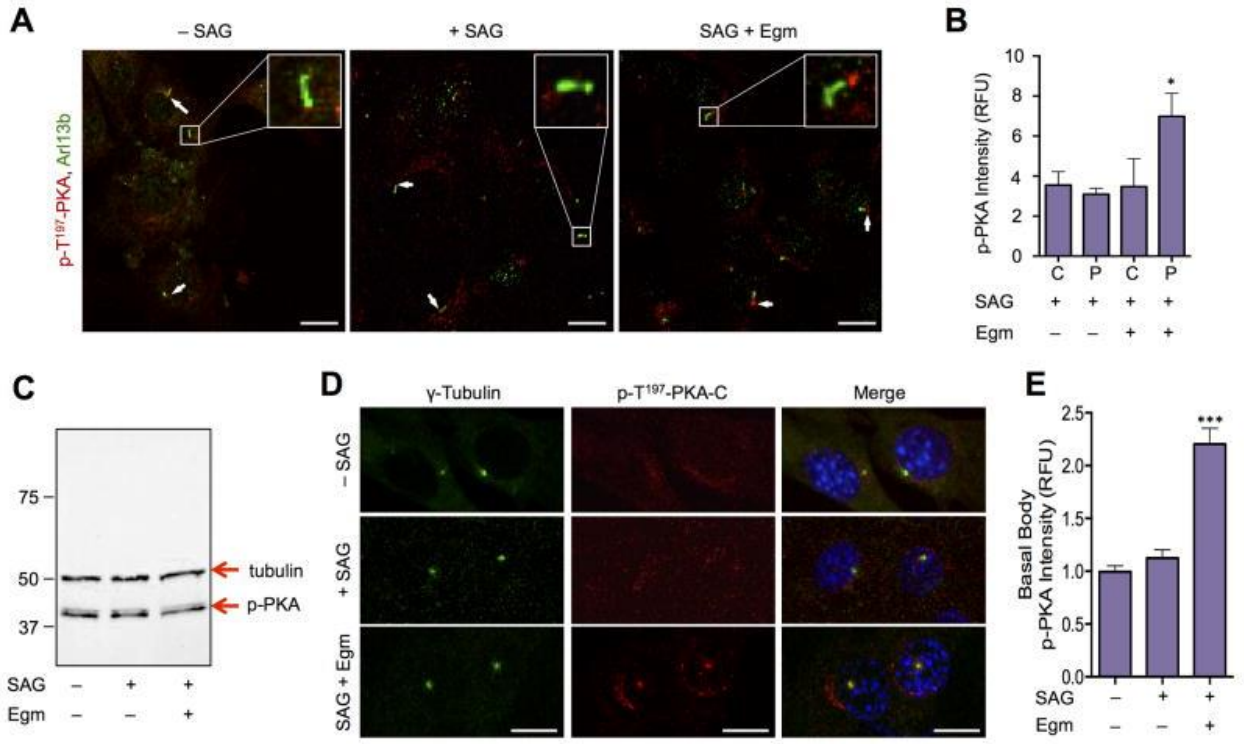

Figure 11 Eggmanone modulates the activity of PKA at the basal body

*(**A**) Immunostaining for the cilia marker Arl13b (green) and the autophosphorylated form of the PKA catalytic subunit (phospho-T^{197}-PKA; red) in NIH3T3 cells unstimulated (left), or stimulated with the Smo agonist SAG (20 nM, middle) demonstrated a low baseline PKA activation; co-treatment with SAG and Egm (5 μM, right) increased local PKA activation at the base of the primary cilium. Representative cilium (white box) magnified in the inset. Scale bars 10 μm. (**B**) Quantitative analysis of the local activation of phospho-T^{197}-PKA at the cilium (C) and peri-cilium (P) (mean ± SEM, n = 3 for each condition, * = 0.031 vs. SAG alone at the peri-cilium), as shown in (**A**). (**C**) Western blot of NIH3T3 whole cell lysates for phospho-T^{197}-PKA (bottom) and α-tubulin (top). SAG was treated at 20 nM and Egm at 5 μM. (**D**) Immunostaining for the basal body marker γ-tubulin (green) and the autophosphorylated PKA catalytic subunit (phospho-T^{197}-PKA; red) in NIH3T3 cells unstimulated (top), or stimulated with SAG (20 nM, middle) and Egm (5 μM) (bottom). Scale bars 10 μm. (**E**) Quantitative analysis of p-PKA intensity at the basal body from (**D**); RFU, relative fluorescence units (mean ± SEM, n = 21 for each condition, *** = <0.0001 vs. SAG alone).*

A

PDE Isoform	Percent Inhibition (20 μM)
PDE1A	7
PDE2A	18
PDE3A	**64**
PDE4D	**98**
PDE5A	-1
PDE7A	17
PDE8A	5
PDE9A	2
PDE10A	**51**
PDE11A	**65**

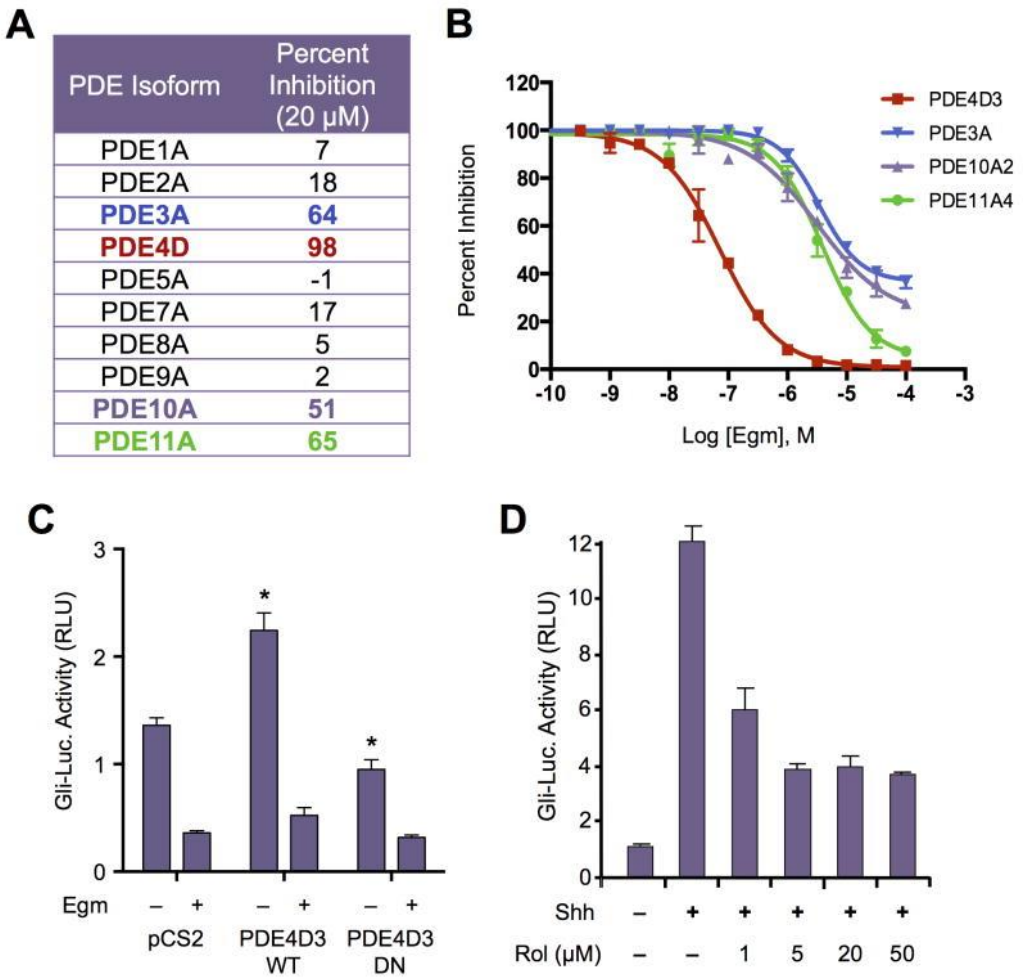

Figure 12 Eggmanone exerts its Hedgehog-inhibitory effects through antagonism of phosphodiesterase 4

*(**A**) In vitro PDE activity assays across ten PDE super-family members by Egm (20 μM). (**B**) Dose response curve of Egm against PDE4D3 (red), PDE3A (blue), PDE10A2 (purple), PDE11A4 (green). IC_{50}s were 0.072 μM, 3.00 μM, 3.05 μM and 4.08 μM respectively. (**C**) Transient overexpression of wild type PDE4D3 induced Hh reporter activity (* = 0.0026 vs. pCS2 control), which was abolished by 5 μM Egm (p <0.0001 vs. PDE4D3 WT). Transient overexpression of dominant negative (DN) PDE4D3 decreased Hh reporter activity (* = 0.0121 vs. pCS2 control). Data is reported at mean ± SEM. (**D**) Rolipram (Rol) inhibited Sonic hedgehog (Shh)-responsive Gli-luciferase (Gli-Luc) reporter activity when stimulated with Shh conditioned medium (n = 4 for each condition, results represented as mean RLU ± SEM, p-value <0.003, starting at 1 μM).*

Eggmanone inhibits hedgehog signaling through antagonism of phosphodiesterase 4

PKA is one of numerous proteins known to localize to the basal body, where it is anchored by A kinase-anchoring proteins (AKAPs) (Terrin et al., 2012). Additionally, PKA activation occurs in response to the ubiquitous secondary messenger cyclic adenosine

monophosphate (cAMP), which is synthesized by adenylyl cyclases (AC) and is degraded by phosphodiesterases (PDE). Following this logic, we hypothesized that eggmanone's Hh-antagonism could be due to PDE inhibition and tested its ability to inhibit PDEs (Figure 12α). Eggmanone potently inhibited PDE4D3 and only inhibited three other family members greater than 50% at 20 μM. No other PDE family members were inhibited by eggmanone more than 18%. This data correlated well with IC_{50} values for four PDE members, where eggmanone displayed potent and selective antagonism of PDE4D3 with an IC_{50} of 0.072 μM, approximately 40- to 50-fold selective over other PDEs (Figure 12B). Conveniently, PDE4D3 has been shown to complex with PKA and AKAP9 at the centrosome, lending additional validity to PDE4 as eggmanone's cellular target (Terrin et al., 2012). Counter-screening of eggmanone against a broad and comprehensive panel of 442 kinases, 158 GPCRs, and 21 phosphatases revealed no other targets inhibited by eggmanone at greater than 50% at 10 μM. Based on these results, eggmanone was confirmed to be a potent and selective PDE4 inhibitor.

PDE4 modulates Hh signaling in vitro

Considering the previous lack of direct correlation between PDE inhibition and Hh blockade, we sought to molecularly confirm this association. First, the PDE isoform most potently inhibited by eggmanone, PDE4D3, was transfected into Shh-Light2 cells and was shown to significantly increase signaling over the levels observed when stimulated with SAG (Figure 12C). This increased signaling was returned to basal level upon treatment with eggmanone. Furthermore, transfection of a dominant negative catalytically inactive PDE4D3 construct led to a reduction in Hh signaling which was further abrogated by

subsequent eggmanone treatment. Finally, if PDE inhibition modulates Hh signaling, we reasoned that the broad-spectrum PDE4 inhibitor rolipram should display inhibitory activity in the Gli-Luc reporter assay. Indeed, Shh-Light2 cells stimulated with Shh followed by treatment with increasing concentrations of rolipram did reduce Hh signaling levels, albeit with lower potency than eggmanone (Figure 12D). These results confirm that decreased cAMP concentrations due to higher PDE4 activity can promote Hh signaling, and the converse situation can lead to Hh inhibition.

Discussion

Hh and PDE4 have been independently identified as promising targets for cancer therapy. As previously mentioned, Hh has been shown to drive tumor progression in BCC, medulloblastoma, and other cancers (Kar et al., 2012; Ng and Curran, 2011). PDE4 has primarily been implicated as a driver of central nervous system (CNS) tumors such as medulloblastoma and glioblastoma as well as lung and breast tumors (Goldhoff et al., 2008; Sengupta et al., 2011). Moreover, much evidence points to overexpression of PDE4 in a wide variety of tumors, and the resulting decrease in cAMP has been associated with increased prevalence of malignancies. In light of this information and our presented data, we show that PKA acts as a linchpin to link PDE4 to Hh signaling.

Based on our data from cellular characterization of eggmanone's Hh-inhibitory activity, we propose a signaling model that illuminates previously unclear portions of the Hh signaling mechanism. During the normal active pathway state, PKA remains minimally active due to low cAMP concentrations associated with PDE4 hydrolytic activity. GliFL does not undergo phosphorylation by PKA and translocates to the nucleus to promote

gene transcription. When PDE4 activity is inhibited, increasing concentrations of cAMP activate PKA leading to Gli phosphorylation and processing to Gli repressor.

Using an unbiased *in vivo* chemical genetic screen for small molecules that perturb Hh signaling, we identified eggmanone, a novel highly selective PDE4 inhibitor and used it as a probe to discover a novel role of PDE4 in regulation of Hh signaling downstream of Smo. To our knowledge, this work represents the first demonstration of a direct and specific link between PDE4 inhibition and Hh blockade. In light of prior associations of PDE4 and Hh with variety of malignancies, our study highlights a novel therapeutic strategy that exploits the dual roles of PDE4 in Hh signaling and cancer.

CHAPTER 4

ZePAC: ZEBRAFISH PHENOTYPIC ANATOMICAL CLUSTERING

Introduction

In the past decade the phenotypic screening has regained interest as a complementary approach to in vitro screening for early drug discovery (Williams and Hong, 2016). A critical component of this resurgence is the rising cost of drug development caused by late stage failures (Swinney and Anthony, 2011). New avenues for discovery of tractable and relevant disease modifying targets are of primary import. Targeting of developmental pathways and signaling cascades represents a resource of untapped potential. For example, CSCs (cancer stem cells) utilize pathways essential for embryonic development and tissue homeostasis, such as WNT, Hedgehog (HH), and Notch pathways (Takebe et al., 2015). The FDA recently approved the first Hedgehog inhibitor Vismodegib, which targets the smoothened receptor, for treatment of basal cell carcinoma (Fecher and Sharfman, 2015). This drug provides the first clinical proof of principle for the development of therapeutics around developmental pathways.

In a previously described phenotypic screen we identified novel small molecule regulators of BMP, VEGF, Hedgehog and WNT (Hao et al., 2010b, 2013; Williams et al., 2015; Yu et al., 2008). Windorphen a novel P300 selective inhibitor was discovered through its ability to perturb dorsoventral patterning in zebrafish development. During zebrafish development WNT plays a bimodal role; during the early phase WNT is critical for establishing the Spemann-mangold organizer which determines the dorsal pole. The

later phase consists of WNT signals in ventrally determined progenitors. The signaling cascade initiates with WNT ligand binding to Frizzled receptors to trigger dissociation of the destruction complex resulting in β-catenin nuclear translocation. The stability of β-catenin is tightly controlled through the degradation complex, which consists of APC, axin, CK1 and GSK3B (Nakamura et al., 1998). CK1 and GSK3B are kinases that phosphorylate B-catenin at various serine residues, allowing degradation through the proteasome (Kimelman and Xu, 2006). Inhibition of these factors leads, or dissociation from the destruction complex are two mean by which WNT activation occurs. Once in the nucleus, β-catenin binds TCF/LEF and recruits the transcriptional co-activators p300 and/or CBP resulting in target gene transcriptional activation. (Ashihara et al., 2015). WNT represents a particularly interesting target for therapeutics, as under normal physiological conditions WNT signaling controls stem cell homeostasis (Klaus and Birchmeier, 2008). Further WNT signaling is thought to drive a large number of cancers, including but not limited to colon and pancreatic cancers (Klaus and Birchmeier, 2008). However, a WNT inhibitor has yet to gain FDA approval, a promising clinical trial of the biologic OMP-54F28/Fzd-Fc has been found to have a negative off target effect of bone mineral density decreases (NCT01608867).

In forward mutagenesis screens, as the genome is more saturated, multiple alleles in the same gene are discovered. Although these mutants are different, the phenotypes would be similar enough that genetic complementation tests are conducted. Therefore, mutations in different loci of the same gene create similar phenotypes, and even mutations in different genes in the same pathway can create similar phenotypes. Building on this concept, chemical probe utilization during development in zebrafish have shown

that specific inhibition of proteins with small molecules can phenocopy loss of function mutations (Yu et al., 2008). In previous chemical screens for modulators of developmental pathways, phenotype of chemical perturbations have been used to associate the compound to a known pathway (Hao et al., 2010b, 2013; Williams et al., 2015; Yu et al., 2008). However, this approach is highly dependent on the depth of human knowledge and is biased toward commonly known phenotypes. Target and pathway identification is possible in numerous contexts through Phenoclustering (Williams and Hong, 2013). Zebrafish have been used in biomedical research for over 40 years, with data from mutants and genetic perturbations aggregated by ZFIN for many years, representing a large data set that is beyond the scope of human processing. To date, this data has not yet been fully utilized toward for target/ pathway identification.

Herein we report the use of a phenotypic clustering platform ZEPAC (Zebrafish Phenotypic Anatomical Clustering), an unsupervised hierarchical clustering method for pathway identification of small molecules using a zebrafish phenotypic screening. In proof of concept we apply ZEPAC to a small molecule, here in called incaskin (ICN), a novel 2-(2-phenylethenyl)quinolone, which antagonizes WNT signaling, both in vivo and in vitro, through CK2α. *Insilico* modelling suggests that ICN binds the CK2α active site with exquisite selectivity. Further, ICN inhibits CK2α in purified enzyme assays and phosphorylation of CK2 specific phosphorylation of PTEN-S370. Finally, ICN differentially inhibits growth of WNT driven tumors. Together these represent a novel chemical biological tool for the study of CK2α in WNT signaling.

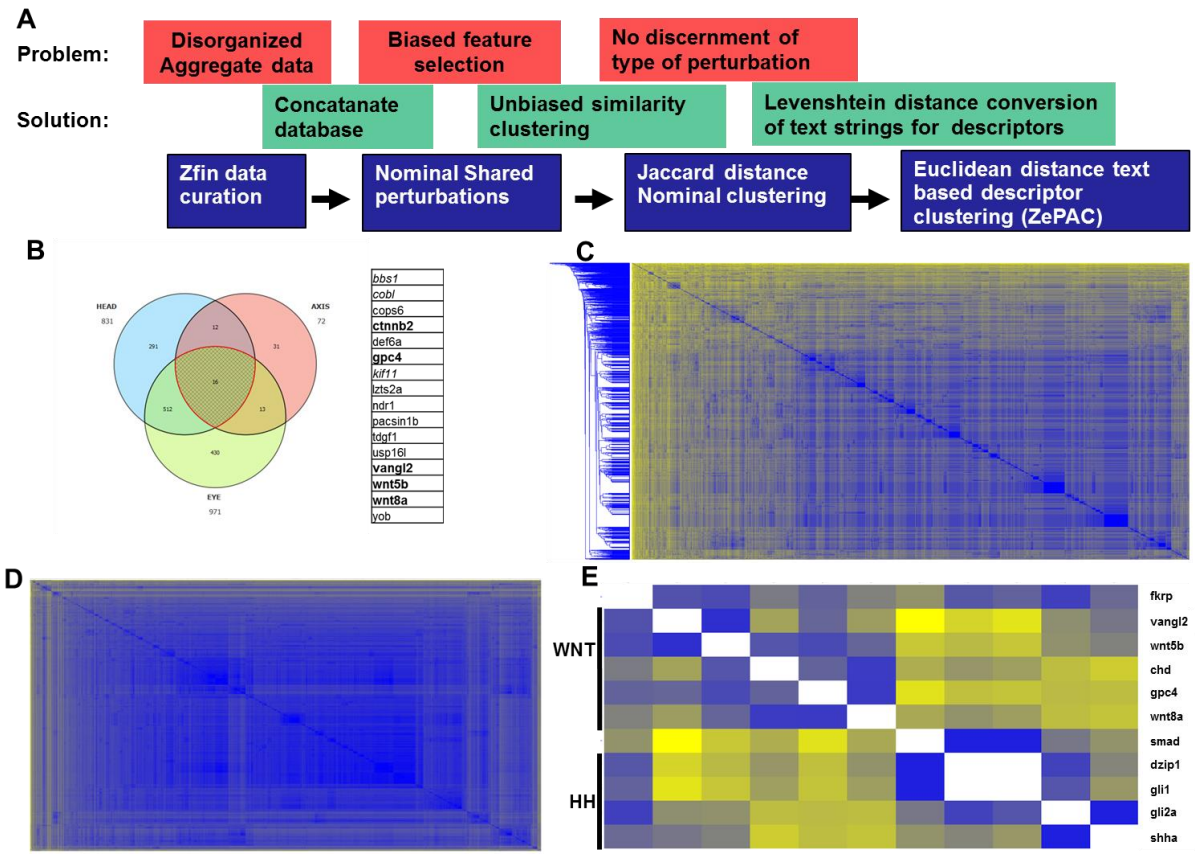

Figure 13 . Development and execution of ZePAC (Zebrafish Phenotypic anatomical clustering) ***(A)*** *Schema for the steps taken to develop ZePAC.* ***(B)*** *Venn diagram of genes with phenotypes annotated in axis, eye, and head anatomical features. Table of 16 genes that are shared in the three categories (Wnt genes: BOLDED, Ciliary Genes: Italicized).* ***(C)*** *Hierarchical clustering of nominal descriptors.* ***(D)****Applying Levenshtein text distance to descriptors allow more granularity of data and gradients to form for hierarchical clustering.* ***(E)*** *Small extract of wnt and hedgehog genes clustered show segregation of genes based on similarity of phenotypes extracted from text descriptors.*

Results

Pathway segregation based on genotype-phenotype association database

We curated data on 29 anatomical features discernable by standard light microscopy in the first 48 hours of embryonic development from ZFIN's publicly available genotype phenotype database consisting of 15439 gene-descriptor-affected structure data points. These were concatenated into 9813 gene-affected structure pairs among 2909 genes. The average gene therefore had 3.4 affected structures. Any structures in

the dataset that did not have phenotype annotations were imputed as normal. This database was then given nominal values of 1 being affected and 0 being unaffected. As a feasibility study, we assessed if this database was capable of finding groups of pathway genes based on affected structures. The WNT pathway is known to affect axis length, head size and retinal development in zebrafish development. By generating a simple Venn diagram of genes containing annotated perturbations in these features, we identify a subset of genes that are enriched for WNT signaling components; interestingly, as cilia are profoundly important for wnt signaling, ciliary proteins bbs1, cobl, and kif11 also were found in this grouping (Figure 13B). However, this was a biased approach selecting specifically for known features and ignoring the rest of the 26 anatomical features. Taking an unbiased approach, genes were hierarchically clustered using unsupervised learning using a jaccard similarity index between the phenotypes. While still clustering WNT components together, other genes were also well represented (Figure 13C). This result indicated that assigning nominal values for data reduction causes loss of data depth, and resultant convergence of dissimilar phenotypes (e.g. loss of structure, vs increased size of structure). To reduce loss of data depth, we restored granularity to the data for affected structures using levenshtein text distance calculations as vector distances for descriptors deviating from “normal” (Figure 13D). Further, clustering this data using Euclidean distance for vectors allows the segregation of signaling pathways like WNT and hedgehog, based on unsupervised clustering using anatomical phenotype descriptors. (Figure 13E).

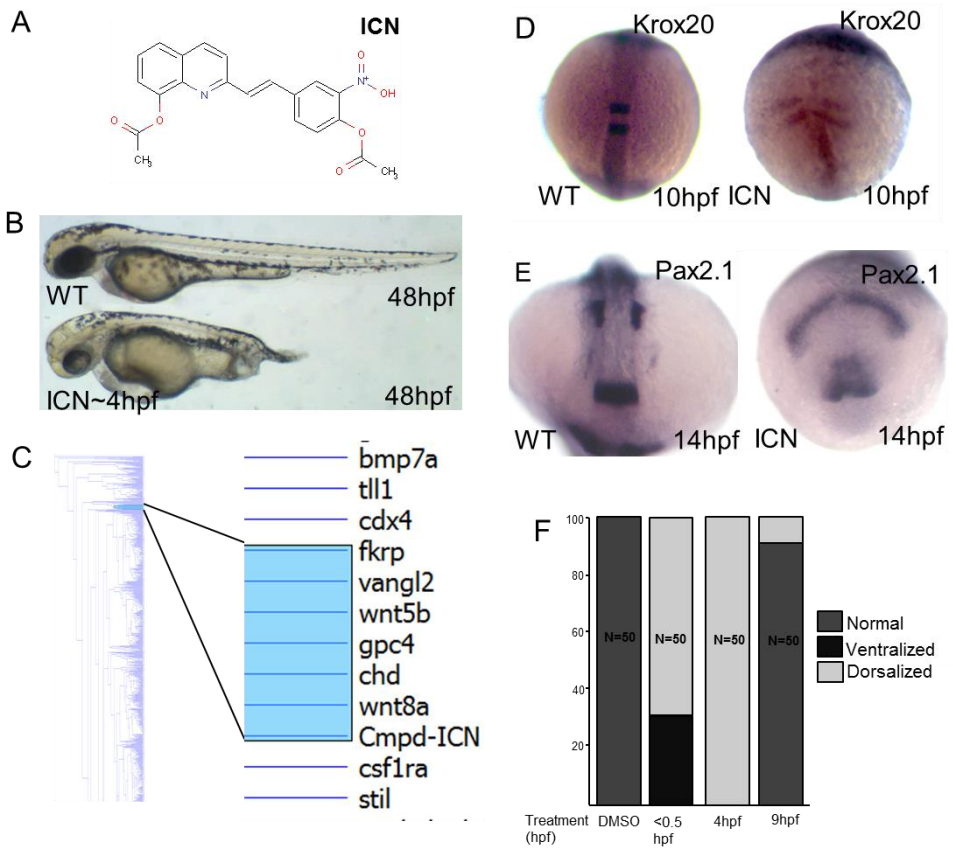

Figure 14 Incaskin 48hpf phenotype clusters with known Wnt pathway mutants and exhibits Wnt like dorsalizing activity

(A) *Chemical structure of Incaskin, 2-[(E)-2-phenylethenyl]quinoline.* ***(B)*** *48hpf Phenotype of embryos treated with ICN at 4hpf.* ***(C)*** *ZePAC clustering results. ICN clusters with Wnt components wnt8a, gpc4, wnt5a and vangl2.* ***(D)*** *In situ hybridization of 6-somite-stage (12-hpf) embryos to evaluate expression of the dorsal markers Krox20, which marks rhombomeres 3 and 5. In comparison to untreated embryos (left), expression is dramatically expanded in incaskin (ICN) treated embryos (right). Dorsal view, anterior is to the bottom.* ***(E)*** *In situ hybridization of 12-somite-stage (16-hpf) embryos to evaluate expression of the dorsal markers pax2.1, which marks mid-hindbrain boundary. In comparison to untreated embryos (left), expression is dramatically expanded in incaskin (ICN) treated embryos (right). Dorsal view, anterior is to the bottom.* ***(F)*** *Differential temporal effects of ICN (10 μM). Treatment of embryos right after fertilization results in loss of anterior structures and ventralization of embryos. Treatment at 4hpf results in shortened axis and dorsalization of embryos is between 4 to 6-hpf. Treatment at 9hpf resulted in few truncated embryos.*

Pheno-clustering of novel small molecule for target pathway identification

To directly assess whether this machine learning approach could predict the target pathway of a novel small molecule based on induced phenotype, we selected a novel unannotated 2-(2-phenylethenyl)quinoline, here in called incaskin (ICN) (Figure 14A). In brief ICN was discovered a screen of approximately 30,000 small molecules for their ability to effect alterations in embryonic zebrafish patterning; fertilized zebrafish embryos were arrayed into 96-well microtiter plates, exposed at 3 to 4-hours post fertilization (hpf) to a 10uM compound library, and then visually assessed for perturbations. ICN was given phenotypic description including but not limited to decreased axis length, abnormal brain morphology, decreased eye size, and increased head size (Figure 14B, Table 1). After calculating levenshtein distances for our phenotypic descriptions against “normal”, we appended ICN into our genotype-phenotype database and clustered the perturbations. ICN clustered closely to WNT signaling components wnt8a, gpc4, vangl2 and wnt5b (Figure 14C). WNT signaling is critical for establishing ventral cell fates between 4-6 hours (Hao et al., 2013; Schier and Talbot, 2005). Incaskin treatment at 4 hours induced marked expansion of the dorsal markers and *krox20*, a marker of rhombomeres 3 and 5 at the 6-somite (Figure 14D), and *pax2.1*, which demarcates mid-hindbrain boundary and otic placode at the 10-somite stage (Figure 14E). In contrast to BMP inhibition, but consistent with the biphasic role of WNT in axis patterning, incaskin treatment also reproducibly caused ventralization of zebrafish embryos when treated during early blastula. (Figure 14F). Taken together these phenotypes predict that incaskin regulates WNT signaling and furthermore causes dorsalization of key markers and exhibits a biphasic role on axis formation, consistent with inhibition of WNT signaling.

Anatomical feature	Descriptors
axis	decreased length
brain	decreased length poorly differentiated
eye	decreased size
forebrain	distended prominent abnormal
head	hydrocephalic
notochord	structure increased width decreased length disrupted
otolith	amount increased
post-vent region	disrupted decreased length decreased size has fewer parts of type curved ventral kinked
somite	decreased amount
trunk	decreased amount
whole organism	decreased length dead dorsalized abnormal shape anterioralized

Table 1 Phenotypic descriptors of ICN treatment

Incaskin inhibits activation of β-catenin and nuclear subsequent nuclear translocation

To define the mode of action of ICN on the canonical WNT signaling pathway, we assessed activation of β-catenin in embryo lysates. Embryos treated with ICN reduce levels of active, non GSK3B phosphorylated, β-catenin. (Figure 15A). Notably there is a small mobility shift in both active and total β-catenin, suggesting a change in phosphorylation. To assess if the target for ICN is conserved in mammalian cells a WNT reporter cell line, STF293, were used. In STF293 cells, addition of WNT3a conditioned media alone robustly induced β-catenin dependent luciferase activity, and this WNT3a-induced reporter activity was blocked by ICN in a dose-dependent manner (Figure 15B). Next, in human colon carcinoma RKO cells, we found that ICN affected WNT3a-induced translocation of β-catenin to the nucleus (Figure 15C). Taken together, these results suggest that ICN selectively targets a signaling component in the WNT pathway that modulates the phosphorylation and translocation of β-catenin.

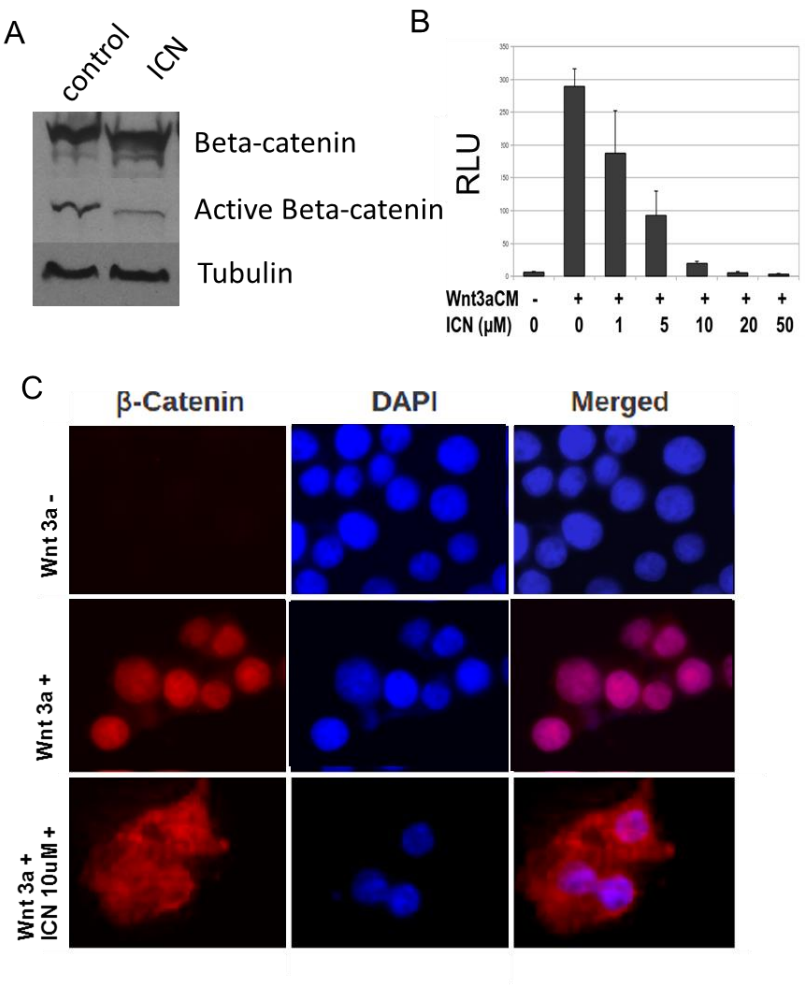

Figure 15 Incaskin inhibits nuclear translocation of B-catenin

(A) *Western blot of B-catenin and active b-catenin. ICN reduces levels of active b-catenin with no significant effect on total b-catenin or tubulin levels. Differences in mobility suggest different phosphorylation states* ***(B)*** *Incaskin (ICN) inhibited Wnt signaling induced by Wnt3a conditioned Media TOPFLASH-luciferase assays in STF293 cells. (n = 4, results represented as mean RLU, relative luciferase units).* ***(C)*** *ICN treatment blocks Wnt3a-induced β-catenin nuclear translocation in RKO cells. RKO cells were immunostained for β-catenin (red) and counterstained with DAPI (blue) following 24-hour incubation without Wnt3a, with Wnt3a, and with Wnt3a plus ICN (10 μM).*

Incaskin is a CK2α inhibitor

β-catenin is tightly regulated by a number of kinases. Building on the evidence above, we examined kinases as a possible molecular target of Incaskin. ICN binding was screened against a diverse panel of 442 kinases (DiscoverRx KINOME***scan***) using an in vitro ATP-site competition binding assay at a concentration of 10 μM. 8 kinases that

exhibited greater than 95% displacement from the immobilized ligand by Incaskin were further assayed in purified enzyme assays (Figure 16A). The *in vitro* purified enzyme assays showed that Incaskin has inhibitory activity against CK2α (casein kinase 2α), CK2α2 and CAMK2□ (calcium/calmodulin-dependent protein kinase II beta); IC50s 687, 4414, and 7089 nM, respectively (Figure 16B). Incaskin exhibited no further inhibitory activity against any other potential targets identified in the Kinomescan.

Crystal structures of CK2α catalytic domains have been determined in the presence of ATP and other ligands (Niefind et al., 1998). The catalytic domain, consisting of a catalytic loop Arg155 to Asn161, for CK2α is somewhat unique and is capable of using ATP and GTP (Niefind et al., 1998). These structures enabled us to perform unbiased docking simulations to identify potential Incaskin binding sites. Incaskin was docked to the structure of CK2α determined by X-ray crystallography (Protein Data Bank identifier 3WAR). Molecular docking software (Pyrx) was run using blind docking over the entire molecule using Genetic algorithm and suggested that ICN competitively binds to the CK2α ATP binding pocket (Figure 16C). This binding pocket was then extracted in iGEMdock and ICN was docked to predict interacting residues and binding modes (Figure 16D). Taken together this molecular model suggests that the north-east nitro group form critical hydrogen bonds with lys68 and asp175 for inhibition of CK2α (Figure 16D, E).

A

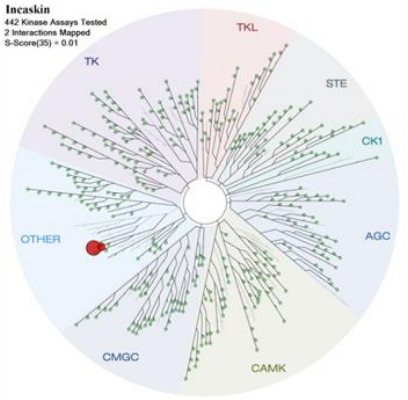

B

IC50 (nM)	ICN
CK2a1	687
CK2a2	4414
CAMK2B	7089

C

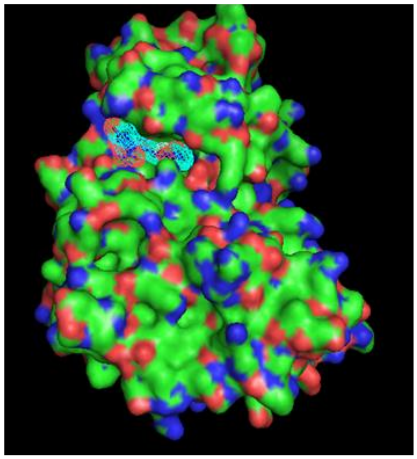

D

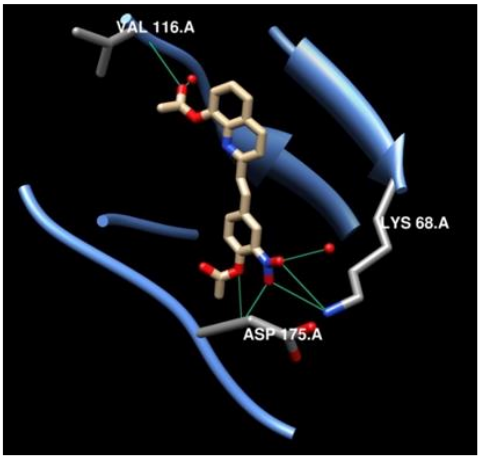

E

PDB:3WAR	Energy	LYS68	VAL116	ASP175
ICN4541	-164.5	-9.49341	-3.5	-14.7226
ICN4343	-149.8	-2.67899	-2.68707	0

Figure 16 Incaskin selectively targets CK2α
(A) *KinomeScan profiling of Incaskin at a concentration of 10 μM against 442 kinases.* ***(B)*** *IC50 results of in vitro purified kinase assays for interacting targets from Kinomescan.* ***(C)*** *Blind Docking simulations of ICN with CK2α (PDBID:3WAR) based on Lamarckian genetic algorithm in PyRx predicts binding in the active site.* ***(D)*** *Docking pose of CK2α (PDBID:3WAR) with incaskin using hex v6 algorithm. The receptor is represented as ribbon form and ligand as solid model.* ***(E)*** *Binding energy was determined as −164 (kcal/mol), predicted hydrogen bond interactions at LYS68, VAL116 and ASP157.*

To test the hypothesis that hydrogen bonds formed by the northeast functionality are important for ICN action two analogs were acquired with a loss of the nitro functional group with either bromine (ICN4343) or ethyl ether functional group (ICN7863) (Figure 17A). The *in vitro* purified enzyme assays showed that ICN, ICN4343 had inhibitory

activity against CK2α (casein kinase 2α), IC50s 687, 23400nM, respectively, while ICN7863 had no CK2α inhibitory activity up to 30uM (Figure 17B). Purified enzyme assays further showed that while ICN had inhibitory activity against CAMK2□, IC50 7089, ICN4343 and ICN7863 had no CAMK2□ inhibitory activity up to 30uM. Furthermore, loss of CK2α inhibitory activity for ICN7863 correlates with loss of WNT antagonism in STF293 assay (Figure 17C). Taken together these findings determine the structural determinant for ICN inhibition of WNT signaling through CK2α.

Genetic manipulation with CK2α modulates zebrafish dorsoventral patterning

The possibility that Incaskin inhibits CK2α to modulate WNT during zebrafish development is consistent with the important role of CK2 in xenopus dorsoventral patterning (Dominguez et al., 2004; Song et al., 2000). However, the role of CK2α in zebrafish has not been established. It is known that CK2α (zgc:86598) is ubiquitously expressed throughout development (Thisse et al., 2004). We hypothesized that injection of kinase inactivated (dominant negative) CK2α should serve to phenocopy pharmacological inhibition of CK2α by Incaskin. Indeed, injection of capped mRNA encoding DN-CK2α resulted in both ventralized embryos and dorsalized embryos (Figure 17D). The dual role, both dorsalizing and ventralizing activities, of Incaskin and KI-CK2α can be explained by the dual functionality of WNT signaling during axis formation in zebrafish where maternal WNT signaling is necessary for establishing the dorsal

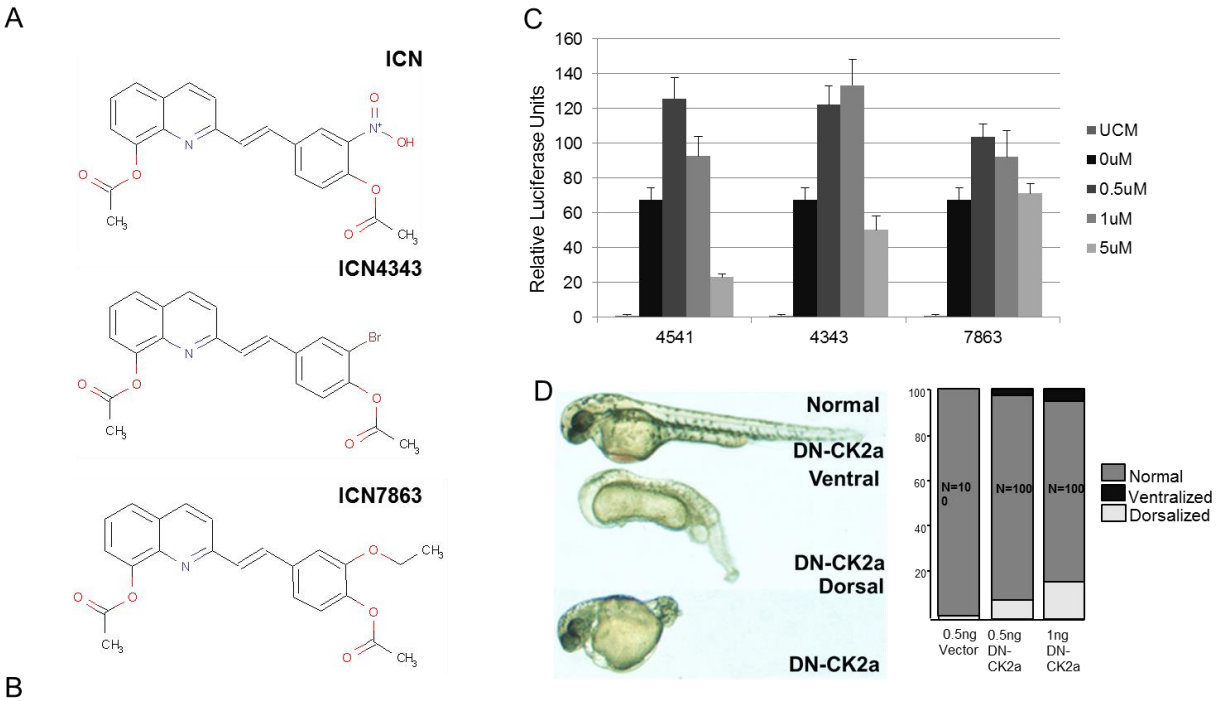

	(nM)CK2a	(nM)CAMK2B
ICN	687	7089
ICN4343	23400	NA
ICN7863	NA	NA

Figure 17 Loss of CK2α kinase activity causes incaskin phenotype
(A) Analogs of Incaskin with altered Northeast portion were obtained. (B) IC50 results of in vitro purified kinase assays for potential relevant targets CK2α and CAMK2B. (C) Alterations of northeast portion of incaskin lose wnt inhibitory ability. (D) Dominant negative CK2α injected zebrafish recapitulate Incaskin phenotype. (E) Incaskin inhibits CK2 specific phosphorylation of PTEN at residue S370 in HEK293 cells.

organizer, and later zygotic WNT plays a role in the formation of tail and ventral structures. Finally, to assess if CK2α kinase activity is affected in cellular contexts we examined the site serine 370 on PTEN, which is a CK2 specific phosphorylation site(Miller et al., 2002). Cells treated with ICN had reduced pS370 PTEN compared to DMSO treatment (Figure 17E). This data with the data above suggest that ICN inhibits CK2α phosphorylation activity which, in turn inhibits WNT signaling in vitro and in vivo.

Incaskin robustly induces apoptosis signaling in Wnt dependent tumor cells

Canonical Wnt/β-catenin signaling has been strongly linked to the development of numerous malignancies, particularly gastrointestinal cancers of which 90% are thought to involve aberrant Wnt signal activation (Clevers, 2006; Moon et al., 2004; Reya and Clevers, 2005). To ascertain therapeutic potential of chemical inhibition of CK2α, we investigated Incaskin's effects on the viability of cancer cells. Cell viability assays with increasing concentrations of ICN for 72 hours reflect that human carcinoma cell lines noted to have activation of Wnt signaling, such as human colon cancer cell lines SW480, HCT116, and RKO and prostate cancer cell lines DU145 and medulloblastoma Daoy (Lu et al., 2009; Suzuki et al., 2008), exhibited sensitivities to killing by incaskin (IC50s of 15.0, 19.2, 21.8, 19.0 μM, respectively; Figure 6A, B). In contrast, Hela cells were relatively refractory to the effects of Incaskin. In human colon adenocarcinoma HCT116 cells, in which Wnt signaling is constitutively activated due to mutant APC (adenomatous polyposis coli) gene that is protected from degradation via the destruction complex, Incaskin (10 μM) prevented nuclear translocation of □-catenin to the nucleus (Figure 6C) and caused activation of apoptosis through cleavage of caspase-3 after 72 hours of treatment (Figure 6D). These observations suggest that selective CK2α inhibitors like Incaskin may be an attractive chemical probe for interrogating Wnt pathway in cancer cells.

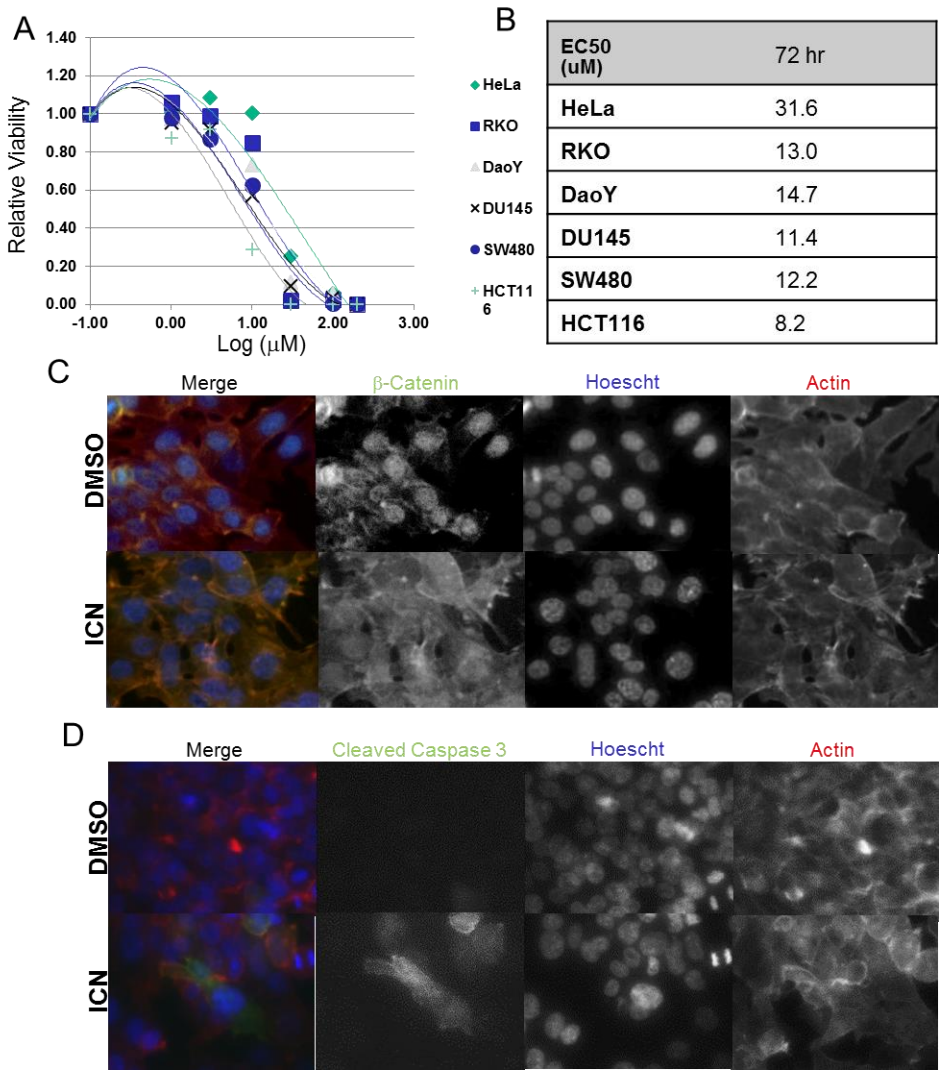

EC50 (uM)	72 hr
HeLa	31.6
RKO	13.0
DaoY	14.7
DU145	11.4
SW480	12.2
HCT116	8.2

Figure 18 Incaskin promotes apoptosis in Wnt dependent tumor cell lines
(A) *Percentage of viable human cancer cells (SW480, RKO, DU145, PC3 DaoY and HCT116), as determined by cell titer assays, following 72-hour treatment with increasing concentrations of ICN (n=4 for each data point).* ***(B)*** *IC 50 values for tumor cell lines.* ***(C)*** *ICN treatment blocks aberrant β-catenin nuclear translocation in HCT116 cells. HCT116 cells were immunostained for β-catenin (green) and counterstained with DAPI (blue) and actin (red) following 24-hour incubation ICN (10 μM).* ***(D)*** *ICN treatment induces cleaved caspase-3 in HCT116 cells. HCT116 cells were immunostained for β-cleaved caspase(green) and counterstained with DAPI (blue) and actin (red) following 24-hour incubation ICN (10 μM).*

Discussion

In this study, we used publicly available genotype-phenotype data to develop a hierarchical clustering method to facilitate pathway identification for small molecule modulators of zebrafish development. We used gene-phenotype association across over 2,900 genes and 29 anatomical features to segregate clusters of gene interactors that modulate elicit a spectrum of anatomical perturbations during the first 48 hours of zebrafish development. We validate that genes that are related are responsible for similar phenotypes and therefore cluster together. For computation of difference between normal and observed differences for the anatomical structures we used Levenshtein distance, string distance based measure, for terms for each anatomical feature from a publicly developed database. However, this is not without flaws. Verbosity of data curators and potential observational bias of curators for some phenotypes over others can introduce artificial “phenotypic noise”. Despite these confounders, a clear segregation of gene families is seen in our hierarchical clustering pathway prediction strategy.

To directly test the feasibility of pathway deconvolution method ZEPAC, we chose to identify the target of a previously unannotated a 2-(2-phenylethenyl)quinolone, ICN. Through use of anatomical phenoclustering we were able to predict that ICN was involved in wnt signaling. Further investigations identified that ICN was a highly selective CK2α inhibitor that inhibits nuclear translocation of β-catenin. Finally, we show that incaskin can selectively kill cancer cells in which Wnt signaling is aberrantly activated. This is concurrent with data from the clinical trial (NCT00891280) using CK2α inhibitor CX-4945 for a wide spectrum of cancers that over express CK2α including but not limited to Lung, Renal, Head and neck, Prostate and Colorectal cancer.

Currently there are a few commercially available CK2α inhibitors used as chemical probes: DMAT, TBB and DRB. DMAT and TBB are derivatives of one another with IC50s of 0.14 and 0.5uM, respectively (Duncan et al., 2008). However, DRB which is structurally distinct has a higher IC50 of 13uM. As with many kinase inhibitors, these compounds are far from specific; a small assay of 80 kinases (less than 1/5th of the human kinome) revealed that TBB and derivatives also target PIM1 (provirus integration site for Moloney murine leukemia virus), PIM2, PIM3, PKD1 (protein kinase D1), HIPK2 (homeodomain-interacting protein kinase 2) and DYRK1a (dual-specificity tyrosine-phosphorylated and -regulated kinase 1a) with some potency (Pagano et al., 2008). While these chemical probes have provided some important insight into CK2α biology there is concern of off target effects. With an IC50 of 0.67uM, Incaskin's potency is equal to or better than currently available CK2α inhibitors. Moreover, it is exquisitely selective for CK2α, with only one other possible target in CAMK2b at a 10-fold lower affinity. Furthermore, having been first characterized in zebrafish, Incaskin has already demonstrated its efficacy in vivo. These features of potency, selectivity, and in vivo efficacy make Incaskin an ideal probe for the study of CK2α in vivo.

As Phenotype-based chemical genetic screening becomes more common and throughput increases, the consequences of a bottleneck of target identification become more significant. Because traditional target identification approaches are linear and labor intensive, targets for only a small number of "hit" compounds can be pursued. By contrast, hierarchical clustering based on phenotypic similarity has the potential to dramatically increase the throughput of small molecule target identification efforts, and mechanism of action studies. These pathway predictions can be done in real time with annotation of the

phenotype. Furthermore, using this methodology as a framework, advancements in machine learning and image analysis/recognition have the potential to supplement this approach and remove observer bias for phenotypic assessment.

CHAPTER 5

OGREMORPHIN

Introduction

Highly malignant, invasive, and metastatic cancers have markedly elevated glycolytic activity, producing an oncogenically favorable acidotic extracellular environment; a phenomenon called the Warburg effect(Vander Heiden et al., 2009). This acidification (pHe < 7.4) of the environment is marked by increases in efflux mechanisms H+ATPases and Na+-H+ exchangers(Martinez-Zaguilan et al., 1993; McLean et al., 2000; Miraglia et al., 2005; Sennoune et al., 2004). Furthermore acidification promotes tumor malignancy, including metabolic reprogramming and invasiveness, the cellular mechanisms that mediate these phenomena are poorly understood(Justus et al., 2013; Webb et al., 2011). Investigations have shown that in numerous animal models of solid tumors, small molecule inhibition of NHE1 can have an effect on tumor growth and metastasis(Matthews et al., 2011).

Melanoma is one of the most aggressive human cancers; patients having metastsatic melanoma have a median survival of less than 12 months(Tas, 2012). Melanomas derives from neural crest derived melanocytes. It has been shown that numerous mechanisms and genes are shared between neural crest cells and melanoma(Gong, 2014; Takahashi et al., 2014, 2013). Neural crest cells initially form from a neuroepethelial population that undergoes a transition into a migratory cell type (Morales et al., 2005). The neural crest cells interpret a complex interplay of proximal and

distal signals to invade the surrounding tissue and migrate to the developmentally relevant location(Takahashi et al., 2013). Therefore small molecules that perturb melanogenesis in zebrafish could potentially identify new therapeutic avenues. Indeed several screens have been conducted to validate this approach(Chen et al., 2012; Cheng et al., 2016; Colanesi et al., 2012). In this investigation, we used the zebrafish embryonic pigmentation model to identify a modulator of neural crest migration, identified as an inhibitor of proton sensing GPCR (G protein coupled receptor), GPR68, that modulates migratory behavior of melanoma cells in vitro and in vivo. Furthermore, Human Phenome wide association study identified 2 variants in GPR68 that significantly increase the risk of tumor metastasis to bone and liver.

Results

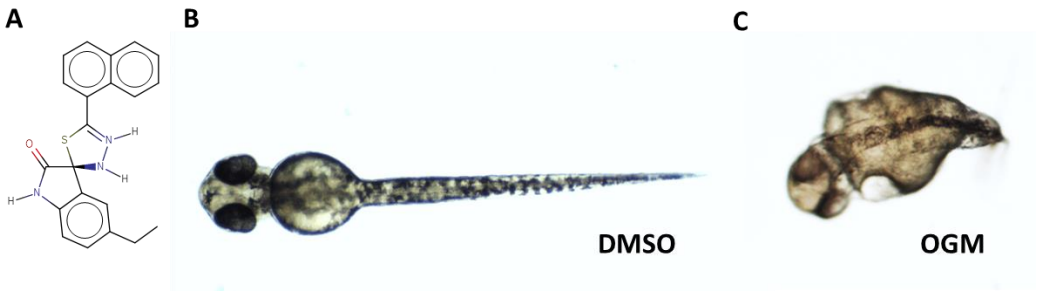

Figure 19 Discovery of Ogremorphin
(A) Structure of Ogremorphin (B) Control Zebrafish embryo at 48hpf (C) OGM treated embryo at 48hpf

Ogremorphin inhibits GPR68

In an unbiased screen of ~30,000 small molecules, assaying for their ability to induce phenotypic changes in morphology, we identified a (3R)-5-ethyl-5'-(naphthalen-1-yl)-1,2-dihydro-3'H-spiro[indole-3,2'-[1,3,4]thiadiazole]-2-one here in called Ogremorphin, based on the formation of a strip of melanocytes along the dorsal ridge of the embryo.

(Figure 19). In addition to pigmentation defects, Ogremorphin reproducibly induced ventral curvature, wavy notochord, shortened body axis, craniofacial defects, and loss of

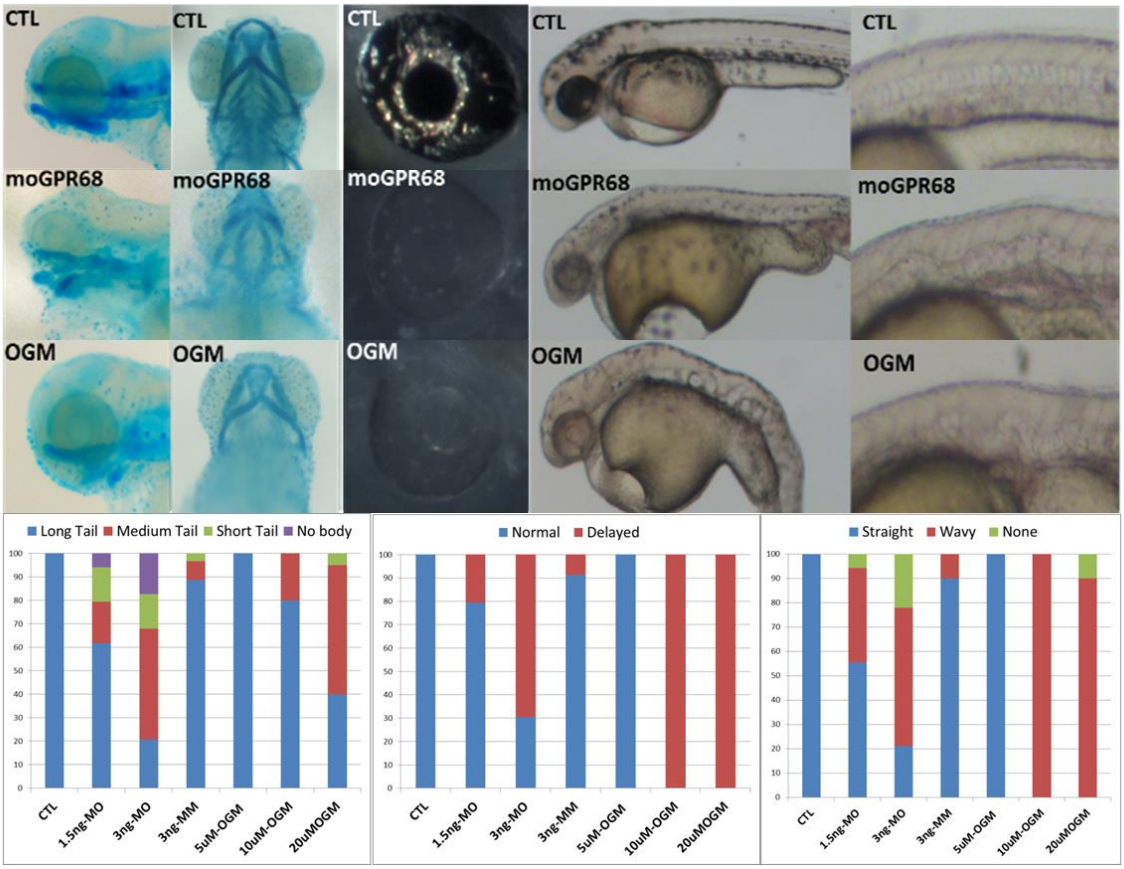

Figure 20 GPR68 knock down phenocopies OGM treatment
Samples: Rows top to bottom; Control embryos, GPR68 morphants, OGM treatment. Phenotypes: columns left to right; Lateral view alcian blue stained 5dpf zebrafish, ventral view of alcian blue stained embryos, retinal iridophores at 3dpf, bright field at 48hpf, bright field of view of notochord at 48 hpf. Bottom row quantification of phenotypes shown above N>100 for each phenotype.

retinal iridophores (Figure 20). The loss of melanophores, iridophores and craniofacial cartilage are consistent abrogation of neural crest development(Kwak et al., 2013). Ogremorphin was assessed for activity against 158 GPCRs based on its chemical structure; in a single point assay and significantly inhibited LPA1, GPR14/UT2R, and GPR68/OGR1 (Figure 21B). Commercially available inhibitors of LPA1 (Ki16425) and GPR14 (SB657510) were both assayed and failed to induce a noticeable phenotype at

concentrations up to 200X the IC50 (Figure 21C). Around a core pharmacophore of Ogremorphin we assayed a series of analogs, and dialed out LPA1 receptor activity (Figure 21). Taken together, the data suggests that inhibition of GPR68 leads to the observed phenotype.

A

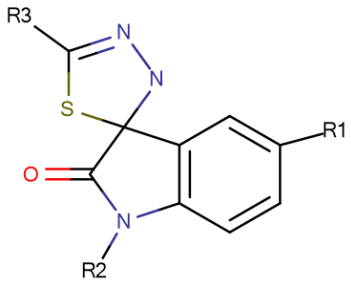

B

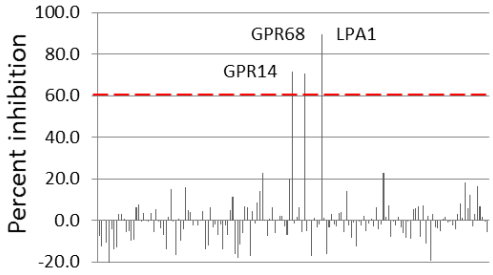

C

ID	R1	R2	R3	Phenotype	GPR68[μM]	LPA1[μM]
1294	H	Methyl	Benz	Y	0.81	----
8437	Methyl	H	Benz	Y	0.76	6.4
8345	Ethyl	H	Benz	Y	0.71	----
2440	Ethyl	H	2-Phen	Y	3.4	1.7
4906	H	Methyl	Napth.	Y	1.5	----
OGM	Ethyl	H	Napth.	Y	0.16	8.7
LPAi	-	-	-	N	-	0.25
UT2i	-	-	-	N	-	-

Figure 21 OGM inhibits GPR68
(A) Core pharmacophore of OGM class (B) GPCRscreen for target identification (C) Small scale SAR and interrogation of targets

Genetic inhibition of GPR68 phenocopies Ogremorphin treatment

Given the chemical evidence that GPR68 inhibition correlated to induction of phenotype, we knocked down GPR68, for which there is only one ortholog in zebrafish.

Increasing doses of GPR68-morpholino induced the same morphological changes as Ogremorphin treatment, namely craniofacial cartilage perturbation, loss of pigmentation and iridophores, and wavy notochord (Figure 20). This data suggests that loss of GPR68 activity is responsible for Ogremorphen induced phenotype in zebrafish.

Molecule	Concentration	Target	Phenotype
DMSO	1%	Vehicle	Normal
Phlorizin	600uM	Na/glucose antagonist	Normal
Bafilomycin	1uM	V-atpase antagonist	Toxic
Concanamycin	1uM	V-atpase antagonist	Toxic
Omeprazole	60uM	H/K atpase antag onist	Phenocopy
Lansoprazole	600uM	H/K atpase antagonist	Phenocopy
EIPA	25uM	NHE antagonist	Developmental delay

Figure 22 H/K ATPase inhibition phenocopies GPR68 inhibition
(Top) Table of H+ extrusion inhibitors and resulting phenotypes. Phlorizin included as a general antiport inhibitor control. (Bottom) Left, Control embryo at 48hpf. Middle, OGM treated embryo, Right, Omeprazole treated embryo

Proton efflux inhibition phenocopies Ogremorphin treatment

GPR68 has been shown to be activated by mild acidification, inactive at pH7.4 but fully active at pH 6.8(Ludwig et al., 2003). Three major proton efflux mechanisms are V-ATPase, H/K ATPase, and NHE. Given these facts we hypothesized that one of these mechanisms lie upstream GPR68 and therefore inhibition of one or more of these mechanisms would result in a similar phenotype. These mechanisms were assayed with by a series of inhibitors and we found that H/K ATPase inhibition, specifically omeprazole and lansoprazole treatments resulted in the same short axis, waxy notochord loss of pigmentation phenotype (Figure 22). As H/K ATPase is an antiporter we show that

blocking other antiport mechanisms such as Na/glucose ATPase does not affect the embryo. Therefore, these results suggest that GPR68 senses protons specifically extruded by H/K-ATPases during development.

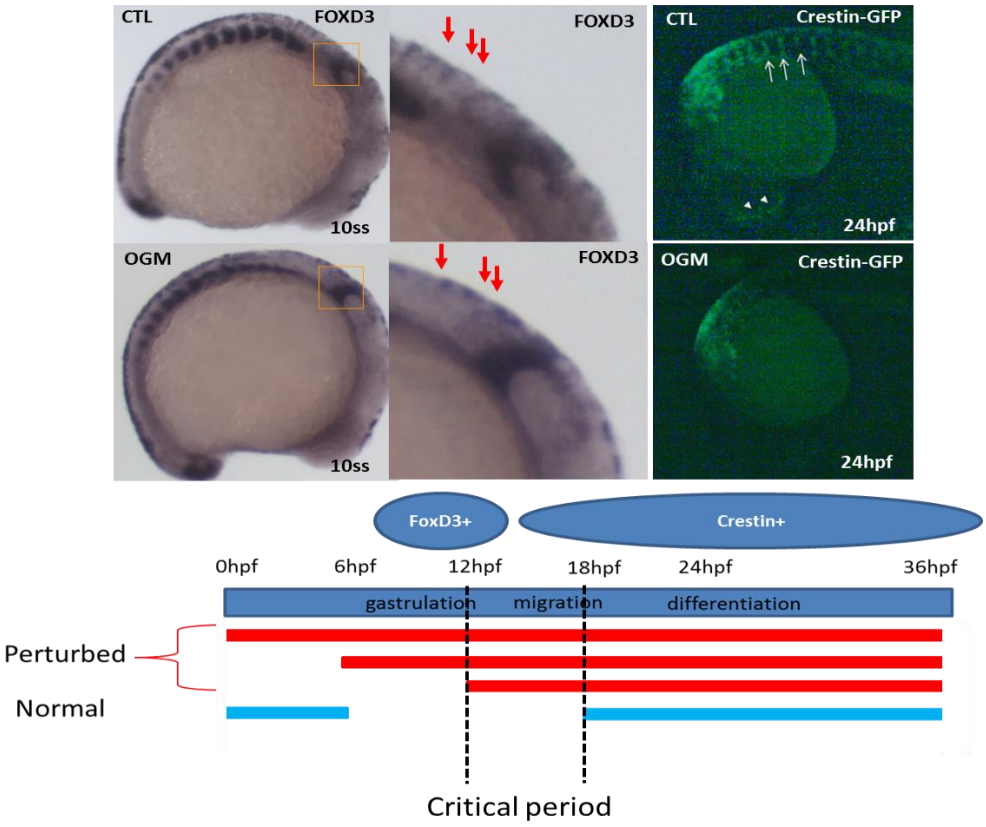

Figure 23 OGM perturbs migration of neural crest cells
(Top) Left, FoxD3 insitu hybridization of CTL and OGM embryos at 10 somite stage. Middle close up of dorsally localized NCC progenitor, OGM progenitors look less ventrally localized. Right, 24hpf embryo expressing Crestin-GFP. OGM embryos have less migratory streams of NCC than CTL.

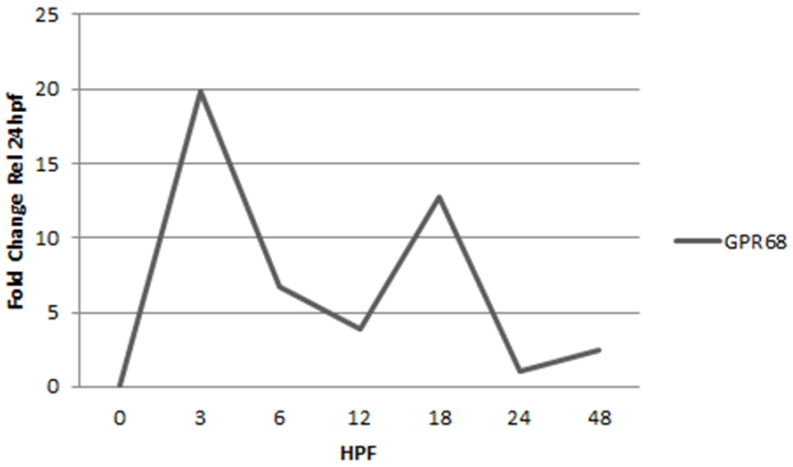

Figure 24 Expression of GPR68 during zebrafish development

Ogremorphen inhibits neural crest migration

Given the perturbations in multiple Neural crest lineages, Ogremorphin could act through altering fate specification of neural crest progenitors. Neural crest are specified through the expression of transcription factor FoxD3(Stewart et al., 2006). FoxD3 expression was comparable in embryos treated with Ogremorphin and control embryos at 10 somite stage (Figure 23). After specification neural crest cell migrate, first ventrally and organized streams and then throughout the rest of the body(Kulesa et al., 2010). These migratory neural crest cells express crestin. Using transgenic crestin:GFP embryos we visualized migration in real time, and found migration severely mitigated in Ogremorphin treated embryos at 24 hpf (Figure 23). This data suggests that GPR68 is necessary for neural crest migration. Leveraging the temporal control that small molecules afford, we inhibited GPR68 in a series of time windows, and determined a critical period for neural crest phenotype to be between 12-18hpf (Figure 23). This window correlates to both the time of neural crest migration and a peak in GPR68 expression

during development (Figure 24). Finally in a scratch assay for migration of human induced pluripotent stem cell (hiPSC)-derived Neural crest cells Ogremorphen treated cells migrated significantly less than the control cells(Figure 25) (Avery and Dalton, 2016). Taken together this data suggests that GPR68 plays a critical role in neural crest migration.

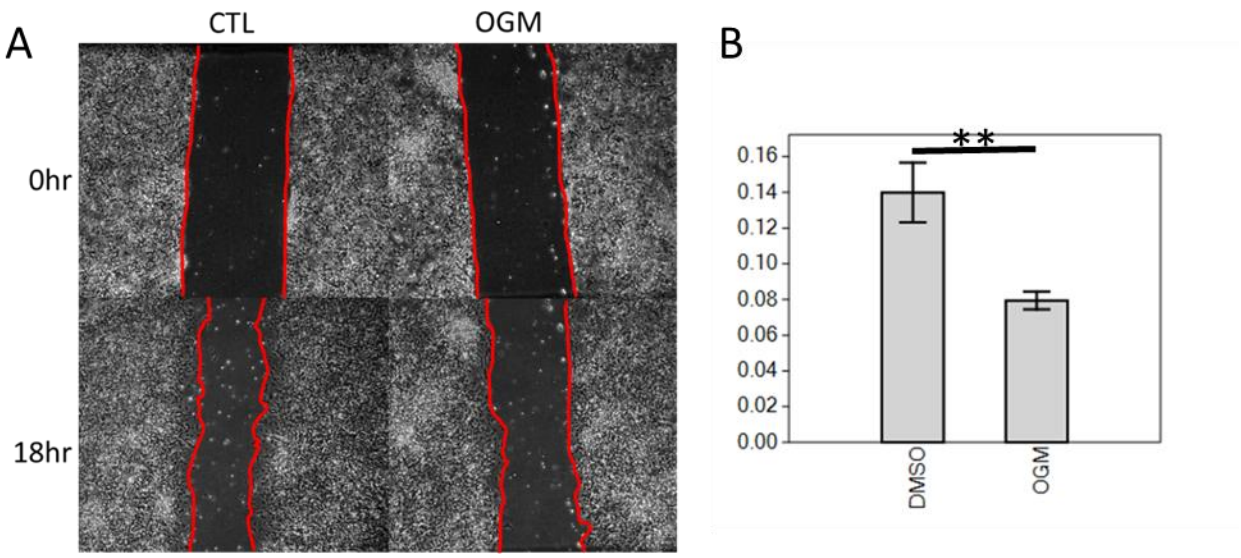

Figure 25 hiPSC NCC migration is abrogated by OGM
*(A) hiPSC-NCC cells were grown to confluence and denuded with p200 tip. Cells were allowed to migrate for 18hours. (B) Quantification of 4 replicates. **P<0.01*

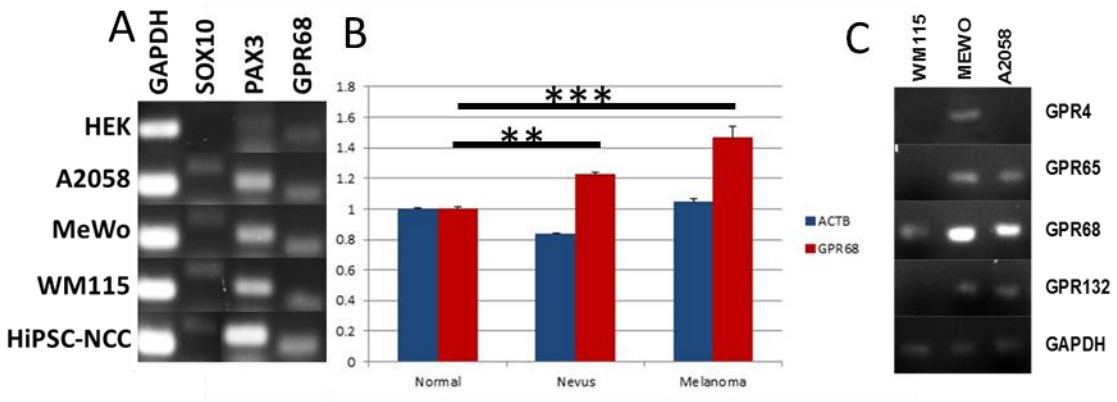

Figure 26 Melanomas express GPR68
*(A) QPCR of neural crest marker SOX10 and PAX3 with GPR68. HiPSC-NCC and melanoma cell lines all express these markers. (B) Data curated from GSE3189. GPR68 expression increases with melanoma progression (C) QPCR of other acid sensing GPRCs in melanoma cell lines ** P<0.01 *** P<0.001*

Ogremorphen inhibits melanoma migration

Numerous parallels are found between neural crest cells and cancer during migration, at the level of expression and behavior(Powell et al., 2013). Having shown a link between GPR68 and neural crest migration, we then examined whether this relationship is retained in human melanoma cell lines. Indeed 3 human melanoma lines A2058, MeWo and WM115 all express neural crest lineage markers, Sox10 and Pax3, and express GPR68(Figure 26). Moreover, it was found that GPR68 expression increases in sequentially in the nevus and melanoma in human melanoma samples(Zhao et al., 2016, GSE3189). Notably GPR68 is the only acid sensing GPCR expressed in all three human cell lines assayed (Figure 26). Behaviorally, it has been shown that transplantation of human SK-Mel 28 melanoma cells into the neural tube of developing embryos causes the cells to migrate along the same streams as the endogenous neural crest cells(Schriek et al., 2005). In a scratch assay for migration of 3 human melanoma cell lines, Ogremorphen treated cells migrated significantly less than the control cells (Figure 27). Furthermore, in a 3D model of melanoma extravasation, Ogremorphen treated WM115 cells migrated significantly less than the control cells (Figure 27). Taken together this data suggests that GPR68 plays a critical role in melanoma migration in vitro.

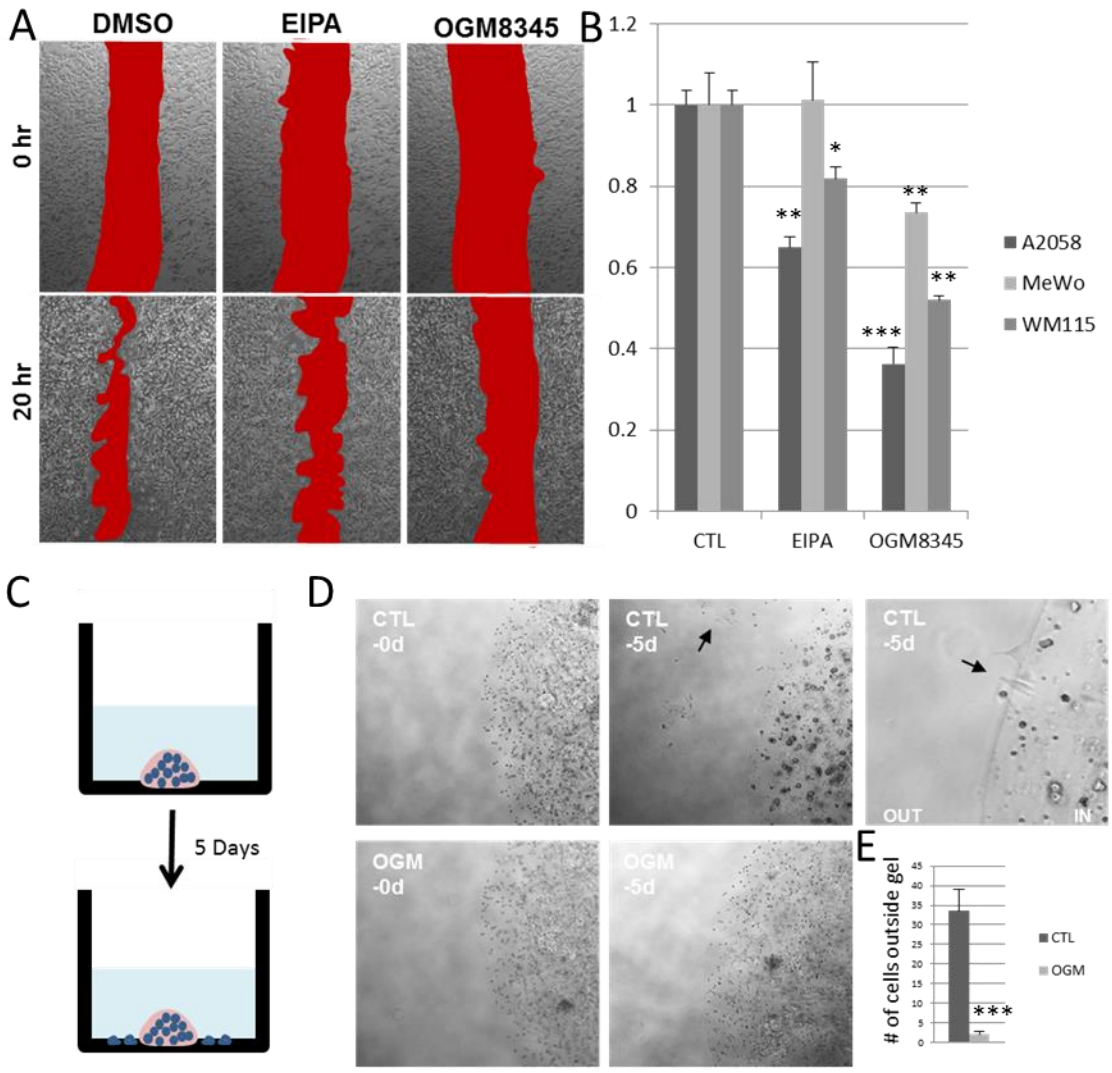

Figure 27 OGM attenuates melanoma migration and extravasation
*(A) Melanoma cell lines cells were grown to confluence and denuded with p200 tip. Cells were allowed to migrate for 18hours in the presence of OGM or EIPA. (B) Quantification of 4 replicates. (C) Schematic of Collagen gel extravasation assay (D) Ctl cells were able to extravasate out of gel readily, OGM treated cell were not able to extravasate (E) Quantitation 4 replicates *P<0.05 **P<0.01 *** P<0.001*

GPR68 regulates cell adhesion

Previous studies in primary human tumor lines showed that acidification of media promotes expression of metastatic factors MMP-2, MMP-9 and IL-8, which are hallmarks of EMT(Rofstad et al., 2006). Therefore, we investigated ogremorphin's affects EMT gene

expression. QPCR of Zeb2, snail2, MMP2, n-cadherin and mmp-9, markers of a mesenchymal cell type were not consistently reduced across cell lines with ogremorphin treatment (Figure 28). To broadly assess transcriptomic changes after 24hours of Ogremorphin treatment, RNAseq was conducted on wm115 cells (Figure 29). This data showed that no epithelial markers increased with 7 out 36 mesenchymal markers decreased more than 1-fold (Figure 30). Pathway analysis of downregulated genes identified significant enrichment in three pathways (-log P <5), ECM-receptor interaction, regulation of actin cytoskeleton, and focal adhesions.

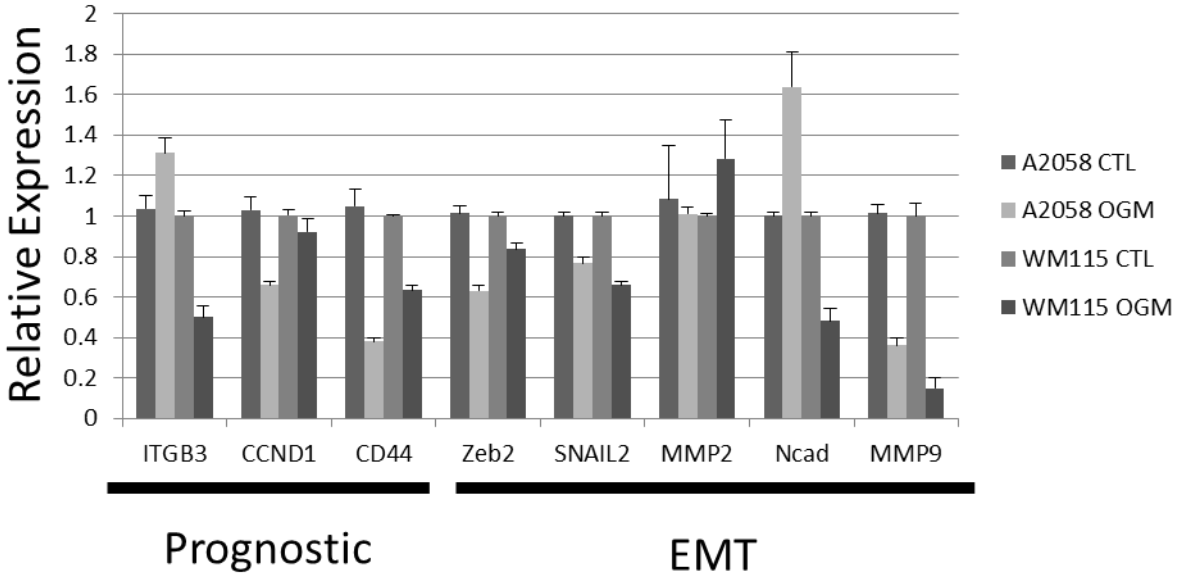

Figure 28 OGM does not act through EMT
QPCR of prognostic markers of Melanoma progression and EMT markers are not consistently reduced with OGM treatment

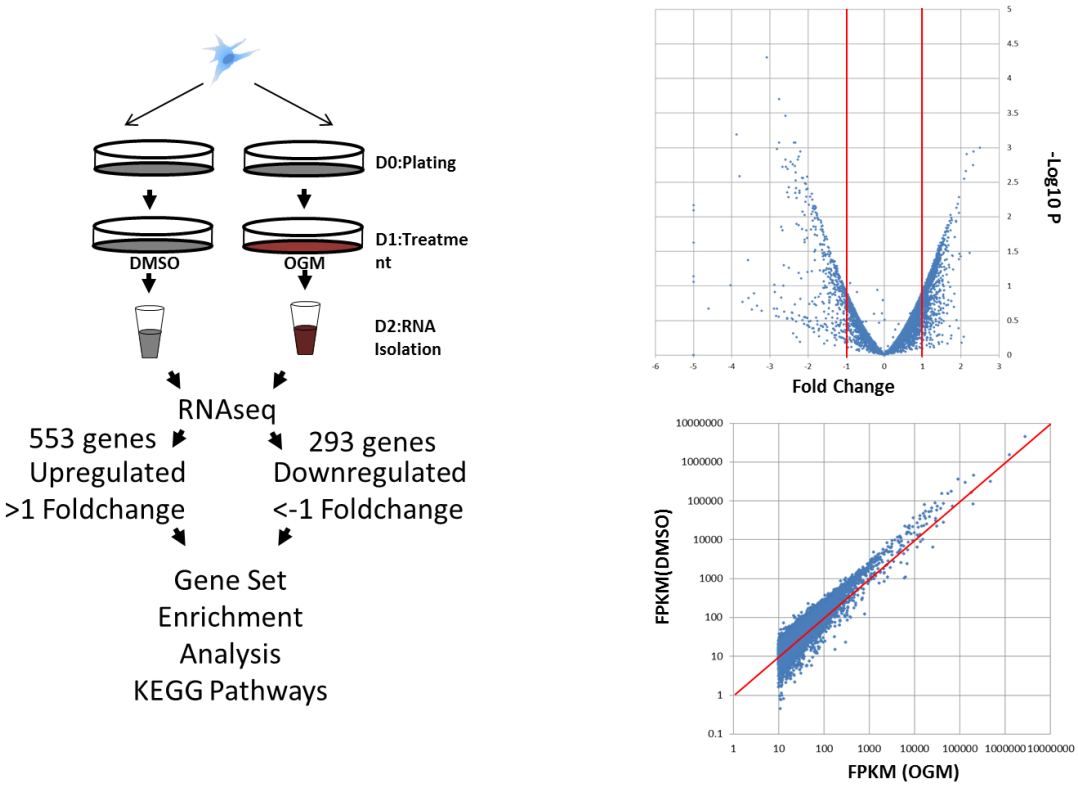

Figure 29 RNAseq of OGM treated WM115

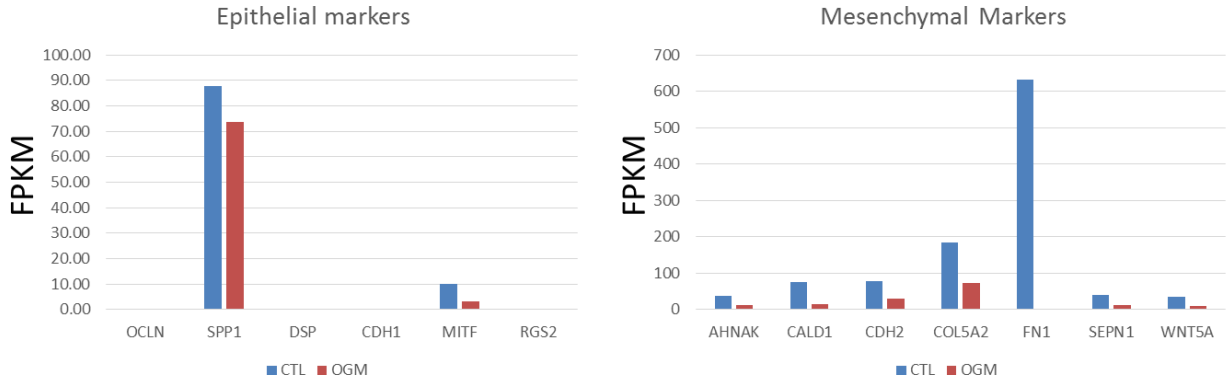

Figure 30 RNAseq results of EMT markers

Term	Count	%	P-Value	Benjamini
ECM-receptor interaction	13	4.4	1.4E-7	1.7E-5
Regulation of actin cytoskeleton	18	6.1	2.1E-6	1.2E-4
Focal adhesion	17	5.8	4.0E-6	1.6E-4
Pathways in cancer	20	6.8	4.8E-5	1.4E-3

Table 2 Pathway Analysis

To confirm an effect of Ogremorphin on cell adhesion, adhesion assays with plastic and fibronectin coated plates in differing pH conditions were carried out. OGM inhibited cell adhesion to fibronectin in acidified media but not pH 7.8 media (Figure 31). Focal adhesions complexes are necessary for adhesion and migration; localization of NHE-1, proton efflux machinery, to focal adhesion complexes has previously been reported(Grinstein et al., 1993; Stüwe et al., 2007a). Given the results above we assayed for formation of FA adhesions in response to acidic pH and GPR68 inhibition. Staining of Paxillin revealed increased focal adhesions in acidified media which was mitigated by Ogremorphin (Figure 31). Taken together, GPR68 regulates focal adhesions to modulate adhesive ability of melanoma cells.

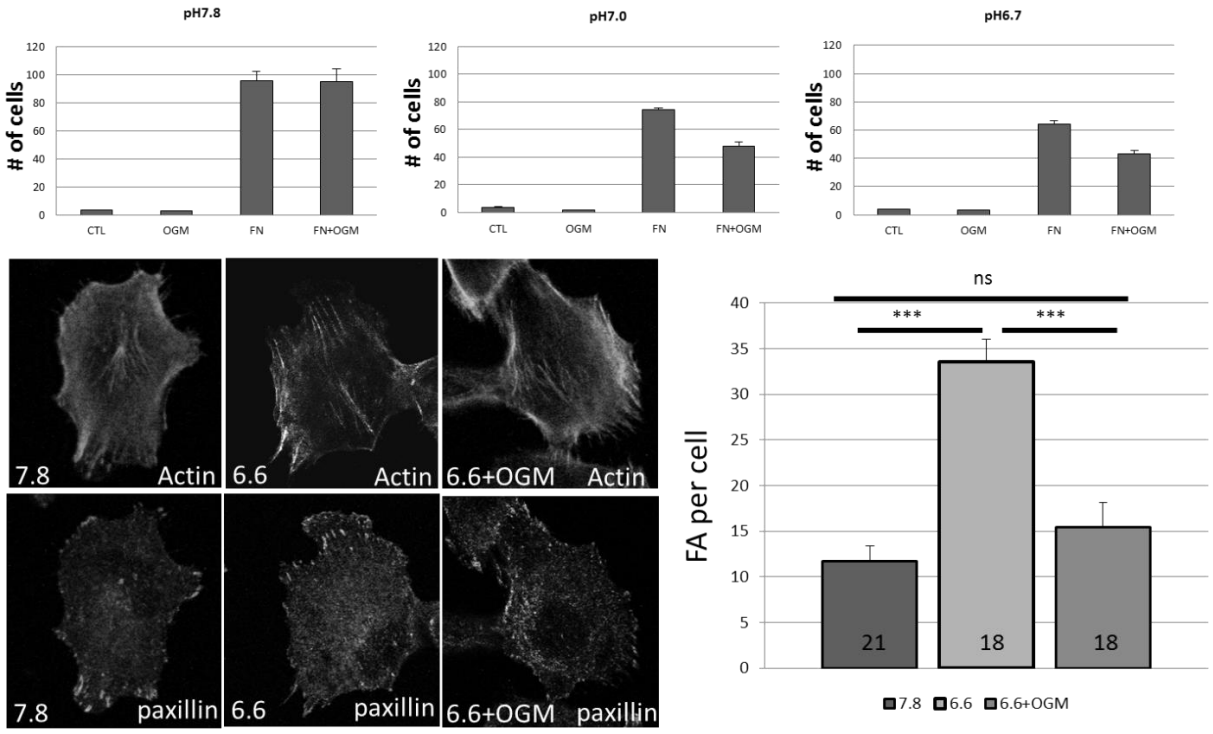

Figure 31 GPR68 modulates Focal adhesion formation
(Top) Number of WM115 cells adherent to 96 well plate after 1 hour with and without Fibronectin coating at varying pH. Total number of cells seeded per well =10,000. OGM Abrogates binding in acidic media. (Bottom left) Immunofluorescence of Actin and focal adhesion marker paxillin. pH 6.6 shows increase in stress fiber like actin bundles and increased paxillin positive loci per cell. This trend is abrogated by OGM (Bottom right) Quantitation of Focal adhesions per cell.

Acidification acutely increases cellular motility through GPR68

Adhesion critically modulates the cellular mechanics of migration. We employed time-lapse microscopy to evaluate the effect of acidification on the velocity of migratory Wm115 cells. 30-minute stimulation of acidic media increased total migratory capacity of cells by 50%, with a corresponding 50% increase in velocity (Figure 32). Additionally, Ogremorphin treatment mitigated the increase in migration and velocity caused by acidification (Figure 32). Following this logic, we hypothesized that GPR68's effect on mobility is through modulation of cellular contraction, and tested it in a collagen gel contraction assay (Figure 32). Stimulation of GPR68 with a published GPR68 agonist

decreased collagen area(Russell et al., 2012). Furthermore, this effect was abrogated with Ogremorphin (Figure 32). Cellular contraction is most proximally mediated through the molecular motor MLC2(Mierke et al., 2008). Notably, MLC2 has also been implicated in focal adhesion maturation(Kuo et al., 2011). To determine if acidification induced mobility is mediated through MLC2, we utilized scratch assays in media pH7.8 and 6.8. Acidification increased the amount of wound closure, this increase in wound closure upon acidification is mitigated in GPR68 (Ogremorphin) and MLC2 (blebbistatin) inhibition, but not mitigated with Rock (Y27632) inhibition (Figure 32). Furthermore, acidification induced phosphorylation of MLC2 which was mitigated by GPR68 inhibition (Figure 32). Based on these results, acid induced GPR68 stimulation promotes phosphorylation of MLC2 and subsequent increase in contraction and mobility.

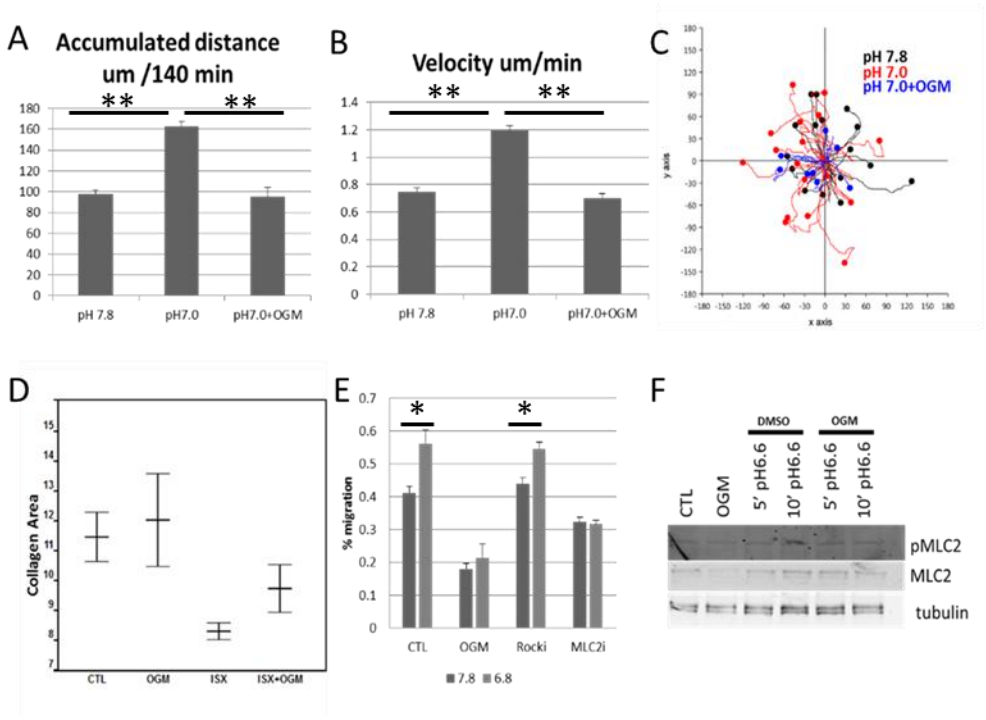

Figure 32 GPR68 stimulates myosin mediated cell contractions
(Top) Migratory behavior of WM115 after 30minute exposure to pH change with or without OGM (A) Quantification of total distance travelled by cells (B) Average velocity of cells during time-lapse. (C) Random selection of paths traveled by WM115 cells in each condition. (D) Collagen gel contraction assay. pH affects rigidity of collagen fibers so small molecule GPR68 agonist was used (E) Quantification of scratch assay conducted with acidic stimulation and inhibitors of Rock and MLC2 (F) Western blot of MLC2 phosphorylation increased after 10minutes of stimulation is abrogated by OGM

GPR68 variants associated with secondary metastasis

Extending the phenotypic discovery of Ogremorphin we hypothesized that variants of human GPR68 that alter the activity could play a disease role in cancer. Deidentified Electronic health records linked to gene sequence information has been used in Phenome-wide association studies(Denny et al., 2016). In a manner inverse to Genome wide association studies, PheWAS allows one to query what phenotypes (expressed as ICD-9 codes) are associated with certain single nucleotide polymorphisms (snps). Querying this database for 6 snps of GPR68, found on the exome chip, and identified 3 variants that were associated with ICD-9 codes (table). These snps rs61745750,

rs61745752, and rs200839166, are coding variants resulting in E330N, E336X and D259N respectively (figure). Notably, secondary malignancy of bone and secondary malignant neoplasm of the liver were signals with P<0.05, and an odds ratio of ~3 for rs61745750, rs61745752 (figure). These two variants exhibit a linkage disequilibrium, and result ultimately in a truncation is on the C-terminal tail of GPR68 (Figure 33). These results suggest that in addition to our in vitro studies that show that GPR68 modulation of in melanoma results in decreased motility, that human variants in GPR68 are linked to a clinical outcome of secondary metastasis.

GPR68 EHR PheWAS

phewas_description	snp		OR	SE	p	allele_freq	carrying_cases	carrying_controls
Cancer of other lymphoid, histiocytic tissue	e330n	rs61745750	2.7973	0.431898	0.017233	0.00137	6	59
Cancer of other lymphoid, histiocytic tissue	e336x	rs61745752	2.792208	0.43191	0.017434	0.001371	6	59
Chronic lymphoid leukemia	e330n	rs61745750	4.283528	0.72349	0.044349	0.001323	2	59
Chronic lymphoid leukemia	e336x	rs61745752	4.259601	0.723504	0.045178	0.001324	2	59
Myeloid leukemia	e336x	rs61745752	4.289663	0.595634	0.014493	0.00134	3	59
Myeloid leukemia	e330n	rs61745750	4.288454	0.595589	0.014505	0.001339	3	59
Myeloid leukemia, acute	e336x	rs61745752	4.761091	0.596056	0.008845	0.001342	3	59
Myeloid leukemia, acute	e330n	rs61745750	4.759119	0.596003	0.008857	0.001341	3	59
Non-Hodgkins lymphoma	e330n	rs61745750	2.522615	0.469207	0.048605	0.001353	5	59
Non-Hodgkins lymphoma	e336x	rs61745752	2.517832	0.46922	0.049075	0.001354	5	59
Prostate cancer	d259d	rs200839166	3.766477	0.663715	0.04571	0.000617	5	23
*Secondary malignancy of bone	e336x	rs61745752	3.005814	0.441537	0.012683	0.001434	6	45
*Secondary malignancy of bone	e330n	rs61745750	3.002216	0.441484	0.01277	0.001433	6	45
*Secondary malignant neoplasm of liver	e336x	rs61745752	3.310794	0.413575	0.003795	0.001459	7	45
*Secondary malignant neoplasm of liver	e330n	rs61745750	3.30349	0.413499	0.003853	0.001458	7	45

Table 3 Cancer related PhEWAS for GPR68 using BioVU database

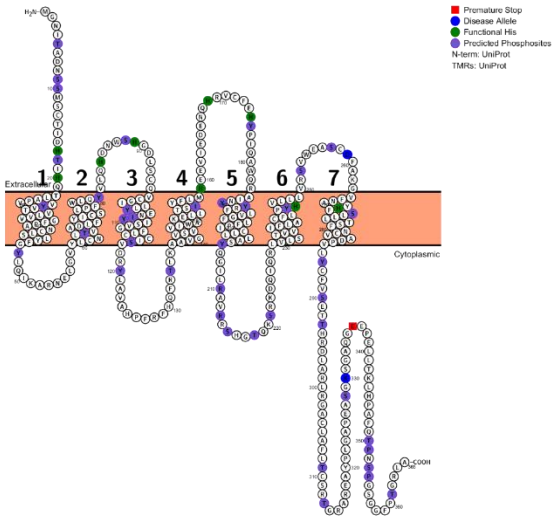

Figure 33 Schematic of coding variants of GPR68 associated with cancer in EHR

Discussion

A close correlation exists between acidosis, as measured by fetal blood pH, and clinical outcome and low Apgar score(Omo-Aghoja, 2014). However, few studies have investigated the role of pH regulation in development. Notably, H+-V-ATPase perturbation has been shown to be critical for development of the posterior part of the embryo, craniofacial morphogenesis, and establishment of right-left asymmetry in xenopus(Adams et al., 2006; Gutknecht et al., 1995; Uzman et al., 1998; Vandenberg et al., 2011). However, how these effluxes are translated into a cellular response is not well understood. In our current study, we show that genetic and pharmacologic inhibition of GPR68 abrogates the neural crest cell migration in zebrafish, furthermore, that this mechanism is present in hiPSC-NCC. We show that, omeprazol and lansoprazole, inhibitors of H+/K+-ATPase, phenocopy GPR68 inhibition. Taken together, this data suggests that neural crest cell migration is dependent on GPR68 sensing protons extruded via H+/K+-ATPase.

Targeting proton dynamics, and the dysregulation of pH has emerged as a possible therapeutic avenue for cancer(Parks et al., 2013; Webb et al., 2011). As mentioned above, acidification promotes tumor malignancy, including metabolic reprogramming and invasiveness, (Justus et al., 2013; Webb et al., 2011). GPR68, when overexpressed in PC3 prostate cancer cells have significantly reduced metastasis.(Singh et al., 2007). Furthermore, in ovarian cancer cells HEY1, overexpression of GPR68 reduced cell migration and increased cell adhesion (Ren and Zhang, 2011). The conclusions drawn from these overexpression studies suggest that GPR68 is a tumor metastasis suppressor. Based on our mechanistic studies, GPR68 does play a critical role in establishing strong ECM contacts under acidified conditions, concurrent with previous studies. However, we also found that these strengthened contacts correlate with increased velocity in Wm115 and with contractile ability of cells in collagen gel assay. Our data suggests that GPR68 activation creates stronger extracellular contacts through focal adhesion complex formation and MLC2 phosphorylation, which increases cellular motility of melanoma. In contrast to previous overexpression studies we examine the role of GPR68 at its basal level, and modulate the activity through acidification and small molecule inhibition with ogremorphin. Membrane proteins in particular are susceptible to generating artifacts through a number of possible mechanisms including activation in the wrong cellular domain and saturation of the proper membrane localization. Recent studies have implicated that proton efflux forms an acidic microenvironment along the leading edge of migrating melanoma cell line MV3(Stock et al., 2007; Stüwe et al., 2007b). Therefore a localized activation of GPR68 along the leading edge of could be convoluted in overexpression experiments by causing increased adhesion through out the cell and

not just the leading edge, thereby skewing interpretation of the results. Notably, GPR68 appears to play a multifaceted role during tumor metastasis, as activity of GPR68 in the host environment is also critical for tumor metastasis in both prostate and melanoma models (Li et al., 2009; Yan et al., 2014). Therefore, based on our data from ogremorphen's activity on human melanoma in vitro, we propose that GPR68 is a chemically tractable target for inhibition of tumor metastasis.

Using an unbiased *in vivo* chemical genetic screen for small molecule modulators of embryonic development, we identified ogremorphin, a first in class inhibitor of proton sensing GPR68 and used it as a probe to elucidate a novel role for GPR68 in regulation of neural crest migration in zebrafish. This inhibitory activity correlated with attenuated migratory capacity in human neural crest cells and human melanoma cell lines in vitro. Finally, an unbiased computational platform with EHR-genotype records identified rare, potentially functional SNPs that increase odds of tumor metastasis. Our study highlights not only a novel therapeutic strategy that exploits the role of GPR68 in melanoma migration, but a phenotype driven discovery platform that leverages the emergent technologies of whole organism based zebrafish screens and human biology of phenome wide association studies.

CHAPTER 6

SUMMARY AND FUTURE DIRECTIONS

The vision of chemical biology is to develop potent and specific small molecule inhibitors for every chemically tractable protein. A targeted, linear approach requires vast amounts of time, man power and expertise. Alternatively, a shotgun approach of targeting developmental pathways during zebrafish development provides a massively parallel system, allowing a “shot gun” approach to discovery. For unbiased screens to reach their full potential, a multiplex approach to target identification should also be taken. The objective of this body of work was to contribute to the pursuit of developing chemical tools for interrogation of novel biology by advancing the use of whole organism screening and phenoclustering for target identification. Through the experiments described in this dissertation, we have advanced multiple fields of biology in multiple ways:

(1) Identification of 3 new molecular tools for interrogation of targets.

(2) Identified a new component of hedgehog signaling

(3) Developed a framework for phenoclustering for parallel target deconvolution

(4) Identified and interrogated developmental role of GPR68 during neural crest development in zebrafish

(5) Show that GPR68 could be a therapeutically tractable target for anti-metastatic molecules

This work generates a plethora of questions the:

(1) How does inhibition of PDE4 with EGM cause selective activation of PKA at the basal body?

(2) Is the mechanism of action for EGM only through PDE4?

(3) How is specificity of CK2α achieved given its exquisite selectivity?

(4) How does CK2α modulate translocation of B-catenin to the nucleus?

(5) Can we expand our phenocluster database in an unbiased fashion for better elucidation of target mechanisms?

(6) Does GPR68 really sense protons gradients in vivo? Where are they coming from?

(7) Can OGM prevent metastasis in vivo?

(8) What are the functional consequences of GPR68 variants?

(9) What proportion of zebrafish active compounds have conserved activity in human systems?

(10) Can phenotype guided discovery efforts be translated in a private sector environment by the pharmaceutical industry?

REFERENCES

Aberle, H., Bauer, A., Stappert, J., Kispert, A., and Kemler, R. (1997). beta-catenin is a target for the ubiquitin-proteasome pathway. EMBO J. *16*, 3797–3804.

Adams, D.S., Robinson, K.R., Fukumoto, T., Yuan, S., Albertson, R.C., Yelick, P., Kuo, L., McSweeney, M., and Levin, M. (2006). Early, H+-V-ATPase-dependent proton flux is necessary for consistent left-right patterning of non-mammalian vertebrates. Dev. Camb. Engl. *133*, 1657–1671.

Arce, L., Yokoyama, N.N., and Waterman, M.L. (2006). Diversity of LEF/TCF action in development and disease. Oncogene *25*, 7492–7504.

Ashihara, E., Takada, T., and Maekawa, T. (2015). Targeting the canonical Wnt/β-catenin pathway in hematological malignancies. Cancer Sci. *106*, 665–671.

Avery, J., and Dalton, S. (2016). Methods for Derivation of Multipotent Neural Crest Cells Derived from Human Pluripotent Stem Cells. Methods Mol. Biol. Clifton NJ *1341*, 197–208.

Baig-Lewis, S., Peterson-Nedry, W., and Wehrli, M. (2007). Wingless/Wnt signal transduction requires distinct initiation and amplification steps that both depend on Arrow/LRP. Dev. Biol. *306*, 94–111.

Barresi, M.J., Stickney, H.L., and Devoto, S.H. (2000). The zebrafish slow-muscle-omitted gene product is required for Hedgehog signal transduction and the development of slow muscle identity. Dev. Camb. Engl. *127*, 2189–2199.

Barua, A.C., Deka, P., and Das, B.N. (1979). Clinical trial of piperazine hydrate and pyrvinium pamoate in ascariasis and oxyuriasis infestation. Indian J. Pediatr. *46*, 182–186.

Becker, J.R., Robinson, T.Y., Sachidanandan, C., Kelly, A.E., Coy, S., Peterson, R.T., and MacRae, C.A. (2012). In vivo natriuretic peptide reporter assay identifies chemical modifiers of hypertrophic cardiomyopathy signalling. Cardiovasc. Res. *93*, 463–470.

Behrens, J., von Kries, J.P., Kühl, M., Bruhn, L., Wedlich, D., Grosschedl, R., and Birchmeier, W. (1996). Functional interaction of beta-catenin with the transcription factor LEF-1. Nature *382*, 638–642.

Bhanot, P., Brink, M., Samos, C.H., Hsieh, J.C., Wang, Y., Macke, J.P., Andrew, D., Nathans, J., and Nusse, R. (1996). A new member of the frizzled family from Drosophila functions as a Wingless receptor. Nature *382*, 225–230.

Bodmer, W.F. (2006). Cancer genetics: colorectal cancer as a model. J. Hum. Genet. *51*, 391–396.

Boulton, S.J., Gartner, A., Reboul, J., Vaglio, P., Dyson, N., Hill, D.E., and Vidal, M. (2002). Combined functional genomic maps of the C. elegans DNA damage response. Science *295*, 127–131.

Bracken, M.B. (2009). Why animal studies are often poor predictors of human reactions to exposure. J. R. Soc. Med. *102*, 120–122.

Brand, J., Smith, E.S.J., Schwefel, D., Lapatsina, L., Poole, K., Omerbasic, D., Kozlenkov, A., Behlke, J., Lewin, G.R., and Daumke, O. (2012). A stomatin dimer modulates the activity of acid-sensing ion channels. EMBO J. *31*, 3635–3646.

Brinkhuizen, T., Reinders, M.G., van Geel, M., Hendriksen, A.J.L., Paulussen, A.D.C., Winnepenninckx, V.J., Keymeulen, K.B., Soetekouw, P.M.M.B., van Steensel, M.A.M., and Mosterd, K. (2014). Acquired resistance to the Hedgehog pathway inhibitor vismodegib due to smoothened mutations in treatment of locally advanced basal cell carcinoma. J. Am. Acad. Dermatol. *71*, 1005–1008.

Bruni, G., Rennekamp, A.J., Velenich, A., McCarroll, M., Gendelev, L., Fertsch, E., Taylor, J., Lakhani, P., Lensen, D., Evron, T., et al. (2016). Zebrafish behavioral profiling identifies multitarget antipsychotic-like compounds. Nat. Chem. Biol. *12*, 559–566.

Burkhardt, M.F., Martinez, F.J., Wright, S., Ramos, C., Volfson, D., Mason, M., Garnes, J., Dang, V., Lievers, J., Shoukat-Mumtaz, U., et al. (2013). A cellular model for sporadic ALS using patient-derived induced pluripotent stem cells. Mol. Cell. Neurosci. *56*, 355–364.

Burns, C.G., Milan, D.J., Grande, E.J., Rottbauer, W., MacRae, C.A., and Fishman, M.C. (2005). High-throughput assay for small molecules that modulate zebrafish embryonic heart rate. Nat. Chem. Biol. *1*, 263–264.

Cadigan, K.M., and Nusse, R. (1996). wingless signaling in the Drosophila eye and embryonic epidermis. Dev. Camb. Engl. *122*, 2801–2812.

Canada, B.A., Thomas, G.K., Cheng, K.C., and Wang, J.Z. (2011). SHIRAZ: an automated histology image annotation system for zebrafish phenomics. Multimed. Tools Appl. *51*, 401–440.

Carney, T.J., and Ingham, P.W. (2013). Drugging Hedgehog: signaling the pathway to translation. BMC Biol. *11*, 37.

Caspary, T., García-García, M.J., Huangfu, D., Eggenschwiler, J.T., Wyler, M.R., Rakeman, A.S., Alcorn, H.L., and Anderson, K.V. (2002). Mouse Dispatched homolog1 is required for long-range, but not juxtacrine, Hh signaling. Curr. Biol. CB *12*, 1628–1632.

Chamoun, Z., Mann, R.K., Nellen, D., von Kessler, D.P., Bellotto, M., Beachy, P.A., and Basler, K. (2001). Skinny hedgehog, an acyltransferase required for palmitoylation and activity of the hedgehog signal. Science *293*, 2080–2084.

Chang, A.L.S., and Oro, A.E. (2012). Initial Assessment of Tumor Regrowth After Vismodegib in Advanced Basal Cell Carcinoma. Arch. Dermatol. *148*, 1324–1325.

Chen, J.K. (2016). I only have eye for ewe: the discovery of cyclopamine and development of Hedgehog pathway-targeting drugs. Nat. Prod. Rep. *33*, 595–601.

Chen, A., Dong, L., Leffler, N.R., Asch, A.S., Witte, O.N., and Yang, L.V. (2011). Activation of GPR4 by acidosis increases endothelial cell adhesion through the cAMP/Epac pathway. PloS One *6*, e27586.

Chen, B., Dodge, M.E., Tang, W., Lu, J., Ma, Z., Fan, C.-W., Wei, S., Hao, W., Kilgore, J., Williams, N.S., et al. (2009a). Small molecule-mediated disruption of Wnt-dependent signaling in tissue regeneration and cancer. Nat. Chem. Biol. *5*, 100–107.

Chen, J.K., Taipale, J., Cooper, M.K., and Beachy, P.A. (2002). Inhibition of Hedgehog signaling by direct binding of cyclopamine to Smoothened. Genes Dev. *16*, 2743–2748.

Chen, L., Ren, X., Liang, F., Li, S., Zhong, H., and Lin, S. (2012). Characterization of two novel small molecules targeting melanocyte development in zebrafish embryogenesis. Pigment Cell Melanoma Res. *25*, 446–453.

Chen, M.-H., Wilson, C.W., Li, Y.-J., Law, K.K.L., Lu, C.-S., Gacayan, R., Zhang, X., Hui, C., and Chuang, P.-T. (2009b). Cilium-independent regulation of Gli protein function by Sufu in Hedgehog signaling is evolutionarily conserved. Genes Dev. *23*, 1910–1928.

Cheng, C., Yang, H.-W., Shang, J.-F., Li, W.-W., Sun, Q.-Z., Chen, X., Cao, Z.-X., Yao, S.-H., and Yang, S.-Y. (2016). Identification of a small molecule that downregulates MITF expression and mediates antimelanoma activity in vitro. Melanoma Res. *26*, 117–124.

Cheng, T., Li, Q., Wang, Y., and Bryant, S.H. (2011). Identifying Compound-Target Associations by Combining Bioactivity Profile Similarity Search and Public Databases Mining. J. Chem. Inf. Model. *51*, 2440–2448.

Cherny, V.V., Markin, V.S., and DeCoursey, T.E. (1995). The voltage-activated hydrogen ion conductance in rat alveolar epithelial cells is determined by the pH gradient. J. Gen. Physiol. *105*, 861–896.

Cianciolo Cosentino, C., Skrypnyk, N.I., Brilli, L.L., Chiba, T., Novitskaya, T., Woods, C., West, J., Korotchenko, V.N., McDermott, L., Day, B.W., et al. (2013). Histone Deacetylase Inhibitor Enhances Recovery after AKI. J. Am. Soc. Nephrol. JASN *24*, 943–953.

Clevers, H. (2006). Wnt/beta-catenin signaling in development and disease. Cell *127*, 469–480.

Cohen, J., Pertsemlidis, A., Kotowski, I.K., Graham, R., Garcia, C.K., and Hobbs, H.H. (2005). Low LDL cholesterol in individuals of African descent resulting from frequent nonsense mutations in PCSK9. Nat. Genet. *37*, 161–165.

Cohen, J.C., Boerwinkle, E., Mosley, T.H., and Hobbs, H.H. (2006). Sequence variations in PCSK9, low LDL, and protection against coronary heart disease. N. Engl. J. Med. *354*, 1264–1272.

Colanesi, S., Taylor, K.L., Temperley, N.D., Lundegaard, P.R., Liu, D., North, T.E., Ishizaki, H., Kelsh, R.N., and Patton, E.E. (2012). Small molecule screening identifies targetable zebrafish pigmentation pathways. Pigment Cell Melanoma Res. *25*, 131–143.

Concordet, J.P., Lewis, K.E., Moore, J.W., Goodrich, L.V., Johnson, R.L., Scott, M.P., and Ingham, P.W. (1996). Spatial regulation of a zebrafish patched homologue reflects the roles of sonic hedgehog and protein kinase A in neural tube and somite patterning. Dev. Camb. Engl. *122*, 2835–2846.

Corbit, K.C., Aanstad, P., Singla, V., Norman, A.R., Stainier, D.Y.R., and Reiter, J.F. (2005). Vertebrate Smoothened functions at the primary cilium. Nature *437*, 1018–1021.

Cozza, G., Meggio, F., and Moro, S. (2011). The dark side of protein kinase CK2 inhibition. Curr. Med. Chem. *18*, 2867–2884.

Daniels, D.L., and Weis, W.I. (2005). Beta-catenin directly displaces Groucho/TLE repressors from Tcf/Lef in Wnt-mediated transcription activation. Nat. Struct. Mol. Biol. *12*, 364–371.

Davidson, G., Wu, W., Shen, J., Bilic, J., Fenger, U., Stannek, P., Glinka, A., and Niehrs, C. (2005). Casein kinase 1 gamma couples Wnt receptor activation to cytoplasmic signal transduction. Nature *438*, 867–872.

Dennler, S., André, J., Alexaki, I., Li, A., Magnaldo, T., ten Dijke, P., Wang, X.-J., Verrecchia, F., and Mauviel, A. (2007). Induction of sonic hedgehog mediators by transforming growth factor-beta: Smad3-dependent activation of Gli2 and Gli1 expression in vitro and in vivo. Cancer Res. *67*, 6981–6986.

Denny, J.C., Bastarache, L., and Roden, D.M. (2016). Phenome-Wide Association Studies as a Tool to Advance Precision Medicine. Annu. Rev. Genomics Hum. Genet.

Dominguez, I., Mizuno, J., Wu, H., Song, D.H., Symes, K., and Seldin, D.C. (2004). Protein kinase CK2 is required for dorsal axis formation in Xenopus embryos. Dev. Biol. *274*, 110–124.

Duncan, J.S., Gyenis, L., Lenehan, J., Bretner, M., Graves, L.M., Haystead, T.A., and Litchfield, D.W. (2008). An unbiased evaluation of CK2 inhibitors by chemoproteomics: characterization of inhibitor effects on CK2 and identification of novel inhibitor targets. Mol. Cell. Proteomics MCP *7*, 1077–1088.

Duraiswamy, A.J., Lee, M.A., Madan, B., Ang, S.H., Tan, E.S.W., Cheong, W.W.V., Ke, Z., Pendharkar, V., Ding, L.J., Chew, Y.S., et al. (2015). Discovery and Optimization of a Porcupine Inhibitor. J. Med. Chem. *58*, 5889–5899.

Echelard, Y., Epstein, D.J., St-Jacques, B., Shen, L., Mohler, J., McMahon, J.A., and McMahon, A.P. (1993). Sonic hedgehog, a member of a family of putative signaling molecules, is implicated in the regulation of CNS polarity. Cell *75*, 1417–1430.

van Eeden, F.J., Granato, M., Schach, U., Brand, M., Furutani-Seiki, M., Haffter, P., Hammerschmidt, M., Heisenberg, C.P., Jiang, Y.J., Kane, D.A., et al. (1996a). Mutations affecting somite formation and patterning in the zebrafish, Danio rerio. Dev. Camb. Engl. *123*, 153–164.

van Eeden, F.J., Granato, M., Schach, U., Brand, M., Furutani-Seiki, M., Haffter, P., Hammerschmidt, M., Heisenberg, C.P., Jiang, Y.J., Kane, D.A., et al. (1996b). Genetic analysis of fin formation in the zebrafish, Danio rerio. Dev. Camb. Engl. *123*, 255–262.

Emami, K.H., Nguyen, C., Ma, H., Kim, D.H., Jeong, K.W., Eguchi, M., Moon, R.T., Teo, J.-L., Oh, S.W., Kim, H.Y., et al. (2004). A small molecule inhibitor of beta-catenin/CREB-binding protein transcription [corrected]. Proc. Natl. Acad. Sci. U. S. A. *101*, 12682–12687.

Fan, H., Oro, A.E., Scott, M.P., and Khavari, P.A. (1997). Induction of basal cell carcinoma features in transgenic human skin expressing Sonic Hedgehog. Nat. Med. *3*, 788–792.

Fate Therapeutics (2016). Fate Therapeutics Provides Update on Adoptive Immunotherapy Programs for Hematopoietic Cell Transplantation (NASDAQ:FATE).

Fecher, L.A., and Sharfman, W.H. (2015). Advanced basal cell carcinoma, the hedgehog pathway, and treatment options – role of smoothened inhibitors. Biol. Targets Ther. *9*, 129–140.

Firestone, A.J., Weinger, J.S., Maldonado, M., Barlan, K., Langston, L.D., O'Donnell, M., Gelfand, V.I., Kapoor, T.M., and Chen, J.K. (2012). Small-molecule inhibitors of the AAA+ ATPase motor cytoplasmic dynein. Nature *484*, 125–129.

Fuchs, F., and Boutros, M. (2006). Cellular phenotyping by RNAi. Brief. Funct. Genomic. Proteomic. *5*, 52–56.

Fujii, N., You, L., Xu, Z., Uematsu, K., Shan, J., He, B., Mikami, I., Edmondson, L.R., Neale, G., Zheng, J., et al. (2007). An Antagonist of Dishevelled Protein-Protein Interaction Suppresses β-Catenin–Dependent Tumor Cell Growth. Cancer Res. *67*, 573–579.

Galli, L.M., Barnes, T.L., Secrest, S.S., Kadowaki, T., and Burrus, L.W. (2007). Porcupine-mediated lipid-modification regulates the activity and distribution of Wnt proteins in the chick neural tube. Development *134*, 3339–3348.

Glitsch, M. (2011). Protons and Ca2+: Ionic Allies in Tumor Progression? Physiology *26*, 252–265.

Goldhoff, P., Warrington, N.M., Limbrick, D.D., Jr, Hope, A., Woerner, B.M., Jackson, E., Perry, A., Piwnica-Worms, D., and Rubin, J.B. (2008). Targeted inhibition of cyclic AMP phosphodiesterase-4 promotes brain tumor regression. Clin. Cancer Res. Off. J. Am. Assoc. Cancer Res. *14*, 7717–7725.

Gomm, W., von Holt, K., Thomé, F., Broich, K., Maier, W., Fink, A., Doblhammer, G., and Haenisch, B. (2016). Association of Proton Pump Inhibitors With Risk of Dementia: A Pharmacoepidemiological Claims Data Analysis. JAMA Neurol. *73*, 410–416.

Gong, S.-G. (2014). Cranial neural crest: migratory cell behavior and regulatory networks. Exp. Cell Res. *325*, 90–95.

Grandy, D., Shan, J., Zhang, X., Rao, S., Akunuru, S., Li, H., Zhang, Y., Alpatov, I., Zhang, X.A., Lang, R.A., et al. (2009). Discovery and Characterization of a Small Molecule Inhibitor of the PDZ Domain of Dishevelled. J. Biol. Chem. *284*, 16256–16263.

Grinstein, S., Woodside, M., Waddell, T.K., Downey, G.P., Orlowski, J., Pouyssegur, J., Wong, D.C., and Foskett, J.K. (1993). Focal localization of the NHE-1 isoform of the Na+/H+ antiport: assessment of effects on intracellular pH. EMBO J. *12*, 5209–5218.

Gross, J.C., Chaudhary, V., Bartscherer, K., and Boutros, M. (2012). Active Wnt proteins are secreted on exosomes. Nat. Cell Biol. *14*, 1036–1045.

Guissart, C., Li, X., Leheup, B., Drouot, N., Montaut-Verient, B., Raffo, E., Jonveaux, P., Roux, A.-F., Claustres, M., Fliegel, L., et al. (2015). Mutation of SLC9A1, encoding the major Na^+/H^+ exchanger, causes ataxia-deafness Lichtenstein-Knorr syndrome. Hum. Mol. Genet. *24*, 463–470.

Gurney, A., Axelrod, F., Bond, C.J., Cain, J., Chartier, C., Donigan, L., Fischer, M., Chaudhari, A., Ji, M., Kapoun, A.M., et al. (2012). Wnt pathway inhibition via the targeting of Frizzled

receptors results in decreased growth and tumorigenicity of human tumors. Proc. Natl. Acad. Sci. U. S. A. *109*, 11717–11722.

Gutknecht, D.R., Koster, C.H., Tertoolen, L.G., de Laat, S.W., and Durston, A.J. (1995). Intracellular acidification of gastrula ectoderm is important for posterior axial development in Xenopus. Dev. Camb. Engl. *121*, 1911–1925.

Haffter, P., Granato, M., Brand, M., Mullins, M.C., Hammerschmidt, M., Kane, D.A., Odenthal, J., Eeden, F.J. van, Jiang, Y.J., Heisenberg, C.P., et al. (1996). The identification of genes with unique and essential functions in the development of the zebrafish, Danio rerio. Development *123*, 1–36.

Han, L., Wang, Y., and Bryant, S.H. (2009). A survey of across-target bioactivity results of small molecules in PubChem. Bioinformatics *25*, 2251–2255.

Hanna, A., and Shevde, L.A. (2016). Hedgehog signaling: modulation of cancer properies and tumor mircroenvironment. Mol. Cancer *15*.

Hao, J., Williams, C.H., Webb, M.E., and Hong, C.C. (2010a). Large scale zebrafish-based in vivo small molecule screen. J. Vis. Exp. JoVE.

Hao, J., Ho, J.N., Lewis, J.A., Karim, K.A., Daniels, R.N., Gentry, P.R., Hopkins, C.R., Lindsley, C.W., and Hong, C.C. (2010b). In vivo structure-activity relationship study of dorsomorphin analogues identifies selective VEGF and BMP inhibitors. ACS Chem. Biol. *5*, 245–253.

Hao, J., Ao, A., Zhou, L., Murphy, C.K., Frist, A.Y., Keel, J.J., Thorne, C.A., Kim, K., Lee, E., and Hong, C.C. (2013). Selective small molecule targeting β-catenin function discovered by in vivo chemical genetic screen. Cell Rep. *4*, 898–904.

Hausmann, G., Bänziger, C., and Basler, K. (2007). Helping Wingless take flight: how WNT proteins are secreted. Nat. Rev. Mol. Cell Biol. *8*, 331–336.

Heemstra, H.E., van Weely, S., Büller, H.A., Leufkens, H.G.M., and de Vrueh, R.L.A. (2009). Translation of rare disease research into orphan drug development: disease matters. Drug Discov. Today *14*, 1166–1173.

Herr, P., and Basler, K. (2012). Porcupine-mediated lipidation is required for Wnt recognition by Wls. Dev. Biol. *361*, 392–402.

van den Heuvel, M., Klingensmith, J., Perrimon, N., and Nusse, R. (1993). Cell patterning in the Drosophila segment: engrailed and wingless antigen distributions in segment polarity mutant embryos. Dev. Camb. Engl. Suppl. 105–114.

Hirsinger, E., Stellabotte, F., Devoto, S.H., and Westerfield, M. (2004). Hedgehog signaling is required for commitment but not initial induction of slow muscle precursors. Dev. Biol. *275*, 143–157.

Hollway, G.E., Maule, J., Gautier, P., Evans, T.M., Keenan, D.G., Lohs, C., Fischer, D., Wicking, C., and Currie, P.D. (2006). Scube2 mediates Hedgehog signalling in the zebrafish embryo. Dev. Biol. *294*, 104–118.

Hong, C.C., and Yu, P.B. (2009). Applications of small molecule BMP inhibitors in physiology and disease. Cytokine Growth Factor Rev. *20*, 409–418.

Hover, L.D., Young, C.D., Bhola, N.E., Wilson, A.J., Khabele, D., Hong, C.C., Moses, H.L., and Owens, P. (2015). Small molecule inhibitor of the bone morphogenetic protein pathway DMH1 reduces ovarian cancer cell growth. Cancer Lett. *368*, 79–87.

Hover, L.D., Owens, P., Munden, A.L., Wang, J., Chambless, L.B., Hopkins, C.R., Hong, C.C., Moses, H.L., and Abel, T.W. (2016). Bone morphogenetic protein signaling promotes tumorigenesis in a murine model of high-grade glioma. Neuro-Oncol. *18*, 928–938.

Howe, K., Clark, M.D., Torroja, C.F., Torrance, J., Berthelot, C., Muffato, M., Collins, J.E., Humphray, S., McLaren, K., Matthews, L., et al. (2013). The zebrafish reference genome sequence and its relationship to the human genome. Nature *496*, 498–503.

Huang, D.W., Sherman, B.T., and Lempicki, R.A. (2009a). Systematic and integrative analysis of large gene lists using DAVID bioinformatics resources. Nat. Protoc. *4*, 44–57.

Huang, S.-M.A., Mishina, Y.M., Liu, S., Cheung, A., Stegmeier, F., Michaud, G.A., Charlat, O., Wiellette, E., Zhang, Y., Wiessner, S., et al. (2009b). Tankyrase inhibition stabilizes axin and antagonizes Wnt signalling. Nature *461*, 614–620.

Hyman, J.M., Firestone, A.J., Heine, V.M., Zhao, Y., Ocasio, C.A., Han, K., Sun, M., Rack, P.G., Sinha, S., Wu, J.J., et al. Small-molecule inhibitors reveal multiple strategies for Hedgehog pathway blockade.

Iorio, F., Bosotti, R., Scacheri, E., Belcastro, V., Mithbaokar, P., Ferriero, R., Murino, L., Tagliaferri, R., Brunetti-Pierri, N., Isacchi, A., et al. (2010). Discovery of drug mode of action and drug repositioning from transcriptional responses. Proc. Natl. Acad. Sci. U. S. A. *107*, 14621–14626.

Ishii, S., Kihara, Y., and Shimizu, T. (2005). Identification of T cell death-associated gene 8 (TDAG8) as a novel acid sensing G-protein-coupled receptor. J. Biol. Chem. *280*, 9083–9087.

Izzi, L., Lévesque, M., Morin, S., Laniel, D., Wilkes, B.C., Mille, F., Krauss, R.S., McMahon, A.P., Allen, B.L., and Charron, F. (2011). Boc and Gas1 each form distinct Shh receptor complexes with Ptch1 and are required for Shh-mediated cell proliferation. Dev. Cell *20*, 788–801.

Ji, Z., Mei, F.C., Xie, J., and Cheng, X. (2007). Oncogenic KRAS activates hedgehog signaling pathway in pancreatic cancer cells. J. Biol. Chem. *282*, 14048–14055.

Johnson, R.W., Nguyen, M.P., Padalecki, S.S., Grubbs, B.G., Merkel, A.R., Oyajobi, B.O., Matrisian, L.M., Mundy, G.R., and Sterling, J.A. (2011). TGF-β promotion of Gli2-induced expression of parathyroid hormone-related protein, an important osteolytic factor in bone metastasis, is independent of canonical Hedgehog signaling. Cancer Res. *71*, 822–831.

Jung, B., Padula, D., Burtscher, I., Landerer, C., Lutter, D., Theis, F., Messias, A.C., Geerlof, A., Sattler, M., Kremmer, E., et al. (2016). Pitchfork and Gprasp2 Target Smoothened to the Primary Cilium for Hedgehog Pathway Activation. PLOS ONE *11*, e0149477.

Jung, D.-W., Oh, E.-S., Park, S.-H., Chang, Y.-T., Kim, C.-H., Choi, S.-Y., and Williams, D.R. (2012). A novel zebrafish human tumor xenograft model validated for anti-cancer drug screening. Mol. Biosyst.

Justus, C.R., Dong, L., and Yang, L.V. (2013). Acidic tumor microenvironment and pH-sensing G protein-coupled receptors. Front. Physiol. *4*.

Kabarowski, J.H., Feramisco, J.D., Le, L.Q., Gu, J.L., Luoh, S.W., Simon, M.I., and Witte, O.N. (2000). Direct genetic demonstration of G alpha 13 coupling to the orphan G protein-coupled receptor G2α leading to RhoA-dependent actin rearrangement. Proc. Natl. Acad. Sci. U. S. A. *97*, 12109–12114.

Kar, S., Deb, M., Sengupta, D., Shilpi, A., Bhutia, S.K., and Patra, S.K. (2012). Intricacies of hedgehog signaling pathways: a perspective in tumorigenesis. Exp. Cell Res. *318*, 1959–1972.

Karet, F.E., Finberg, K.E., Nelson, R.D., Nayir, A., Mocan, H., Sanjad, S.A., Rodriguez-Soriano, J., Santos, F., Cremers, C.W., Di Pietro, A., et al. (1999). Mutations in the gene encoding B1 subunit of H+-ATPase cause renal tubular acidosis with sensorineural deafness. Nat. Genet. *21*, 84–90.

Kawahara, G., and Kunkel, L.M. (2013). Zebrafish based small molecule screens for novel DMD drugs. Drug Discov. Today Technol. *10*, e91–e96.

Kimelman, D., and Xu, W. (2006). beta-catenin destruction complex: insights and questions from a structural perspective. Oncogene *25*, 7482–7491.

Kinch, M.S., Haynesworth, A., Kinch, S.L., and Hoyer, D. (2014). An overview of FDA-approved new molecular entities: 1827–2013. Drug Discov. Today *19*, 1033–1039.

Kise, Y., Morinaka, A., Teglund, S., and Miki, H. (2009). Sufu recruits GSK3beta for efficient processing of Gli3. Biochem. Biophys. Res. Commun. *387*, 569–574.

Klaus, A., and Birchmeier, W. (2008). Wnt signalling and its impact on development and cancer. Nat. Rev. Cancer *8*, 387–398.

Kogerman, P., Grimm, T., Kogerman, L., Krause, D., Undén, A.B., Sandstedt, B., Toftgård, R., and Zaphiropoulos, P.G. (1999). Mammalian Suppressor-of-Fused modulates nuclear–cytoplasmic shuttling of GLI-1. Nat. Cell Biol. *1*, 312–319.

Kokel, D., and Peterson, R.T. (2011). Using the Zebrafish Photomotor Response for Psychotropic Drug Screening. Methods Cell Biol. *105*, 517–524.

Kotowski, I.K., Pertsemlidis, A., Luke, A., Cooper, R.S., Vega, G.L., Cohen, J.C., and Hobbs, H.H. (2006). A spectrum of PCSK9 alleles contributes to plasma levels of low-density lipoprotein cholesterol. Am. J. Hum. Genet. *78*, 410–422.

Krauss, S., Johansen, T., Korzh, V., and Fjose, A. (1991). Expression of the zebrafish paired box gene pax[zf-b] during early neurogenesis. Development *113*, 1193–1206.

Krauss, S., Concordet, J.P., and Ingham, P.W. (1993). A functionally conserved homolog of the Drosophila segment polarity gene hh is expressed in tissues with polarizing activity in zebrafish embryos. Cell *75*, 1431–1444.

Kulak, O., and Lum, L. (2013). A Multiplexed Luciferase-based Screening Platform for Interrogating Cancer-associated Signal Transduction in Cultured Cells. J. Vis. Exp. JoVE.

Kulak, O., Yamaguchi, K., and Lum, L. (2015). Identification of Therapeutic Small-Molecule Leads in Cultured Cells Using Multiplexed Pathway Reporter Readouts. Methods Mol. Biol. Clifton NJ *1263*, 3–14.

Kulesa, P.M., Bailey, C.M., Kasemeier-Kulesa, J.C., and McLennan, R. (2010). Cranial neural crest migration: New rules for an old road. Dev. Biol. *344*, 543–554.

Kuo, J.-C., Han, X., Hsiao, C.-T., Yates Iii, J.R., and Waterman, C.M. (2011). Analysis of the myosin-II-responsive focal adhesion proteome reveals a role for β-Pix in negative regulation of focal adhesion maturation. Nat. Cell Biol. *13*, 383–393.

Kwak, J., Park, O.K., Jung, Y.J., Hwang, B.J., Kwon, S.-H., and Kee, Y. (2013). Live Image Profiling of Neural Crest Lineages in Zebrafish Transgenic Lines. Mol. Cells *35*, 255–260.

Lagna, G., Carnevali, F., Marchioni, M., and Hemmati-Brivanlou, A. (1999). Negative regulation of axis formation and Wnt signaling in Xenopus embryos by the F-box/WD40 protein beta TrCP. Mech. Dev. *80*, 101–106.

Lamb, J., Crawford, E.D., Peck, D., Modell, J.W., Blat, I.C., Wrobel, M.J., Lerner, J., Brunet, J.-P., Subramanian, A., Ross, K.N., et al. (2006). The Connectivity Map: using gene-expression signatures to connect small molecules, genes, and disease. Science *313*, 1929–1935.

Lander, E.S. (2015). Brave New Genome. N. Engl. J. Med. *373*, 5–8.

Lauth, M., Bergström, Å., Shimokawa, T., and Toftgård, R. (2007). Inhibition of GLI-mediated transcription and tumor cell growth by small-molecule antagonists. Proc. Natl. Acad. Sci. U. S. A. *104*, 8455–8460.

Le, P.N., McDermott, J.D., and Jimeno, A. (2015). Targeting the Wnt pathway in human cancers: therapeutic targeting with a focus on OMP-54F28. Pharmacol. Ther. *146*, 1–11.

Li, H., Wang, D., Singh, L.S., Berk, M., Tan, H., Zhao, Z., Steinmetz, R., Kirmani, K., Wei, G., and Xu, Y. (2009). Abnormalities in osteoclastogenesis and decreased tumorigenesis in mice deficient for ovarian cancer G protein-coupled receptor 1. PloS One *4*, e5705.

Li, J., Wang, C., Pan, Y., Bai, Z., and Wang, B. (2011). Increased proteolytic processing of full-length Gli2 transcription factor reduces the Hedgehog pathway activity in vivo. Dev. Dyn. Off. Publ. Am. Assoc. Anat. *240*, 766–774.

Li, Y.-H., Luo, J., Mosley, Y.-Y.C., Hedrick, V.E., Paul, L.N., Chang, J., Zhang, G., Wang, Y.-K., Banko, M.R., Brunet, A., et al. (2015). AMP-activated Protein Kinase Directly Phosphorylates and Destabilizes Hedgehog Pathway Transcription Factor GLI1 in Medulloblastoma. Cell Rep. *12*, 599–609.

Liu, J., Pan, S., Hsieh, M.H., Ng, N., Sun, F., Wang, T., Kasibhatla, S., Schuller, A.G., Li, A.G., Cheng, D., et al. (2013a). Targeting Wnt-driven cancer through the inhibition of Porcupine by LGK974. Proc. Natl. Acad. Sci. *110*, 20224–20229.

Liu, J.-P., Komachi, M., Tomura, H., Mogi, C., Damirin, A., Tobo, M., Takano, M., Nochi, H., Tamoto, K., Sato, K., et al. (2010). Ovarian cancer G protein-coupled receptor 1-dependent and -independent vascular actions to acidic pH in human aortic smooth muscle cells. Am. J. Physiol. Heart Circ. Physiol. *299*, H731-742.

Liu, X., Rubin, J.S., and Kimmel, A.R. (2005). Rapid, Wnt-induced changes in GSK3beta associations that regulate beta-catenin stabilization are mediated by Galpha proteins. Curr. Biol. CB *15*, 1989–1997.

Liu, Y., Asnani, A., Zou, L., Bentley, V.L., Yu, M., Wang, Y., Dellaire, G., Sarkar, K.S., Dai, M., Chen, H.H., et al. (2014). Visnagin protects against doxorubicin-induced cardiomyopathy through modulation of mitochondrial malate dehydrogenase. Sci. Transl. Med. *6*, 266ra170.

Liu, Y.-J., Fan, H.-B., Jin, Y., Ren, C.-G., Jia, X.-E., Wang, L., Chen, Y., Dong, M., Zhu, K.-Y., Dong, Z.-W., et al. (2013b). Cannabinoid receptor 2 suppresses leukocyte inflammatory migration by modulating the JNK/c-Jun/Alox5 pathway. J. Biol. Chem. *288*, 13551–13562.

Long, J., Li, B., Rodriguez-Blanco, J., Pastori, C., Volmar, C.-H., Wahlestedt, C., Capobianco, A., Bai, F., Pei, X.-H., Ayad, N.G., et al. (2014). The BET Bromodomain Inhibitor I-BET151 Acts

Downstream of Smoothened Protein to Abrogate the Growth of Hedgehog Protein-driven Cancers. J. Biol. Chem. *289*, 35494–35502.

Lu, W., Tinsley, H.N., Keeton, A., Qu, Z., Piazza, G.A., and Li, Y. (2009). Suppression of Wnt/beta-catenin signaling inhibits prostate cancer cell proliferation. Eur. J. Pharmacol. *602*, 8–14.

Ludwig, M.-G., Vanek, M., Guerini, D., Gasser, J.A., Jones, C.E., Junker, U., Hofstetter, H., Wolf, R.M., and Seuwen, K. (2003). Proton-sensing G-protein-coupled receptors. Nature *425*, 93–98.

Manoukian, A.S., Yoffe, K.B., Wilder, E.L., and Perrimon, N. (1995). The porcupine gene is required for wingless autoregulation in Drosophila. Dev. Camb. Engl. *121*, 4037–4044.

Mao, J., Wang, J., Liu, B., Pan, W., Farr, G.H., Flynn, C., Yuan, H., Takada, S., Kimelman, D., Li, L., et al. (2001). Low-density lipoprotein receptor-related protein-5 binds to Axin and regulates the canonical Wnt signaling pathway. Mol. Cell *7*, 801–809.

Martinez-Zaguilan, R., Lynch, R.M., Martinez, G.M., and Gillies, R.J. (1993). Vacuolar-type H(+)-ATPases are functionally expressed in plasma membranes of human tumor cells. Am. J. Physiol. *265*, C1015-1029.

Mattei, M.G., Sardet, C., Franchi, A., and Pouysségur, J. (1988). The human amiloride-sensitive Na+/H+ antiporter: localization to chromosome 1 by in situ hybridization. Cytogenet. Cell Genet. *48*, 6–8.

Matthews, H., Ranson, M., and Kelso, M.J. (2011). Anti-tumour/metastasis effects of the potassium-sparing diuretic amiloride: An orally active anti-cancer drug waiting for its call-of-duty? Int. J. Cancer *129*, 2051–2061.

Mazhab-Jafari, M.T., and Rubinstein, J.L. (2016). Cryo-EM studies of the structure and dynamics of vacuolar-type ATPases. Sci. Adv. *2*.

McLean, L.A., Roscoe, J., Jorgensen, N.K., Gorin, F.A., and Cala, P.M. (2000). Malignant gliomas display altered pH regulation by NHE1 compared with nontransformed astrocytes. Am. J. Physiol. Cell Physiol. *278*, C676-688.

McMahon, A.P., and Moon, R.T. (1989a). Ectopic expression of the proto-oncogene int-1 in Xenopus embryos leads to duplication of the embryonic axis. Cell *58*, 1075–1084.

McMahon, A.P., and Moon, R.T. (1989b). int-1--a proto-oncogene involved in cell signalling. Dev. Camb. Engl. *107 Suppl*, 161–167.

Merriam, J.M., Rubenstein, A.B., and Klymkowsky, M.W. (1997). Cytoplasmically anchored plakoglobin induces a WNT-like phenotype in Xenopus. Dev. Biol. *185*, 67–81.

Mierke, C.T., Rösel, D., Fabry, B., and Brábek, J. (2008). Contractile forces in tumor cell migration. Eur. J. Cell Biol. *87*, 669–676.

Miller, S.J., Lou, D.Y., Seldin, D.C., Lane, W.S., and Neel, B.G. (2002). Direct identification of PTEN phosphorylation sites. FEBS Lett. *528*, 145–153.

Minke, K.S., Staib, P., Puetter, A., Gehrke, I., Gandhirajan, R.K., Schlösser, A., Schmitt, E.K., Hallek, M., and Kreuzer, K.-A. (2009). Small molecule inhibitors of WNT signaling effectively induce apoptosis in acute myeloid leukemia cells. Eur. J. Haematol. *82*, 165–175.

Miraglia, E., Viarisio, D., Riganti, C., Costamagna, C., Ghigo, D., and Bosia, A. (2005). Na+/H+ exchanger activity is increased in doxorubicin-resistant human colon cancer cells and its modulation modifies the sensitivity of the cells to doxorubicin. Int. J. Cancer *115*, 924–929.

Mogi, C., Tobo, M., Tomura, H., Murata, N., He, X., Sato, K., Kimura, T., Ishizuka, T., Sasaki, T., Sato, T., et al. (2009). Involvement of proton-sensing TDAG8 in extracellular acidification-induced inhibition of proinflammatory cytokine production in peritoneal macrophages. J. Immunol. Baltim. Md 1950 *182*, 3243–3251.

Mohammed, M.K., Shao, C., Wang, J., Wei, Q., Wang, X., Collier, Z., Tang, S., Liu, H., Zhang, F., Huang, J., et al. (2016). Wnt/β-catenin signaling plays an ever-expanding role in stem cell self-renewal, tumorigenesis and cancer chemoresistance. Genes Dis. *3*, 11–40.

Molina, G., Vogt, A., Bakan, A., Dai, W., Queiroz de Oliveira, P., Znosko, W., Smithgall, T.E., Bahar, I., Lazo, J.S., Day, B.W., et al. (2009). Zebrafish chemical screening reveals an inhibitor of Dusp6 that expands cardiac cell lineages. Nat. Chem. Biol. *5*, 680–687.

Moon, R.T., Kohn, A.D., De Ferrari, G.V., and Kaykas, A. (2004). WNT and beta-catenin signalling: diseases and therapies. Nat. Rev. Genet. *5*, 691–701.

Morales, A.V., Barbas, J.A., and Nieto, M.A. (2005). How to become neural crest: From segregation to delamination. Semin. Cell Dev. Biol. *16*, 655–662.

Mosimann, C., Hausmann, G., and Basler, K. (2009). Beta-catenin hits chromatin: regulation of Wnt target gene activation. Nat. Rev. Mol. Cell Biol. *10*, 276–286.

Mueller, R.L., and Scheidt, S. (1994). History of drugs for thrombotic disease. Discovery, development, and directions for the future. Circulation *89*, 432–449.

Mullard, A. (2015). The phenotypic screening pendulum swings. Nat. Rev. Drug Discov. *14*, 807–809.

Mullins, M.C., Hammerschmidt, M., Kane, D.A., Odenthal, J., Brand, M., Eeden, F.J. van, Furutani-Seiki, M., Granato, M., Haffter, P., Heisenberg, C.P., et al. (1996). Genes establishing dorsoventral pattern formation in the zebrafish embryo: the ventral specifying genes. Development *123*, 81–93.

Murakami, N., Yokomizo, T., Okuno, T., and Shimizu, T. (2004). G2α is a proton-sensing G-protein-coupled receptor antagonized by lysophosphatidylcholine. J. Biol. Chem. *279*, 42484–42491.

Nakamura, T., Hamada, F., Ishidate, T., Anai, K., Kawahara, K., Toyoshima, K., and Akiyama, T. (1998). Axin, an inhibitor of the Wnt signalling pathway, interacts with beta-catenin, GSK-3beta and APC and reduces the beta-catenin level. Genes Cells Devoted Mol. Cell. Mech. *3*, 395–403.

Nakamura, Y., Nishisho, I., Kinzler, K.W., Vogelstein, B., Miyoshi, Y., Miki, Y., Ando, H., Horii, A., and Nagase, H. (1991). Mutations of the adenomatous polyposis coli gene in familial polyposis coli patients and sporadic colorectal tumors. Princess Takamatsu Symp. *22*, 285–292.

Nath, A.K., Roberts, L.D., Liu, Y., Mahon, S.B., Kim, S., Ryu, J.H., Werdich, A., Januzzi, J.L., Boss, G.R., Rockwood, G.A., et al. (2013). Chemical and metabolomic screens identify novel biomarkers and antidotes for cyanide exposure. FASEB J. *27*, 1928–1938.

Ng, J.M.Y., and Curran, T. (2011). The Hedgehog's tale: developing strategies for targeting cancer. Nat. Rev. Cancer *11*, 493–501.

Ni, T.T., Rellinger, E.J., Mukherjee, A., Xie, S., Stephens, L., Thorne, C.A., Kim, K., Hu, J., Lee, E., Marnett, L., et al. (2011). Discovering small molecules that promote cardiomyocyte generation by modulating Wnt signaling. Chem. Biol. *18*, 1658–1668.

Niefind, K., Guerra, B., Pinna, L.A., Issinger, O.G., and Schomburg, D. (1998). Crystal structure of the catalytic subunit of protein kinase CK2 from Zea mays at 2.1 A resolution. EMBO J. *17*, 2451–2462.

Niewiadomski, P., Kong, J.H., Ahrends, R., Ma, Y., Humke, E.W., Khan, S., Teruel, M.N., Novitch, B.G., and Rohatgi, R. (2014). Gli Protein Activity Is Controlled by Multisite Phosphorylation in Vertebrate Hedgehog Signaling. Cell Rep. *6*, 168–181.

Nishiya, N., Oku, Y., Kumagai, Y., Sato, Y., Yamaguchi, E., Sasaki, A., Shoji, M., Ohnishi, Y., Okamoto, H., and Uehara, Y. (2014). A Zebrafish Chemical Suppressor Screening Identifies Small Molecule Inhibitors of the Wnt/β-catenin Pathway. Chem. Biol. *21*, 530–540.

Nolan-Stevaux, O., Lau, J., Truitt, M.L., Chu, G.C., Hebrok, M., Fernández-Zapico, M.E., and Hanahan, D. (2009). GLI1 is regulated through Smoothened-independent mechanisms in neoplastic pancreatic ducts and mediates PDAC cell survival and transformation. Genes Dev. *23*, 24–36.

Norman, J.N. (1985). William Withering and the Purple Foxglove: A Bicentennial Tribute. J. Clin. Pharmacol. *25*, 479–483.

North, T.E., Goessling, W., Walkley, C.R., Lengerke, C., Kopani, K.R., Lord, A.M., Weber, G.J., Bowman, T.V., Jang, I.-H., Grosser, T., et al. (2007). Prostaglandin E2 regulates vertebrate haematopoietic stem cell homeostasis. Nature *447*, 1007–1011.

Nüsslein-Volhard, C., and Wieschaus, E. (1980). Mutations affecting segment number and polarity in Drosophila. Nature *287*, 795–801.

Odunewu-Aderibigbe, A., and Fliegel, L. (2014). The Na(+) /H(+) exchanger and pH regulation in the heart. IUBMB Life *66*, 679–685.

Oh, S., Kato, M., Zhang, C., Guo, Y., and Beachy, P.A. (2015). A Comparison of Ci/Gli Activity as Regulated by Sufu in Drosophila and Mammalian Hedgehog Response. PLoS ONE *10*.

Okajima, F. (2013). Regulation of inflammation by extracellular acidification and proton-sensing GPCRs. Cell. Signal. *25*, 2263–2271.

Omo-Aghoja, L. (2014). Maternal and Fetal Acid-Base Chemistry: A Major Determinant of Perinatal Outcome. Ann. Med. Health Sci. Res. *4*, 8–17.

Oro, A.E., Higgins, K.M., Hu, Z., Bonifas, J.M., Epstein, E.H., and Scott, M.P. (1997). Basal cell carcinomas in mice overexpressing sonic hedgehog. Science *276*, 817–821.

Owens, P., Polikowsky, H., Pickup, M.W., Gorska, A.E., Jovanovic, B., Shaw, A.K., Novitskiy, S.V., Hong, C.C., and Moses, H.L. (2013). Bone Morphogenetic Proteins stimulate mammary fibroblasts to promote mammary carcinoma cell invasion. PloS One *8*, e67533.

Owens, P., Pickup, M.W., Novitskiy, S.V., Giltnane, J.M., Gorska, A.E., Hopkins, C.R., Hong, C.C., and Moses, H.L. (2015). Inhibition of BMP signaling suppresses metastasis in mammary cancer. Oncogene *34*, 2437–2449.

Oxtoby, E., and Jowett, T. (1993). Cloning of the zebrafish krox-20 gene (krx-20) and its expression during hindbrain development. Nucleic Acids Res. *21*, 1087–1095.

Ozawa, M., Baribault, H., and Kemler, R. (1989). The cytoplasmic domain of the cell adhesion molecule uvomorulin associates with three independent proteins structurally related in different species. EMBO J. *8*, 1711–1717.

Pagano, M.A., Bain, J., Kazimierczuk, Z., Sarno, S., Ruzzene, M., Di Maira, G., Elliott, M., Orzeszko, A., Cozza, G., Meggio, F., et al. (2008). The selectivity of inhibitors of protein kinase CK2: an update. Biochem. J. *415*, 353–365.

Parks, S.K., Chiche, J., and Pouysségur, J. (2013). Disrupting proton dynamics and energy metabolism for cancer therapy. Nat. Rev. Cancer *13*, 611–623.

Peal, D.S., Mills, R.W., Lynch, S.N., Mosley, J.M., Lim, E., Ellinor, P.T., January, C.T., Peterson, R.T., and Milan, D.J. (2011). Novel chemical suppressors of long QT syndrome identified by an in vivo functional screen. Circulation *123*, 23–30.

Pedersen, L.B., and Akhmanova, A. (2014). Kif7 keeps cilia tips in shape. Nat. Cell Biol. *16*, 623–625.

Peppard, J.V., Rugg, C., Smicker, M., Dureuil, C., Ronan, B., Flamand, O., Durand, L., and Pasquier, B. (2014). Identifying Small Molecules which Inhibit Autophagy: a Phenotypic Screen Using Image-Based High-Content Cell Analysis. Curr. Chem. Genomics Transl. Med. *8*, 3–15.

Perrot, C.Y., Javelaud, D., and Mauviel, A. (2013). Overlapping activities of TGF-β and Hedgehog signaling in cancer: Therapeutic targets for cancer treatment. Pharmacol. Ther. *137*, 183–199.

Peterson, R.T., Link, B.A., Dowling, J.E., and Schreiber, S.L. (2000). Small molecule developmental screens reveal the logic and timing of vertebrate development. Proc. Natl. Acad. Sci. *97*, 12965–12969.

Peterson, R.T., Shaw, S.Y., Peterson, T.A., Milan, D.J., Zhong, T.P., Schreiber, S.L., MacRae, C.A., and Fishman, M.C. (2004). Chemical suppression of a genetic mutation in a zebrafish model of aortic coarctation. Nat. Biotechnol. *22*, 595–599.

Piano, F., Schetter, A.J., Morton, D.G., Gunsalus, K.C., Reinke, V., Kim, S.K., and Kemphues, K.J. (2002). Gene clustering based on RNAi phenotypes of ovary-enriched genes in C. elegans. Curr. Biol. CB *12*, 1959–1964.

Porter, J.A., von Kessler, D.P., Ekker, S.C., Young, K.E., Lee, J.J., Moses, K., and Beachy, P.A. (1995). The product of hedgehog autoproteolytic cleavage active in local and long-range signalling. Nature *374*, 363–366.

Porter, J.A., Ekker, S.C., Park, W.J., von Kessler, D.P., Young, K.E., Chen, C.H., Ma, Y., Woods, A.S., Cotter, R.J., Koonin, E.V., et al. (1996). Hedgehog patterning activity: role of a lipophilic modification mediated by the carboxy-terminal autoprocessing domain. Cell *86*, 21–34.

Powell, D.R., Blasky, A.J., Britt, S.G., and Artinger, K.B. (2013). Riding the crest of the wave: parallels between the neural crest and cancer in epithelial-to-mesenchymal transition and migration. Wiley Interdiscip. Rev. Syst. Biol. Med. *5*, 511–522.

Radu, C.G., Nijagal, A., McLaughlin, J., Wang, L., and Witte, O.N. (2005). Differential proton sensitivity of related G protein-coupled receptors T cell death-associated gene 8 and G2α expressed in immune cells. Proc. Natl. Acad. Sci. U. S. A. *102*, 1632–1637.

Ren, J., and Zhang, L. (2011). Effects of ovarian cancer G protein coupled receptor 1 on the proliferation, migration, and adhesion of human ovarian cancer cells. Chin. Med. J. (Engl.) *124*, 1327–1332.

Rennekamp, A.J., and Peterson, R.T. (2015). 15 years of zebrafish chemical screening. Curr. Opin. Chem. Biol. *24*, 58–70.

Rennekamp, A.J., Huang, X.-P., Wang, Y., Patel, S., Lorello, P.J., Cade, L., Gonzales, A.P.W., Yeh, J.-R.J., Caldarone, B.J., Roth, B.L., et al. (2016). σ1 receptor ligands control a switch between passive and active threat responses. Nat. Chem. Biol. *12*, 552–558.

Reya, T., and Clevers, H. (2005). Wnt signalling in stem cells and cancer. Nature *434*, 843–850.

Reynolds, A.L., Alvarez, Y., Sasore, T., Waghorne, N., Butler, C.T., Kilty, C., Smith, A.J., McVicar, C., Wong, V.H.Y., Galvin, O., et al. (2016). Phenotype-based Discovery of 2-[(E)-2-(Quinolin-2-yl)vinyl]phenol as a Novel Regulator of Ocular Angiogenesis. J. Biol. Chem. *291*, 7242–7255.

Riggleman, B., Schedl, P., and Wieschaus, E. (1990). Spatial expression of the Drosophila segment polarity gene armadillo is posttranscriptionally regulated by wingless. Cell *63*, 549–560.

Rihel, J., Prober, D.A., Arvanites, A., Lam, K., Zimmerman, S., Jang, S., Haggarty, S.J., Kokel, D., Rubin, L.L., Peterson, R.T., et al. (2010). Zebrafish behavioral profiling links drugs to biological targets and rest/wake regulation. Science *327*, 348–351.

Rimm, D.L., Caca, K., Hu, G., Harrison, F.B., and Fearon, E.R. (1999). Frequent Nuclear/Cytoplasmic Localization of β-Catenin without Exon 3 Mutations in Malignant Melanoma. Am. J. Pathol. *154*, 325–329.

Robarge, K.D., Brunton, S.A., Castanedo, G.M., Cui, Y., Dina, M.S., Goldsmith, R., Gould, S.E., Guichert, O., Gunzner, J.L., Halladay, J., et al. (2009). GDC-0449-a potent inhibitor of the hedgehog pathway. Bioorg. Med. Chem. Lett. *19*, 5576–5581.

Robertson, A.L., Holmes, G.R., Bojarczuk, A.N., Burgon, J., Loynes, C.A., Chimen, M., Sawtell, A.K., Hamza, B., Willson, J., Walmsley, S.R., et al. (2014). A Zebrafish Compound Screen

Reveals Modulation of Neutrophil Reverse Migration as an Anti-Inflammatory Mechanism. Sci. Transl. Med. *6*, 225ra29-225ra29.

Roelink, H., Augsburger, A., Heemskerk, J., Korzh, V., Norlin, S., Ruiz i Altaba, A., Tanabe, Y., Placzek, M., Edlund, T., and Jessell, T.M. (1994). Floor plate and motor neuron induction by vhh-1, a vertebrate homolog of hedgehog expressed by the notochord. Cell *76*, 761–775.

Rofstad, E.K., Mathiesen, B., Kindem, K., and Galappathi, K. (2006). Acidic extracellular pH promotes experimental metastasis of human melanoma cells in athymic nude mice. Cancer Res. *66*, 6699–6707.

Roth, B.L., Sheffler, D.J., and Kroeze, W.K. (2004). Magic shotguns versus magic bullets: selectively non-selective drugs for mood disorders and schizophrenia. Nat. Rev. Drug Discov. *3*, 353–359.

Rubinfeld, B., Souza, B., Albert, I., Müller, O., Chamberlain, S.H., Masiarz, F.R., Munemitsu, S., and Polakis, P. (1993). Association of the APC gene product with beta-catenin. Science *262*, 1731–1734.

Russell, J.L., Goetsch, S.C., Aguilar, H.R., Coe, H., Luo, X., Liu, N., van Rooij, E., Frantz, D.E., and Schneider, J.W. (2012). Regulated expression of pH sensing G Protein-coupled receptor-68 identified through chemical biology defines a new drug target for ischemic heart disease. ACS Chem. Biol. *7*, 1077–1083.

Ryan, K.E., and Chiang, C. (2012). Hedgehog secretion and signal transduction in vertebrates. J. Biol. Chem. *287*, 17905–17913.

Sabaliauskas, N.A., Foutz, C.A., Mest, J.R., Budgeon, L.R., Sidor, A.T., Gershenson, J.A., Joshi, S.B., and Cheng, K.C. (2006). High-throughput zebrafish histology. Methods San Diego Calif *39*, 246–254.

Saxena, H., Deshpande, D.A., Tiegs, B.C., Yan, H., Battafarano, R.J., Burrows, W.M., Damera, G., Panettieri, R.A., Dubose, T.D.J., An, S.S., et al. (2012). The GPCR OGR1 (GPR68) mediates diverse signalling and contraction of airway smooth muscle in response to small reductions in extracellular pH. Br. J. Pharmacol. *166*, 981–990.

Scannell, J.W., Blanckley, A., Boldon, H., and Warrington, B. (2012). Diagnosing the decline in pharmaceutical R&D efficiency. Nat. Rev. Drug Discov. *11*, 191–200.

Schier, A.F., and Talbot, W.S. (2005). Molecular genetics of axis formation in zebrafish. Annu. Rev. Genet. *39*, 561–613.

Schrader, E.K., Harstad, K.G., Holmgren, R.A., and Matouschek, A. (2011). A Three-part Signal Governs Differential Processing of Gli1 and Gli3 Proteins by the Proteasome. J. Biol. Chem. *286*, 39051–39058.

Schriek, G., Oppitz, M., Busch, C., Just, L., and Drews, U. (2005). Human SK-Mel 28 melanoma cells resume neural crest cell migration after transplantation into the chick embryo. Melanoma Res. *15*, 225–234.

Sengupta, R., Sun, T., Warrington, N.M., and Rubin, J.B. (2011). Treating brain tumors with PDE4 inhibitors. Trends Pharmacol. Sci. *32*, 337–344.

Sennoune, S.R., Bakunts, K., Martínez, G.M., Chua-Tuan, J.L., Kebir, Y., Attaya, M.N., and Martínez-Zaguilán, R. (2004). Vacuolar H+-ATPase in human breast cancer cells with distinct metastatic potential: distribution and functional activity. Am. J. Physiol. Cell Physiol. *286*, C1443-1452.

Seto, M., Ohta, M., Asaoka, Y., Ikenoue, T., Tada, M., Miyabayashi, K., Mohri, D., Tanaka, Y., Ijichi, H., Tateishi, K., et al. (2009). Regulation of the hedgehog signaling by the mitogen-activated protein kinase cascade in gastric cancer. Mol. Carcinog. *48*, 703–712.

Seuwen, K., Ludwig, M.-G., and Wolf, R.M. (2006). Receptors for protons or lipid messengers or both? J. Recept. Signal Transduct. Res. *26*, 599–610.

Sharpe, H.J., Pau, G., Dijkgraaf, G.J., Basset-Seguin, N., Modrusan, Z., Januario, T., Tsui, V., Durham, A.B., Dlugosz, A.A., Haverty, P.M., et al. (2015). Genomic Analysis of Smoothened Inhibitor Resistance in Basal Cell Carcinoma. Cancer Cell *27*, 327–341.

Shelton, E.L., Galindo, C.L., Williams, C.H., Pfaltzgraff, E., Hong, C.C., and Bader, D.M. (2013). Autotaxin signaling governs phenotypic heterogeneity in visceral and parietal mesothelia. PloS One *8*, e69712.

Shi, Q., Li, S., Li, S., Jiang, A., Chen, Y., and Jiang, J. (2014). Hedgehog-induced phosphorylation by CK1 sustains the activity of Ci/Gli activator. Proc. Natl. Acad. Sci. U. S. A. *111*, E5651-5660.

Shoemaker, R.H. (2006). The NCI60 human tumour cell line anticancer drug screen. Nat. Rev. Cancer *6*, 813–823.

Siegfried, E., Wilder, E.L., and Perrimon, N. (1994). Components of wingless signalling in Drosophila. Nature *367*, 76–80.

Singh, L.S., Berk, M., Oates, R., Zhao, Z., Tan, H., Jiang, Y., Zhou, A., Kirmani, K., Steinmetz, R., Lindner, D., et al. (2007). Ovarian cancer G protein-coupled receptor 1, a new metastasis suppressor gene in prostate cancer. J. Natl. Cancer Inst. *99*, 1313–1327.

Sinha, S., and Chen, J.K. (2006). Purmorphamine activates the Hedgehog pathway by targeting Smoothened. Nat. Chem. Biol. *2*, 29–30.

Skrypnyk, N.I., Sanker, S., Brilli-Skvarca, L., Novitskaya, T., Woods, C., Chiba, T., Patel, K., Goldberg, N.D., McDermott, L., Vinson, P.N., et al. (2015). Delayed treatment with PTBA analogs reduces post injury renal fibrosis after kidney injury. Am. J. Physiol. - Ren. Physiol. ajprenal.00503.2015.

Song, D.H., Sussman, D.J., and Seldin, D.C. (2000). Endogenous protein kinase CK2 participates in Wnt signaling in mammary epithelial cells. J. Biol. Chem. *275*, 23790–23797.

Stamos, J.L., and Weis, W.I. (2013). The β-Catenin Destruction Complex. Cold Spring Harb. Perspect. Biol. *5*.

Stanganello, E., and Scholpp, S. (2016). Role of cytonemes in Wnt transport. J Cell Sci *129*, 665–672.

Stanganello, E., Hagemann, A.I.H., Mattes, B., Sinner, C., Meyen, D., Weber, S., Schug, A., Raz, E., and Scholpp, S. (2015). Filopodia-based Wnt transport during vertebrate tissue patterning. Nat. Commun. *6*, 5846.

Stanton, B.Z., Peng, L.F., Maloof, N., Nakai, K., Wang, X., Duffner, J.L., Taveras, K.M., Hyman, J.M., Lee, S.W., Koehler, A.N., et al. (2009). A small molecule that binds Hedgehog and blocks its signaling in human cells. Nat. Chem. Biol. *5*, 154–156.

Stecca, B., and Pandolfi, S. (2015). Hedgehog-Gli signaling in basal cell carcinoma and other skin cancers: prospects for therapy. Res. Rep. Biol. 55.

Stelzer, G., Rosen, N., Plaschkes, I., Zimmerman, S., Twik, M., Fishilevich, S., Stein, T.I., Nudel, R., Lieder, I., Mazor, Y., et al. (2016). The GeneCards Suite: From Gene Data Mining to Disease Genome Sequence Analyses. Curr. Protoc. Bioinforma. Ed. Board Andreas Baxevanis Al *54*, 1.30.1-1.30.33.

Stewart, R.A., Arduini, B.L., Berghmans, S., George, R.E., Kanki, J.P., Henion, P.D., and Look, A.T. (2006). Zebrafish foxd3 is selectively required for neural crest specification, migration and survival. Dev. Biol. *292*, 174–188.

Stock, C., Mueller, M., Kraehling, H., Mally, S., Noël, J., Eder, C., and Schwab, A. (2007). pH nanoenvironment at the surface of single melanoma cells. Cell. Physiol. Biochem. Int. J. Exp. Cell. Physiol. Biochem. Pharmacol. *20*, 679–686.

Stover, E., Borthwick, K., Bavalia, C., Eady, N., Fritz, D., Rungroj, N., Giersch, A., Morton, C., Axon, P., Akil, I., et al. (2002). Novel ATP6V1B1 and ATP6V0A4 mutations in autosomal recessive distal renal tubular acidosis with new evidence for hearing loss. J. Med. Genet. *39*, 796–803.

Stüwe, L., Müller, M., Fabian, A., Waning, J., Mally, S., Noël, J., Schwab, A., and Stock, C. (2007a). pH dependence of melanoma cell migration: protons extruded by NHE1 dominate protons of the bulk solution. J. Physiol. *585*, 351–360.

Stüwe, L., Müller, M., Fabian, A., Waning, J., Mally, S., Noël, J., Schwab, A., and Stock, C. (2007b). pH dependence of melanoma cell migration: protons extruded by NHE1 dominate protons of the bulk solution. J. Physiol. *585*, 351–360.

Sugimoto, A. (2004). High-throughput RNAi in Caenorhabditis elegans: genome-wide screens and functional genomics. Differ. Res. Biol. Divers. *72*, 81–91.

Sun, X., Yang, L.V., Tiegs, B.C., Arend, L.J., McGraw, D.W., Penn, R.B., and Petrovic, S. (2010). Deletion of the pH sensor GPR4 decreases renal acid excretion. J. Am. Soc. Nephrol. JASN *21*, 1745–1755.

Suzuki, H., Masuda, N., Shimura, T., Araki, K., Kobayashi, T., Tsutsumi, S., Asao, T., and Kuwano, H. (2008). Nuclear beta-catenin expression at the invasive front and in the vessels predicts liver metastasis in colorectal carcinoma. Anticancer Res. *28*, 1821–1830.

Swinney, D.C., and Anthony, J. (2011). How were new medicines discovered? Nat. Rev. Drug Discov. *10*, 507–519.

Taipale, J., Chen, J.K., Cooper, M.K., Wang, B., Mann, R.K., Milenkovic, L., Scott, M.P., and Beachy, P.A. (2000). Effects of oncogenic mutations in Smoothened and Patched can be reversed by cyclopamine. Nature *406*, 1005–1009.

Takahashi, M., Suzawa, T., Yamada, A., Yamaguchi, T., Mishima, K., Osumi, N., Maki, K., and Kamijo, R. (2014). Identification of gene expression profile of neural crest-derived cells isolated from submandibular glands of adult mice. Biochem. Biophys. Res. Commun. *446*, 481–486.

Takahashi, Y., Sipp, D., and Enomoto, H. (2013). Tissue interactions in neural crest cell development and disease. Science *341*, 860–863.

Takaki, K., Cosma, C.L., Troll, M.A., and Ramakrishnan, L. (2012). An In Vivo Platform for Rapid High-Throughput Antitubercular Drug Discovery. Cell Rep. *2*, 175–184.

Takebe, N., Miele, L., Harris, P.J., Jeong, W., Bando, H., Kahn, M., Yang, S.X., and Ivy, S.P. (2015). Targeting Notch, Hedgehog, and Wnt pathways in cancer stem cells: clinical update. Nat. Rev. Clin. Oncol. *12*, 445–464.

Tanaka, M., Bateman, R., Rauh, D., Vaisberg, E., Ramachandani, S., Zhang, C., Hansen, K.C., Burlingame, A.L., Trautman, J.K., Shokat, K.M., et al. (2005). An Unbiased Cell Morphology–Based Screen for New, Biologically Active Small Molecules. PLoS Biol. *3*.

Tang, S., Xie, M., Cao, N., and Ding, S. (2016). Patient-Specific Induced Pluripotent Stem Cells for Disease Modeling and Phenotypic Drug Discovery. J. Med. Chem. *59*, 2–15.

Tang, Y., Gholamin, S., Schubert, S., Willardson, M.I., Lee, A., Bandopadhayay, P., Bergthold, G., Masoud, S., Nguyen, B., Vue, N., et al. (2014). Epigenetic targeting of Hedgehog pathway transcriptional output through BET bromodomain inhibition. Nat. Med. *20*, 732–740.

Tas, F. (2012). Metastatic Behavior in Melanoma: Timing, Pattern, Survival, and Influencing Factors. J. Oncol. *2012*, e647684.

Terrin, A., Monterisi, S., Stangherlin, A., Zoccarato, A., Koschinski, A., Surdo, N.C., Mongillo, M., Sawa, A., Jordanides, N.E., Mountford, J.C., et al. (2012). PKA and PDE4D3 anchoring to AKAP9 provides distinct regulation of cAMP signals at the centrosome. J. Cell Biol. *198*, 607–621.

Thisse, B., Heyer, V., Lux, A., Alunni, V., Degrave, A., Seiliez, I., Kirchner, J., Parkhill, J.-P., and Thisse, C. (2004). Spatial and temporal expression of the zebrafish genome by large-scale in situ hybridization screening. Methods Cell Biol. *77*, 505–519.

Thorne, C.A., Hanson, A.J., Schneider, J., Tahinci, E., Orton, D., Cselenyi, C.S., Jernigan, K.K., Meyers, K.C., Hang, B.I., Waterson, A.G., et al. (2010). Small-molecule inhibition of Wnt signaling through activation of casein kinase 1α. Nat. Chem. Biol. *6*, 829–836.

Tran, T.C., Sneed, B., Haider, J., Blavo, D., White, A., Aiyejorun, T., Baranowski, T.C., Rubinstein, A.L., Doan, T.N., Dingledine, R., et al. (2007). Automated, quantitative screening assay for antiangiogenic compounds using transgenic zebrafish. Cancer Res. *67*, 11386–11392.

Trifirò, G., Corrao, S., Alacqua, M., Moretti, S., Tari, M., Caputi, A.P., and Arcoraci, V. (2006). Interaction risk with proton pump inhibitors in general practice: significant disagreement between different drug-related information sources. Br. J. Clin. Pharmacol. *62*, 582–590.

Tukachinsky, H., Lopez, L.V., and Salic, A. (2010). A mechanism for vertebrate Hedgehog signaling: recruitment to cilia and dissociation of SuFu-Gli protein complexes. J. Cell Biol. *191*, 415–428.

Uzman, J.A., Patil, S., Uzgare, A.R., and Sater, A.K. (1998). The role of intracellular alkalinization in the establishment of anterior neural fate in Xenopus. Dev. Biol. *193*, 10–20.

Vandenberg, L.N., Morrie, R.D., and Adams, D.S. (2011). V-ATPase-dependent ectodermal voltage and pH regionalization are required for craniofacial morphogenesis. Dev. Dyn. Off. Publ. Am. Assoc. Anat. *240*, 1889–1904.

Vander Heiden, M.G., Cantley, L.C., and Thompson, C.B. (2009). Understanding the Warburg Effect: The Metabolic Requirements of Cell Proliferation. Science *324*, 1029–1033.

Von Hoff, D.D., LoRusso, P.M., Rudin, C.M., Reddy, J.C., Yauch, R.L., Tibes, R., Weiss, G.J., Borad, M.J., Hann, C.L., Brahmer, J.R., et al. (2009). Inhibition of the hedgehog pathway in advanced basal-cell carcinoma. N. Engl. J. Med. *361*, 1164–1172.

Voronkov, A., Holsworth, D.D., Waaler, J., Wilson, S.R., Ekblad, B., Perdreau-Dahl, H., Dinh, H., Drewes, G., Hopf, C., Morth, J.P., et al. (2013). Structural Basis and SAR for G007-LK, a Lead Stage 1,2,4-Triazole Based Specific Tankyrase 1/2 Inhibitor. J. Med. Chem. *56*, 3012–3023.

Vyas, N., Walvekar, A., Tate, D., Lakshmanan, V., Bansal, D., Cicero, A.L., Raposo, G., Palakodeti, D., and Dhawan, J. (2014). Vertebrate Hedgehog is secreted on two types of extracellular vesicles with different signaling properties. Sci. Rep. *4*, 7357.

Wada, N., Javidan, Y., Nelson, S., Carney, T.J., Kelsh, R.N., and Schilling, T.F. (2005). Hedgehog signaling is required for cranial neural crest morphogenesis and chondrogenesis at the midline in the zebrafish skull. Dev. Camb. Engl. *132*, 3977–3988.

Walsh, A.J., Cook, R.S., Manning, H.C., Hicks, D.J., Lafontant, A., Arteaga, C.L., and Skala, M.C. (2013). Optical metabolic imaging identifies glycolytic levels, subtypes, and early-treatment response in breast cancer. Cancer Res. *73*, 6164–6174.

Walsh, A.J., Cook, R.S., Sanders, M.E., Aurisicchio, L., Ciliberto, G., Arteaga, C.L., and Skala, M.C. (2014). Quantitative optical imaging of primary tumor organoid metabolism predicts drug response in breast cancer. Cancer Res. *74*, 5184–5194.

Wang, J.-Q., Kon, J., Mogi, C., Tobo, M., Damirin, A., Sato, K., Komachi, M., Malchinkhuu, E., Murata, N., Kimura, T., et al. (2004). TDAG8 is a proton-sensing and psychosine-sensitive G-protein-coupled receptor. J. Biol. Chem. *279*, 45626–45633.

Wang, L., Trebicka, E., Fu, Y., Ellenbogen, S., Hong, C.C., Babitt, J.L., Lin, H.Y., and Cherayil, B.J. (2012). The bone morphogenetic protein-hepcidin axis as a therapeutic target in inflammatory bowel disease. Inflamm. Bowel Dis. *18*, 112–119.

Wang, T.-M., Holzhausen, L.C., and Kramer, R.H. (2014). Imaging an optogenetic pH sensor reveals that protons mediate lateral inhibition in the retina. Nat. Neurosci. *17*, 262–268.

van de Water, S., van de Wetering, M., Joore, J., Esseling, J., Bink, R., Clevers, H., and Zivkovic, D. (2001). Ectopic Wnt signal determines the eyeless phenotype of zebrafish masterblind mutant. Dev. Camb. Engl. *128*, 3877–3888.

Webb, B.A., Chimenti, M., Jacobson, M.P., and Barber, D.L. (2011). Dysregulated pH: a perfect storm for cancer progression. Nat. Rev. Cancer *11*, 671–677.

Weger, B.D., Weger, M., Jung, N., Lederer, C., Bräse, S., and Dickmeis, T. (2013). A Chemical Screening Procedure for Glucocorticoid Signaling with a Zebrafish Larva Luciferase Reporter System. J. Vis. Exp. JoVE.

Wehrli, M., Dougan, S.T., Caldwell, K., O'Keefe, L., Schwartz, S., Vaizel-Ohayon, D., Schejter, E., Tomlinson, A., and DiNardo, S. (2000). arrow encodes an LDL-receptor-related protein essential for Wingless signalling. Nature *407*, 527–530.

Wemmie, J.A., Taugher, R.J., and Kreple, C.J. (2013). Acid-sensing ion channels in pain and disease. Nat. Rev. Neurosci. *14*, 461–471.

Westerfield, M. (2000). The zebrafish book : a guide for the laboratory use of zebrafish (Eugene, OR: University of Oregon Press).

White, R.M., Cech, J., Ratanasirintrawoot, S., Lin, C.Y., Rahl, P.B., Burke, C.J., Langdon, E., Tomlinson, M.L., Mosher, J., Kaufman, C., et al. (2011). DHODH modulates transcriptional elongation in the neural crest and melanoma. Nature *471*, 518–522.

Willert, K., and Jones, K.A. (2006). Wnt signaling: is the party in the nucleus? Genes Dev. *20*, 1394–1404.

Williams, C., and Hong, C. (2013). Making Models Work: Library Annotation through Phenoclustering. Drug Discov. Today Dis. Models *10*.

Williams, C.H., and Hong, C.C. (2011). Multi-step usage of in vivo models during rational drug design and discovery. Int. J. Mol. Sci. *12*, 2262–2274.

Williams, C.H., and Hong, C.C. (2015). High content screening for modulators of cardiovascular or global developmental pathways in zebrafish. Methods Mol. Biol. Clifton NJ *1263*, 167–174.

Williams, C.H., and Hong, C.C. (2016). Zebrafish small molecule screens: Taking the phenotypic plunge. Comput. Struct. Biotechnol. J. *14*, 350–356.

Williams, C.H., Hempel, J.E., Hao, J., Frist, A.Y., Williams, M.M., Fleming, J.T., Sulikowski, G.A., Cooper, M.K., Chiang, C., and Hong, C.C. (2015). An in vivo chemical genetic screen identifies phosphodiesterase 4 as a pharmacological target for hedgehog signaling inhibition. Cell Rep. *11*, 43–50.

Wolman, M.A., Jain, R.A., Liss, L., and Granato, M. (2011). Chemical modulation of memory formation in larval zebrafish. Proc. Natl. Acad. Sci. *108*, 15468–15473.

Wong, H.-C., Bourdelas, A., Krauss, A., Lee, H.-J., Shao, Y., Wu, D., Mlodzik, M., Shi, D.-L., and Zheng, J. (2003). Direct binding of the PDZ domain of Dishevelled to a conserved internal sequence in the C-terminal region of Frizzled. Mol. Cell *12*, 1251–1260.

Worp, H.B. van der, Howells, D.W., Sena, E.S., Porritt, M.J., Rewell, S., O'Collins, V., and Macleod, M.R. (2010). Can Animal Models of Disease Reliably Inform Human Studies? PLOS Med *7*, e1000245.

Xiao, R., and Xu, X.Z.S. (2011). C. elegans TRP channels. Adv. Exp. Med. Biol. *704*, 323–339.

Yan, D., Wu, Y., Feng, Y., Lin, S.-C., and Lin, X. (2009). The core protein of glypican Dally-like determines its biphasic activity in Wingless morphogen signaling. Dev. Cell *17*, 470–481.

Yan, L., Singh, L.S., Zhang, L., and Xu, Y. (2014). Role of OGR1 in myeloid-derived cells in prostate cancer. Oncogene *33*, 157–164.

Yang, L.V., Radu, C.G., Roy, M., Lee, S., McLaughlin, J., Teitell, M.A., Iruela-Arispe, M.L., and Witte, O.N. (2007). Vascular abnormalities in mice deficient for the G protein-coupled receptor GPR4 that functions as a pH sensor. Mol. Cell. Biol. *27*, 1334–1347.

Yauch, R.L., Dijkgraaf, G.J.P., Alicke, B., Januario, T., Ahn, C.P., Holcomb, T., Pujara, K., Stinson, J., Callahan, C.A., Tang, T., et al. (2009). Smoothened mutation confers resistance to a Hedgehog pathway inhibitor in medulloblastoma. Science *326*, 572–574.

Ye, X., Linton, J.M., Schork, N.J., Buck, L.B., and Petrascheck, M. (2014). A pharmacological network for lifespan extension in Caenorhabditis elegans. Aging Cell *13*, 206–215.

Yu, P.B., Hong, C.C., Sachidanandan, C., Babitt, J.L., Deng, D.Y., Hoyng, S.A., Lin, H.Y., Bloch, K.D., and Peterson, R.T. (2008). Dorsomorphin inhibits BMP signals required for embryogenesis and iron metabolism. Nat. Chem. Biol. *4*, 33–41.

Zeng, W.-Z., Liu, D.-S., and Xu, T.-L. (2014). Acid-sensing ion channels: trafficking and pathophysiology. Channels Austin Tex *8*, 481–487.

Zeng, W.-Z., Liu, D.-S., Liu, L., She, L., Wu, L.-J., and Xu, T.-L. (2015). Activation of acid-sensing ion channels by localized proton transient reveals their role in proton signaling. Sci. Rep. *5*, 14125.

Zeng, X., Goetz, J.A., Suber, L.M., Scott, W.J., Schreiner, C.M., and Robbins, D.J. (2001). A freely diffusible form of Sonic hedgehog mediates long-range signalling. Nature *411*, 716–720.

Zeng, X., Tamai, K., Doble, B., Li, S., Huang, H., Habas, R., Okamura, H., Woodgett, J., and He, X. (2005). A dual-kinase mechanism for Wnt coreceptor phosphorylation and activation. Nature *438*, 873–877.

Zhao, J., Zeng, X., Song, P., Wu, X., and Shi, H. (2016). AKT1 as the PageRank hub gene is associated with melanoma and its functional annotation is highly related to the estrogen signaling pathway that may regulate the growth of melanoma. Oncol. Rep. *36*, 2087–2093.

Zhao, X., Ponomaryov, T., Ornell, K.J., Zhou, P., Dabral, S.K., Pak, E., Li, W., Atwood, S.X., Whitson, R.J., Chang, A.L.S., et al. (2015). RAS/MAPK Activation Drives Resistance to Smo Inhibition, Metastasis, and Tumor Evolution in Shh Pathway-Dependent Tumors. Cancer Res. *75*, 3623–3635.

Zhao, Z., Tuakli-Wosornu, Y., Lagace, T.A., Kinch, L., Grishin, N.V., Horton, J.D., Cohen, J.C., and Hobbs, H.H. (2006). Molecular characterization of loss-of-function mutations in PCSK9 and identification of a compound heterozygote. Am. J. Hum. Genet. *79*, 514–523.